Development of multifunctional block copolymers for the delivery of nucleic acid vaccines

Connie Cheng

A dissertation

submitted in partial fulfillment of the

requirements for the degree of

Doctor of Philosophy

University of Washington

2013

Reading Committee:

James D. Bryers, Chair

Suzie H. Pun

Patrick S. Stayton

Program Authorized to Offer Degree:

Bioengineering

University of Washington

Abstract

Development of multifunctional block copolymers for the delivery of nucleic acid vaccines

Connie Cheng

Chair of the Supervisory Committee:
Professor James D. Bryers
Bioengineering

Plasmid DNA (pDNA) and messenger RNA (mRNA) vaccines hold significant potential as versatile, safe, and cost-effective technologies for the treatment of cancer and infectious diseases. However, clinical applications are currently limited by poor immunogenicity attributable to limitations in nucleic acid delivery efficacy. Synthetic nonviral delivery vectors represent a promising approach to improving vaccine potency through the enhancement of gene transfection. This dissertation describes the development of multifunctional block copolymers as delivery platforms for nucleic acid vaccines. Polymers were synthesized via reversible addition-fragmentation chain transfer (RAFT) polymerization, a technique enabling the facile production of well-defined block copolymers with complex architectures. First, a series of block copolymers composed of discrete cationic, endosomolytic, and hydrophilic segments was evaluated for mRNA delivery. Polymer designs producing highly stable mRNA polyplexes were associated with high *in vitro* transfection efficiencies and successfully delivered antigen-encoding mRNA to dendritic cells (DCs) for T cell activation. Second, glycopolymer micelles

incorporating an endosomolytic core and mannosylated corona for DC targeting were assessed for pDNA vaccine delivery efficacy in mice. Compared to uncomplexed pDNA and untargeted micelles, mannosylated micelles exhibited enhanced uptake by DCs in lymph nodes and elicited increased antigen-specific antibody responses. Overall, these findings demonstrate the potential of multifunctional RAFT-based polymers for improving the delivery of nucleic acid therapeutics for vaccination strategies.

Table of Contents

List of Figures

List of Tables

List of Abbreviations

AcGalEMA	acetylated galactose ethyl methacrylate
AcManEMA	acetylated mannose ethyl methacrylate
AIBN	2,2-azobisisobutyronitrile
APC	antigen-presenting cell
BMA	butyl methacrylate
BMDC	bone marrow-derived dendritic cell
ConA	concanavalin A
CRD	carbohydrate recognition domain
CTA	chain transfer agent
CTL	cytotoxic T lymphocyte
CTP	4-cyanopentanoic acid dithiobenzoate
DC	dendritic cell
DEAEMA	diethylaminoethyl methacrylate
DLS	dynamic light scattering
DMAEMA	dimethylaminoethyl methacrylate
DMEM	Dulbecco's Modified Eagle Medium
DP	degree of polymerization
DPBS	Dulbecco's phosphate-buffered saline
ECT	4-cyano-4-(ethylsulfanylthiocarbonyl) sulfanylvpentanoic acid
ELISA	enzyme-linked immunosorbent assay
FBS	fetal bovine serum
GalEMA	galactose ethyl methacrylate
GFP	green fluorescent protein

GM-CSF	granulocyte macrophage colony-stimulating factor
GPC	gel permeation chromatography
HBG	HEPES-buffered glucose
IVT	*in vitro* transcribed
LF	Lipofectamine 2000™
LRP	living free radical polymerization
ManEMA	mannose ethyl methacrylate
MHC	major histocompatibility complex
MMR	macrophage mannose receptor
mRNA	messenger RNA
NMR	nuclear magnetic resonance
PDI	polydispersity index
pDNA	plasmid DNA
PEG	poly(ethylene glycol)
PEGMA	poly(ethylene glycol) methyl ether methacrylate
PEI	poly(ethyleneimine)
PLL	poly(L-lysine)
RAFT	reversible addition-fragmentation chain transfer
siRNA	small interfering RNA
V-40	1,1'-azobis(cyclohexane-1-carbonitrile)
V-70	2,2′-azobis(4-methoxy-2,4-dimethyl valeronitrile)
V-501	4,4-azobis(4-cyanopentanoic acid)

Acknowledgements

I would like to express my deepest gratitude to everyone who supported me throughout my graduate career – colleagues, collaborators, faculty, fellow students, friends, and family. In particular, I wish to thank my advisor, James Bryers, for his dedicated mentorship and wholehearted encouragement of my scientific pursuits – whether they involved starting new collaborations, exploring novel avenues of research, or seeing pandas in Chengdu. I am also extremely grateful to Pat Stayton, my unofficial co-advisor, for his intellectual guidance and for asking the tough questions that pushed me to hold myself to higher standards of scientific reasoning and problem-solving. I am indebted to my collaborator, Matt Manganiello, who helped me on everything from polymer chemistry to mouse studies, was a key part of the glycopolymer research described in this thesis, and boosted morale through his enthusiasm and humor. Finally, I would like to thank my better half, William Cheng, and my family for their unwavering support throughout my graduate tenure.

Chapter 1

Nucleic acid vaccines: therapeutic potential and delivery challenges

1. Introduction

The first demonstration of nucleic acid vaccination was described in 1992, when Tang *et al*. reported that biolistic delivery of antigen-encoding plasmid DNA (pDNA) into the skin of mice elicited antigen-specific antibody responses [1]. Subsequently, Ulmer *et al*. observed that intramuscular delivery of pDNA encoding influenza A nucleoprotein conferred protection against viral challenges in mice, demonstrating that pDNA vaccines could generate viral antigens for immune presentation without the limitations of direct peptide delivery and viral vectors [2]. Research efforts in the following decades have proven that nucleic acid vaccines are safe, versatile, cost-efficient, and capable of eliciting humoral and cellular immune responses similar to those induced by live attenuated vaccines [3–5]. Both pDNA and messenger RNA (mRNA) have been explored for prophylactic vaccination against a wide variety of pathogens (*e.g.* HIV, influenza virus, anthrax, malarial parasites), as well as for therapeutic anti-cancer vaccination [3,4,6]. However, the performance of these vaccines in human clinical trials has thus far not matched their success in preclinical animal models, underscoring the need for the development of more potent vaccine technologies.

This chapter provides a review of the immunology of nucleic acid vaccines, followed by a brief summary of pDNA and mRNA vaccines, with a focus on mRNA as an emerging alternative to pDNA for immunotherapies. The final section gives an overview of the approach taken in this

work for enhancing vaccine potency: developing synthetic polymer carrier systems engineered to improve the intracellular delivery efficacy of nucleic acid therapeutics.

2. Immunology of nucleic acid vaccines

The induction of an antigen-specific immune response requires that vaccine antigens be processed by professional antigen-presenting cells (APCs) for loading onto major histocompatibility complex (MHC) molecules and presentation to T cells. Dendritic cells (DCs) are the primary APCs involved in the initiation of adaptive immunity and are important targets for vaccination strategies [7]. Immature DCs are highly endocytic cells that survey peripheral tissues for antigens. In the absence of foreign pathogens, presentation of environmental and self antigens induces tolerance [8]. When exposed to maturation stimuli, such as microbial products and inflammatory cytokines, DCs undergo maturation and migrate to the T cell regions of lymphoid organs to activate T cell-mediated immunity.

The origin of the antigen influences the subsequent immune response (**Figure 1.1**) [9]. Endogenous antigens are presented on MHC I molecules for recognition by CD8+ T cells for initiation of cell-mediated immunity. Exogenous antigens are presented on MHC II molecules for recognition by CD4+ T cells, which then activate B cells for the initiation of humoral immunity. These two pathways are not entirely distinct, as the "cross-presentation" mechanism in DCs allows for the presentation of exogenous antigens on MHC I molecules, and some CD4+ helper T cell subsets play a role in stimulating cellular immunity. Depending on the specific application, optimal vaccine efficacy may require activation of both cell-mediated and humoral immune responses.

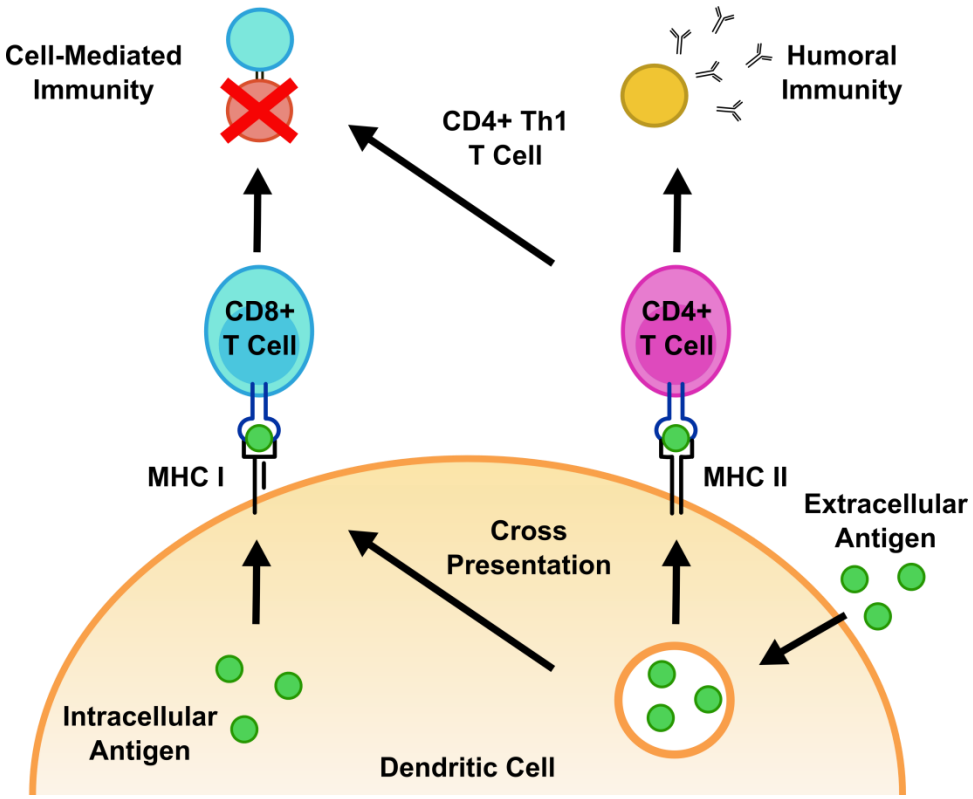

Figure 1.1. Pathways of the adaptive immune response.

Peptide and protein vaccines directly provide exogenous antigens for uptake by DCs, which biases the resultant responses towards MHC II presentation and antibody-mediated immunity. In contrast, nucleic acid vaccines generate endogenous antigens through the transfection of local host cells, which more closely mimics the activity of live pathogens and enables these vaccines to induce both cellular and humoral mmunity [5]. There are two potential mechanisms by which these host-expressed antigens are introduced into DCs for processing: (1) direct transfection of DCs and (2) transfection of bystander cells (*e.g.* keratinocytes, myocytes, fibroblasts) which express antigens for subsequent capture by DCs [5,10]. Current evidence suggests that both pathways can contribute to immunity, although their relative importance may be influenced by the route of administration (intramuscular, subcutaneous, intradermal) [5,11,12].

3. pDNA vaccines

The seminal work of Wolff *et al.* in 1990 established that intramuscular delivery of naked pDNA could generate gene expression in local myocytes [13]. As discussed in the Introduction, this study was followed by reports from Tang *et al*. [1] and Ulmer *et al.* [2] demonstrating that protein expression from injected pDNA elicited protective antigen-specific immune responses. Since then, pDNA vaccines have been extensively evaluated in animal models and human clinical trials, most commonly for the treatment of cancer and infectious diseases [3]. While pDNA therapies have been documented to be safe and well tolerated, the magnitude of the immune response elicited by these vaccines in humans is thus far insufficient for protective or therapeutic efficacy [4]. Nevertheless, the recent approval of three pDNA vaccines for veterinary use – one against viral infection in horses [14], one against viral infection in fish [15], and a melanoma treatment for dogs [16] – is an encouraging advancement that further validates the clinical potential of this technology.

Recent efforts in the field of pDNA vaccination have focused on improving vaccine potency through a variety of approaches. These include: (1) co-delivery of plasmids encoding cytokines, chemokines, or costimulatory molecules as vaccine adjuvants [17], (2) heterologous immunization strategies utilizing a pDNA vaccine for priming followed by a recombinant viral or protein boost [18], (3) next-generation delivery formats such as electroporation and gene gun [19], and (4) formulating pDNA with carrier systems, such as liposomes, polymers, and nanoparticles, in order to improve delivery characteristics and gene transfection efficiency [20,21].

4. mRNA vaccines

4.1. Advantages of mRNA as a gene therapeutic

Eukaryotic mature mRNA is a linear, single-stranded molecule composed of five major components: the 5' cap (m^7GpppN, where N is any nucleotide), a 5' untranslated region (UTR), an open reading frame, a 3' UTR, and a poly(A) tail consisting of 100-250 adenosine residues [22]. mRNAs used for vaccination typically range from 100-10,000 bases in length [6], and are produced by *in vitro* transcription from a pDNA template.

One of the primary advantages of mRNA compared to pDNA is that mRNA does not require nuclear entry for its activity, resulting in significantly higher and faster levels of gene expression [22,23]. Nuclear entry is a formidable barrier to pDNA transfection – some studies have estimated that less than 1% of pDNA delivered to the cytoplasm reaches the nucleus [24,25] – and the mechanisms by which this process occurs for synthetic delivery systems are extremely poorly characterized [26]. This is particularly significant for gene delivery to slowly- or non-dividing mammalian cells, whose relative intransigence to pDNA transfection has been attributed to the unavailability of passive nuclear import via the mitotically induced breakdown of the nuclear envelope [27–29]. In contrast, mRNA-based gene therapies render the nuclear entry barrier irrelevant, and thus represent a promising alternative to pDNA for delivery to hard-to-transfect cell types.

In terms of safety, mRNA is preferable to pDNA for clinical applications since mRNA cannot integrate into the host genome, thus eliminating the risk of insertional mutagenesis, and is only transiently expressed. While the usage of mRNA for long-term gene therapies is limited due to

this short-term expression profile, mRNA is extremely suitable for applications where only transient production of the gene product is required. In the case of prophylactic or therapeutic vaccination strategies, multiple administrations of mRNA may be needed, but this is a perfectly feasible approach given the relative facility, efficiency, and cost-effectiveness of producing *in vitro* transcribed (IVT) mRNA in accordance with good manufacturing practice (GMP) guidelines [30].

4.2. Applications of mRNA vaccination

Administration of mRNA for *in vivo* protein expression was also first demonstrated by Wolff *et al*. in their seminal 1990 report [13]. In 1993, successful mRNA vaccination was first reported by Martinon *et al*., who observed the induction of an antigen-specific cytotoxic T cell response in mice following immunization with liposome-entrapped mRNA [31]. Boczkowski *et al*. subsequently demonstrated in 1996 that mRNA-transfected DCs could be used to generate protective antitumor immune responses [32]. Despite these successes, the use of mRNA for vaccination has lagged behind plasmid pDNA largely because mRNA was long considered to be too unstable for clinical applications. However, mRNA is now increasingly being recognized as a promising alternative to pDNA in gene therapy strategies.

Thus far, mRNA has been predominantly investigated as a gene vaccination agent for cancer immunotherapy, with the vast majority of these studies utilizing autologous DCs transfected with mRNA *ex vivo* [6,33–38]. mRNA offers the potential for vaccination with both predefined tumor antigens or patient-specific antigenic mixtures in the form of tumor-derived mRNA, with the latter option being particularly useful for situations where the optimal antigenic targets are

unknown [35]. Despite the relative instability of unprotected mRNA, early phase clinical studies have successfully utilized passive transfection of DCs with naked mRNA [39–46] or direct injection of naked mRNA [47,48] to induce antitumor immune responses. Vaccine efficacy in clinical trials has also been observed using DCs transfected by electroporation [49–53] and lipofection [54]. In general, mRNA vaccination treatments have been well tolerated by patients with no major toxicity observed.

mRNA vaccination has also been explored in preclinical studies for other immunotherapy applications. The use of mRNA vaccines and mRNA-transfected DC vaccines as anti-infective immunotherapies has been reported in murine models using antigens for influenza virus [31,55], lymphocytic choriomeningitis virus [56], hepatitis C virus [57], human papillomavirus type 16 [58], and human immunodeficiency virus (HIV) [59]. Additionally, Roesler *et al*. recently reported the use of mRNA delivered by direct injection in mice for preventative vaccination against type I allergies [60].

5. Designing polymer vehicles for nucleic acid vaccine delivery

The primary disadvantage of nucleic acid vaccination is that vaccine efficacy is dependent upon gene transfection: low levels of antigen expression reduce the potency of the subsequent immune responses [61]. To overcome this limitation, many research efforts have focused on developing delivery technologies for improving the transfection efficiency of nucleic acid vaccines. Synthetic nonviral vectors are highly versatile and avoid the safety concerns associated with viral delivery, but are typically less efficient. To successfully deliver pDNA or mRNA for cellular expression, delivery vehicles must navigate a wide variety of extracellular and intracellular

barriers (**Figure 1.2)** [26]. Viruses have evolved numerous functionalities to surmount each of these obstacles and mediate highly efficient gene transduction. In contrast, the relatively low transfection efficiencies obtained with synthetic carriers can be attributed to the fact that these systems typically only address a subset of these barriers.

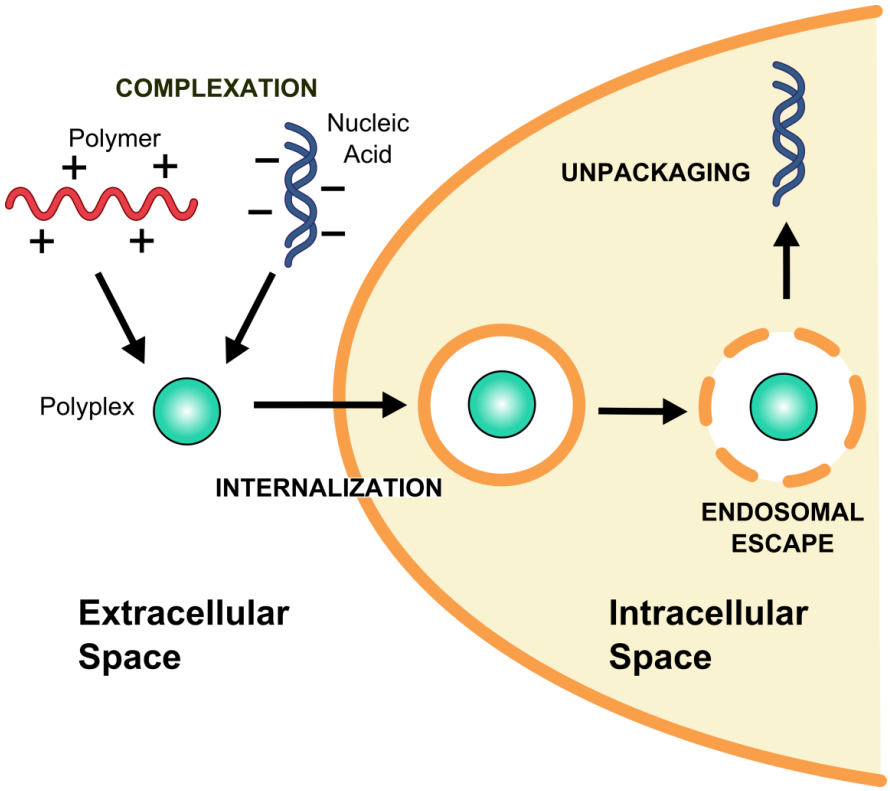

Figure 1.2. Major steps in polymer-mediated intracellular gene delivery.

5.1. Navigating the extracellular space

The extracellular milieu contains nucleases that rapidly degrade any unprotected nucleic acids. This is a particularly significant issue for mRNA, since it is very labile to degradation by ubiquitous RNases. Cationic polymers such as poly(ethyleneimine) (PEI), poly(L-lysine) (PLL), and poly(dimethylaminoethyl methacrylate) (pDMAEMA) confer protection from degradation by condensing nucleic acids into a particulate "polyplex" via electrostatic interactions. Cationic condensation also enhances cellular uptake of nucleic acids by compacting nucleic acids into a

size range favorable for endocytosis and facilitating association with anionic cellular membranes [26,62].

However, the cationic surface charge associated with polyplexes can cause problems *in vivo* with regards to colloidal instability, aggregation, and toxicity, due to undesirable interactions with negatively charged biomacromolecules such as serum proteins, cellular blood components, complement factors, and cell surface glycosaminoglycans [63]. Such interactions may also destabilize polyplexes, causing premature extracellular release of the nucleic acid [63,64]. Many delivery systems incorporate neutral hydrophilic polymers such as poly(ethylene glycol) (PEG), N-(2-hydroxypropyl) methacrylamide (HPMA), and various oligosaccharides that reduce these interactions and shield the cationic surface charge via the creation of a steric barrier [26,64].

5.2. Cell-specific targeting

Although APCs can internalize polyplexes through the nonspecific processes of macropinocytosis and phagocytosis, additional enhancement of uptake efficiency can be achieved through the use of cell-specific targeting ligands to direct polyplexes into the receptor-mediated endocytic pathway. Targeting strategies typically involve chemically modifying delivery vectors with targeting moieties such as carbohydrates, small molecules, peptides, and antibodies [26]. For vaccines, commonly targeted DC receptors include the macrophage mannose receptor (MMR, described in greater detail in Chapter 5), DEC-205, DC-SIGN, and the Fcγ receptors [65,66].

5.3. Escaping the endolysosomal pathway

Once endocytosed, polyplexes are entrapped in early endosomes, which acidify, mature into late endosomes, and fuse with lysosomes containing degradative enzymes (**Figure 1.3**) [67,68]. To avoid destruction of the nucleic acid cargo, polyplexes must escape from entrapment in endolysosomal compartments. While endosomal escape remains a formidable obstacle for synthetic gene delivery vectors [26], viruses and intracellular pathogens have evolved very effective escape mechanisms that manipulate the intracellular trafficking pathway [68]. For instance, in the acidic endolysosomal environment, the viral protein hemagglutinin undergoes a conformational change from a hydrophilic to a hydrophobic form that can fuse with and disrupt membrane lipid bilayers [69].

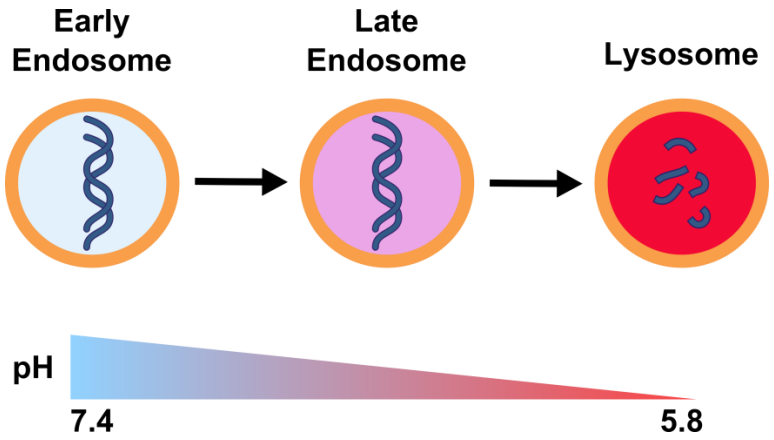

Figure 1.3. Acidifying pH gradient of the endolysosomal trafficking pathway.

Alternatively, synthetic polymer systems that exhibit high buffering capacities such as PEI are hypothesized to achieve cytosolic delivery through the proton sponge effect, in which an influx of counterions and water ruptures the endosomal vesicle through an increase in osmotic pressure [70]. More recently, pH-responsive polymer systems that mimic the ability of viral proteins to

undergo conformational changes to a hydrophobic, endosomolytic state have been reported [71,72], and are described in greater detail in Chapter 2.

5.4. Polyplex unpackaging and gene expression

Successful gene expression requires that the nucleic acid ultimately be released from the condensing polymer. It remains unclear at what point in the intracellular delivery process this polyplex unpackaging occurs, although there is some evidence that negatively-charged biomacromolecules resident in the cytosolic space may facilitate decomplexation [73–75]. Extremely stable polymer-nucleic acid interactions may cause inefficient nucleic acid unpackaging from the polyplex, leading to reduced transfection efficiencies [76]. Common approaches to facilitating polyplex unpackaging include reducing the overall cationic charge, using lower molecular weight polycations, using biodegradable or reducible polymer systems, and incorporating neutral hydrophilic segments [26,77]. However, reducing the stability of nucleic acid binding may conversely lead to premature polyplex dissociation in the extracellular space, so polymeric gene carriers must be carefully designed to enable both protection from degradation and timely intracellular release.

Following decomplexation, mRNA translation takes place in the cytosol, whereas pDNA must be trafficked into the nucleus for transcription to occur. As previously discussed, elimination of the nuclear localization requirement is a significant advantage of mRNA transfection, since the nuclear transport of pDNA is a poorly characterized process that remains a significant barrier to efficient pDNA transfection. While the use of peptides containing nuclear localization signals

has been explored as a means of overcoming this barrier, there is significant controversy over the effectiveness of this approach [78,79] .

5.5. Block copolymers as multifunctional gene delivery vectors

An ideal gene carrier system would incorporate multiple functionalities, each engineered to address a specific delivery barrier. Block copolymer vectors satisfy this requirement by allowing for the modular incorporation of discrete functional polymer segments. For instance, various di-, tri-, and pentablock copolymer architectures consisting of alternating cationic blocks, for nucleic acid condensation, and neutral hydrophilic blocks, for conferring polyplex stability and biocompatibility, have been developed for gene delivery [80]. Studies performed with these systems have underscored the observation that delivery vector development frequently involves balancing competing design requirements: the improved stability and reduced cytotoxicity associated with these block copolymer vectors often comes at the cost of lower transfection efficiencies compared to cationic homopolymers, possibly due to alterations in polyplex internalization and intracellular trafficking [81].

Amphiphilic block copolymers composed of hydrophilic and hydrophobic segments that self-assemble into micellar structures have also received significant research attention in the context of delivery vector development [82,83]. Gary *et al*. reported that amphiphilic triblock copolymer micelles composed of PEG, pDMAEMA, and hydrophobic poly(*n*-butyl acrylate) (PnBA) exhibited superior *in vitro* and *in vivo* small interfering RNA (siRNA) delivery characteristics compared to non-micellar PEG and PEG-pDMAEMA carriers, and hypothesized that the

"micelleplexes" were directed towards internalization and intracellular trafficking pathways more favorable for efficient transfection [84].

5.6. Reversible addition-fragmentation chain transfer (RAFT) polymerization

The development of multifunctional polymer vectors requires excellent synthetic control over polymer composition and structure. Living free radical polymerization (LRP) techniques such as stable free radical polymerization (SFRP), atom transfer radical polymerization (ATRP), and reversible addition-fragmentation chain transfer (RAFT) polymerization enable the synthesis of well-defined block copolymers with predetermined molecular weights, specific polymer architectures, and narrow polydispersity indices (PDIs), and are commonly used to synthesize vehicles for drug and gene delivery [80,85]. These attributes also make LRP methodologies particularly suitable for studies that seek to systematically elucidate structure-function principles for rational gene carrier design.

RAFT polymerization, first described in 1998 [86], exhibits several unique advantages in that it is applicable to a wide variety of vinyl monomers, does not require the use of toxic metallic catalysts, and allows for facile functionalization of polymer chain ends. The RAFT mechanism utilizes a chain transfer agent (CTA) which typically contains a thiocarbonylthio moiety reactive towards radical species (**Figure 1.4**). Uniform chain growth is achieved through a reversible chain transfer process between active propagating polymeric radicals and these thiocarbonylthio groups on dormant "macroCTA" chains. Under the appropriate conditions, the polymerization molecular weight is controlled by the initial monomer to CTA ratio ($[M]_0/[CTA]_0$), allowing for the synthesis of polymers with predetermined block sizes [83]. The "living" nature of the

polymer chain end enables the fabrication of more advanced multiblock architectures, while additional end group functionalities, such as targeting moieties and bioconjugation sites, can be incorporated through the use of appropriately modified CTAs [83]. RAFT techniques are amenable to many monomers commonly used in the context of delivery applications, including DMAEMA, HPMA, poly(ethylene glycol) methyl ether methacrylate (PEGMA), and N-isopropylacrylamide (NIPAAm) [85].

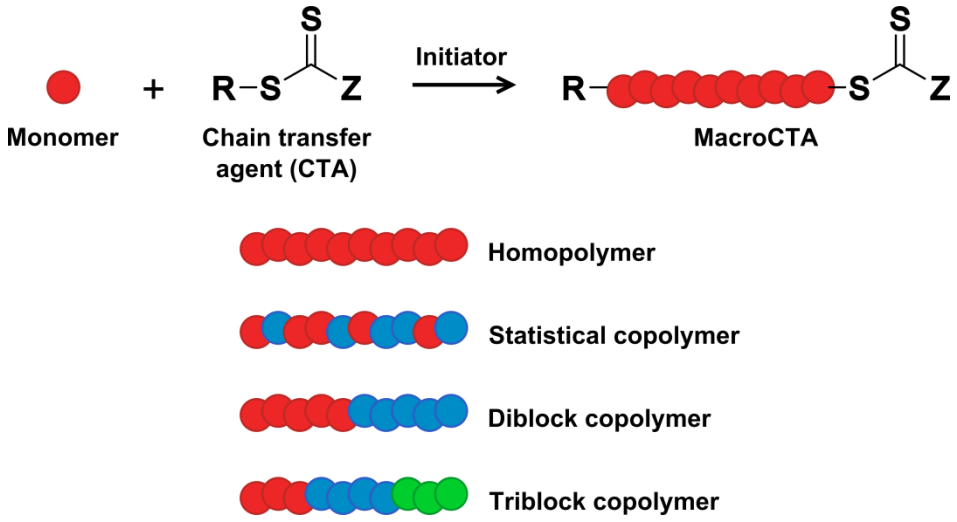

Figure 1.4. RAFT polymerization methodology and potential polymer architectures. The activity of the CTA depends upon the properties of the radical leaving group, R, and the activating group, Z.

Chapter 2

Synthesis of multifunctional block copolymers for mRNA delivery

Abstract

This chapter describes the development, synthesis, and characterization of multifunctional block copolymer delivery vehicles for intracellular mRNA delivery. The overall polymer architecture incorporates three discrete polymer blocks with distinct functionalities: (1) a DMAEMA block for the cationic condensation of mRNA, (2) a PEGMA block for stabilization and biocompatibility, and (3) a copolymer of diethylaminoethyl methacrylate (DEAEMA) and butyl methacrylate (BMA) for enabling pH-triggered endosomal escape. RAFT polymerization was used to synthesize a polymer series that rationally varied block order and PEGMA block size. The resultant polymers were characterized by NMR spectroscopy, gel permeation chromatography (GPC), dynamic light scattering (DLS), and an erythrocyte hemolysis assay. Successful block copolymerization was demonstrated by GPC traces indicating relatively unimodal molecular weight distributions with clear shifts to lower retention times. All synthesized polymers exhibited block sizes and compositions close to the targeted values. Polymers in aqueous solution formed approximately 22-36 nm micelles that were capable of disrupting cellular membranes at endosomal/lysosomal pH values, while remaining inert under physiological pH conditions.

1. Introduction

While synthetic polymer systems have been widely explored for pDNA and siRNA delivery, there are relatively few reports of such systems being applied towards mRNA delivery. Previous findings have observed that commonly used polycations such as PEI [87–90], PLL [87,89], and pDMAEMA [91] are typically less effective for mRNA delivery, although high transfection efficiencies have been reported with PEI in certain studies [91,92]. Improvements in mRNA delivery have been achieved with modified polymer systems, including peptide-conjugated low molecular weight PEI [87], reducible histidine-PLL copolymers [90], copolymers of DMAEMA and oligo(ethylene glycol) methyl ether methacrylate (p(DMAEMA-*co*-OEGMA)) [91], ternary complexes of PEI and PEI-poly(ethylene glycol) (PEI-PEG) copolymers [92], and PEG-polyamino acid block copolymers [93]. Hybrid polymer-lipid delivery systems have also been developed, including ternary complexes of DOTAP and reducible linear poly(amido amines) [94], lipid-enveloped poly(β-amino ester) nanoparticles [95], and ternary complexes of PEGylated histidylated PLL (PEG-HpK) and L-histidine-(N,N-di-*n*-hexadecylamine)ethylamide:cholesterol (HDHE:chol) [96].

Block copolymer systems allow for the modular incorporation of multiple functionalities into a single polymer structure and have been widely explored for gene delivery applications. Typical polymer architectures may include: (A) cationic segments for condensing nucleic acids, (B) hydrophilic segments for enhancing stability and biocompatibility, and (C) pH-responsive segments capable of mediating escape from acidic endolysosomal compartments [82,83,97]. Various ABC-type triblock copolymer systems have been previously reported in the context of pDNA [98–104] and siRNA [105–107] transfection, but not for mRNA delivery.

pDMAEMA and DMAEMA-based copolymers have received significant research attention for gene delivery applications [108–113]. pDMAEMA is a polycation capable of condensing nucleic acids via its tertiary amines, which are partially protonated at physiological pH (pK_a ~7.5) [114]. This interaction results in a compact particle that confers protection from nucleases and enhances cellular association via electrostatic interactions between the cationic polyplexes and negatively charged cellular membranes [26]. The facile synthesis of well-defined DMAEMA-based systems using LRP methodologies represents a significant advantage over other commonly used polycations such as PEI and PLL. However, further improvements in the design of DMAEMA-based delivery systems are still needed in order to bring them into clinical relevance: high molecular weight pDMAEMA homopolymers have been observed to be extremely cytotoxic, while low molecular weight pDMAEMA does not mediate efficient gene transfer [115,116].

RAFT techniques have been used to develop pH-sensitive amphiphilic block copolymer systems that achieve improved gene delivery efficiencies through the enhancement of endosomal escape capabilities. These systems mimic the conformational changes exhibited by viral fusogenic proteins and peptides in the acidic endolysosomal environment. Convertine *et al*. reported the synthesis of a diblock copolymer system for siRNA transfection composed of a DMAEMA segment and a copolymer of propylacrylic acid (PAA), BMA, and DMAEMA [71]. The pH-triggered protonation of PAA causes the diblock copolymer to transition into a hydrophobic, membrane-interactive state, enabling the cytosolic release of the carrier and its cargo.

Recently, Manganiello *et al*. reported a micellar diblock copolymer for pDNA delivery composed of a DMAEMA segment and a copolymer of diethylaminoethyl methacrylate and butyl methacrylate (DEAEMA-*co*-BMA) [72]. The protonation of DEAEMA upon exposure to acidic conditions induces a micelle to unimer transition that exposes hydrophobic BMA units that disrupt endosomal membranes. In the work reported here, this carrier system was modified into a triblock copolymer system with the addition of a hydrophilic PEGMA segment to enhance polyplex stability by steric shielding. RAFT polymerization was used to synthesize a polymer series that varied blocking order and PEGMA block size in order to investigate the effect of polymer architecture on delivery characteristics.

2. Experimental methods

2.1. Materials

Chemicals were supplied by Sigma-Aldrich unless otherwise specified. DMAEMA, DEAEMA, and BMA were distilled prior to use. PEGMA (average M_n = 300 Da) was passed through a basic alumina column prior to use. 2,2-azobisisobutyronitrile (AIBN) was recrystallized from methanol. 4-cyanopentanoic acid dithiobenzoate (CTP) and 4,4-azobis(4-cyanopentanoic acid) (V-501) were used as received.

2.2. Synthesis of pDMAEMA macroCTA

The RAFT polymerization of DMAEMA (6 g, 38.2 mmol) was conducted in dioxane (9 g, 102 mmol) at 60 °C (40 wt% monomer to solvent) under a nitrogen atmosphere for 18 h using CTP (142 mg, 0.509 mmol) and V-501 (36 mg, 0.127 mmol) as the chain transfer agent (CTA) and

radical initiator, respectively. The initial monomer to CTA ratio ($[M]_0/[CTA]_0$) and the initial CTA to initiator ratio ($[CTA]_0/[I]_0$) were 75:1 and 4:1, respectively. The resultant macroCTA was isolated by precipitation into pentane (x5) and dried overnight *in vacuo*.

2.3. Synthesis of pPEGMA macroCTA

The RAFT polymerization of PEGMA (2 g, 6.67 mmol) was conducted in dioxane (18 g, 204 mmol) at 60 °C (10 wt% monomer to solvent) under a nitrogen atmosphere for 18 h using CTP (29 mg, 0.103 mmol) and AIBN (1.7 mg, 0.0103 mmol), with $[M]_0/[CTA]_0$ and $[CTA]_0/[I]_0$ ratios of 65:1 and 10:1, respectively. The resultant macroCTA was isolated by precipitation and dried.

2.4. Synthesis of diblock copolymer DE

DEAEMA (224 mg, 1.21 mmol) and BMA (74 mg, 0.518 mmol) monomers (30% mole fraction BMA) were added to pDMAEMA macroCTA (200 mg, 0.0173 mmol) dissolved in dioxane (746 mg, 8.47 mmol) (40 wt% monomer and macroCTA to solvent) at a $[M]_0/[CTA]_0$ ratio of 100:1. The reaction was conducted at 60 °C under a nitrogen atmosphere for 18 h using V-501 (1.2 mg, 4.32 μmol) with $[CTA]_0/[I]_0$ ratio 4:1, and the final polymer was isolated by precipitation and dried.

2.5. Synthesis of triblock copolymers DPE1, DPE2, DPE3

PEGMA monomer was added to pDMAEMA macroCTA dissolved in dioxane (10 wt% monomer and macroCTA to solvent) at $[M]_0/[CTA]_0$ ratios of 40:1 (DPE1), 100:1 (DPE2), or

150:1 (DPE3). Reactions were conducted at 60 °C under a nitrogen atmosphere using AIBN with $[CTA]_0/[I]_0$ ratio 10:1, and the resultant macroCTAs were isolated by precipitation and dried. These macroCTAs were used in the block copolymerization of DEAEMA and BMA at $[M]_0/[CTA]_0$ ratios of 100:1 (DPE1, DPE2) or 175:1 (DPE3), with all other reaction conditions and purification procedures the same as previously described for polymer DE.

2.6. Synthesis of triblock copolymers PDE, PED

Polymer PDE was synthesized in a two-step procedure: (1) block copolymerization of DMAEMA from a pPEGMA macroCTA with $[M]_0/[CTA]_0$ ratio 75:1, followed by (2) block copolymerization of DEAEMA and BMA from the resultant diblock macroCTA with $[M]_0/[CTA]_0$ ratio 100:1. Polymer PED was synthesized by: (1) block copolymerization of DEAEMA and BMA from a pPEGMA macroCTA with $[M]_0/[CTA]_0$ ratio 100:1, followed by (2) block copolymerization of DMAEMA from the resultant diblock macroCTA with $[M]_0/[CTA]_0$ ratio 75:1. All other conditions and procedures for the polymerizations of DMAEMA or DEAEMA-*co*-BMA were the same as previously described.

2.7. Chromatographic purification and preparation of polymer stock solutions

Dried polymers were dissolved into ethanol followed by addition into Dulbecco's phosphate-buffered saline (DPBS) (10 vol% ethanol, 8-12 mg/mL polymer), purified by chromatographic separation via a PD-10 desalting column (GE Healthcare), and lyophilized. Polymer stock solutions were prepared by redissolving lyophilized polymers into ethanol followed by addition into DPBS (2 vol% ethanol, 2 mg/mL polymer).

2.8. Nuclear magnetic resonance (NMR) spectroscopy

The ^{1}H-NMR spectra of all dried macroCTA intermediates and final lyophilized polymers were acquired using a Bruker AV 500 at 10-20 mg/mL polymer in $CDCl_3$. The monomer compositions of the DEAEMA-*co*-BMA "E" block were determined by the integration of the peaks described in **Figure 2.2**.

2.9. Gel permeation chromatography (GPC)

Molecular weights and polydisperity indices were determined using Tosoh SEC TSK-GEL R-3000 and R-4000 columns connected in series to an Agilent 1200 series liquid chromatography system, Wyatt miniDAWN TREOS triple-angle MALS light scattering detector, and Optilab-rEX refractive index detector. HPLC-grade DMF containing 0.1 wt% LiBr at 60 ^{o}C was used as the mobile phase at a flow rate of 1 mL/min. Polymer molecular weights were determined using dn/dc values calculated separately for each macroCTA and polymer.

2.10. Dynamic light scattering (DLS) characterization of polymer micelle size

DLS measurements were conducted on a ZetaSizer Nano ZS (Malvern) at a constant scattering angle of 173° at 25 °C. Measurements for polymer micelles were conducted using 2 mg/mL polymer solutions in DPBS.

2.11. Hemolysis assay

An erythrocyte hemolysis assay was performed as previously described [117]. Briefly, polymer solutions were incubated with red blood cells in 100 mM sodium phosphate buffer at pH values

of 7.4, 7.0, 6.6, 6.2, or 5.8. In order to normalize hemolytic activity to the total amount of endosomolytic units available per polymer, the concentration of each polymer solution was calculated such that the final mass concentration of the DEAEMA-*co*-BMA block was 20 μg/mL. Triton X-100 (1% v/v in water) was used as a positive control. After 1 h incubation at 37 °C, the amount of released hemoglobin was measured via absorbance at 492 nm.

3. Results

3.1. RAFT-mediated polymer synthesis and characterization

RAFT-mediated synthesis (**Scheme 2.1)** was used to construct a series of block copolymers composed of DMAEMA, PEGMA, and DEAEMA-*co*-BMA (**Scheme 2.2, Table 2.1**). Triblock copolymers DPE1, PDE, and PED were designed to investigate the effect of different block arrangements without altering the lengths of their constitutive blocks. Copolymer series DE, DPE1, DPE2, and DPE3 were designed to maintain the same block order while increasing the targeted size of the central PEGMA block: 0 g/mol (DE), 10,000 g/mol (DPE1), 20,000 g/mol (DPE2), and 30,000 g/mol (DPE3). Targeted molecular weights for the DMAEMA and DEAEMA-*co*-BMA blocks in all polymers were 10,000 g/mol and 15,000 g/mol, respectively, with a monomer feed ratio of 30% BMA in the DEAEMA-*co*-BMA block.

GPC traces of the intermediate macroCTAs and final polymer showed relatively unimodal molecular weight distributions with clear shifts to lower retention times, indicating successful block copolymerization (**Figure 2.1**). NMR analysis confirmed that the synthesized polymers exhibited all expected resonances and were free of residual monomers (**Figure 2.2**). All

polymers exhibited narrow polydispersities (PDI ≤ 1.14) with block sizes and compositions close to the targeted values.

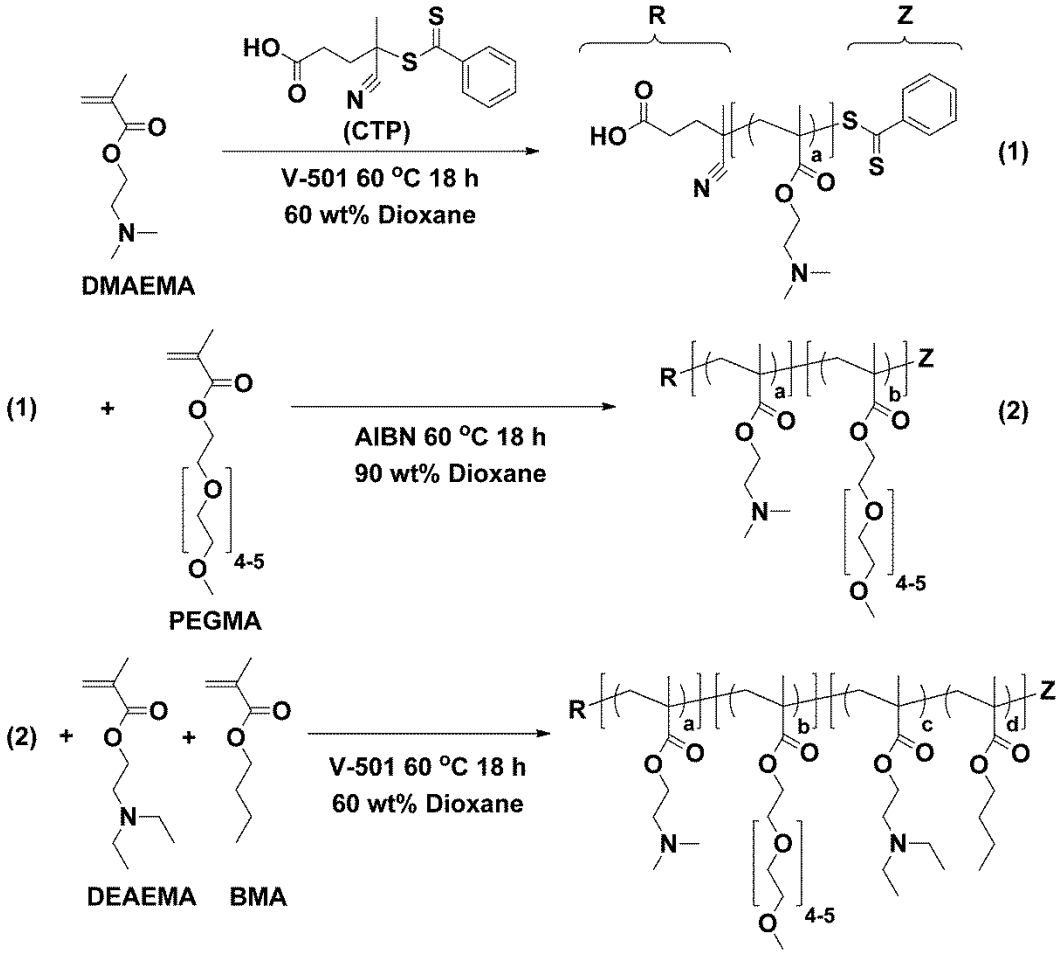

Scheme 2.1. RAFT-mediated synthesis of triblock copolymers composed of DMAEMA, PEGMA, and DEAEMA-*co*-BMA. A representative synthetic scheme for polymers DPE1, DPE2, and DPE3 is shown.

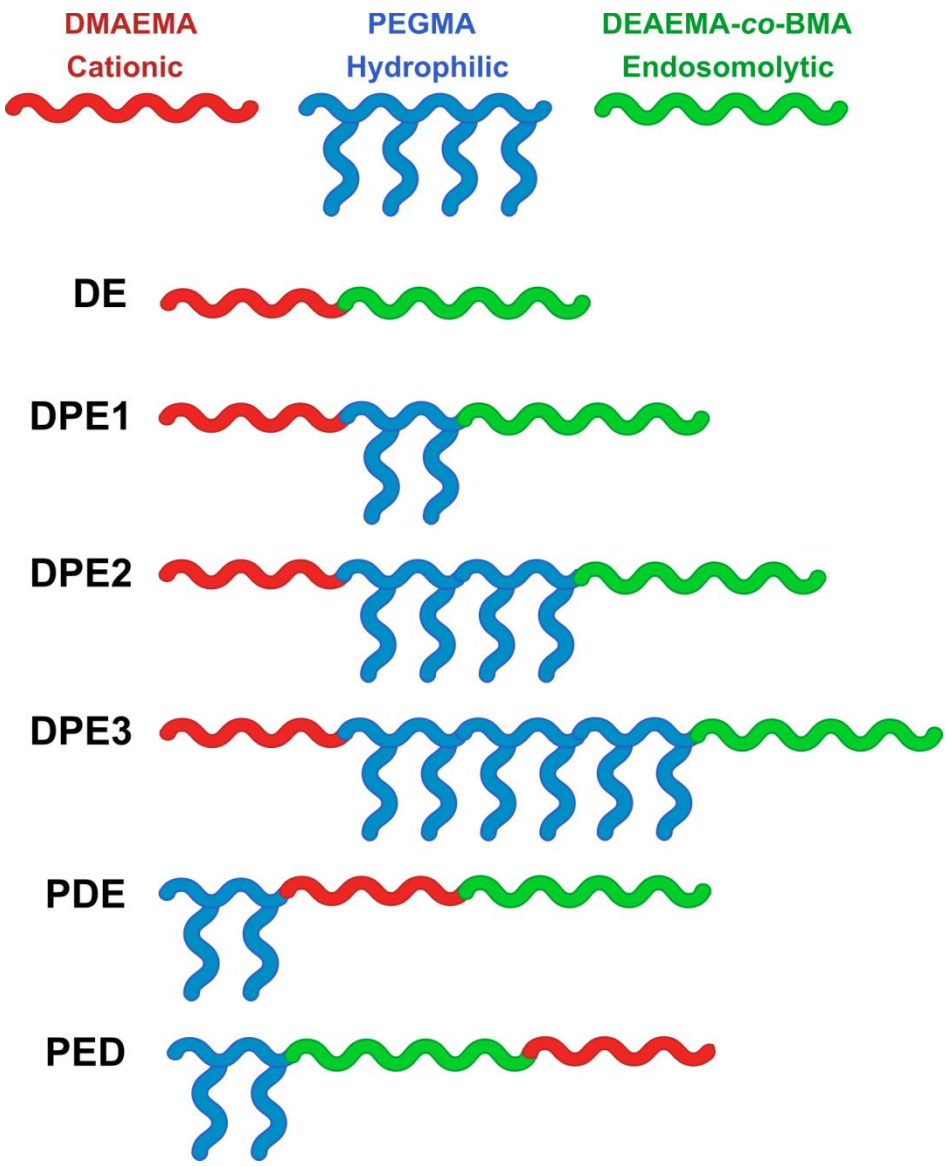

Scheme 2.2. Block copolymer designs prepared in this study and their nomenclature.

Table 2.1. Blocking orders, molecular weights, polydispersities, and monomer compositions for polymer designs.

Polymer	Block order[a]	M_n 1st block[b] (g/mol)	DP 1st block[b]	M_n 2nd block[b] (g/mol)	DP 2nd block[b]	M_n 3rd block[b] (g/mol)	DP 3rd block[b]	Total M_n[b] (g/mol)	PDI[b]	%BMAE block[c]
DE	D-E	11600	74	13500	79	-	-	25100	1.07	34
DPE1	D-P-E	11600	74	8400	28	15500	90	35500	1.08	31
DPE2	D-P-E	11600	74	19700	66	14300	84	45600	1.12	36
DPE3	D-P-E	11600	74	33100	110	17100	100	61700	1.14	34
PDE	P-D-E	10900	36	10300	66	13100	77	34400	1.08	34
PED	P-E-D	10900	36	16200	95	8100	52	35200	1.11	33

[a] Denotes the ordering of the DMAEMA (D), PEGMA (P), and DEAEMA-*co*-BMA (E) blocks (1st block-2nd block -3rd block).
[b] As determined by GPC.
[c] The monomer composition of the DEAEMA-*co*-BMA (E) block, as determined by ^{1}H-NMR ($CDCl_3$) spectroscopy (Bruker AV 500).

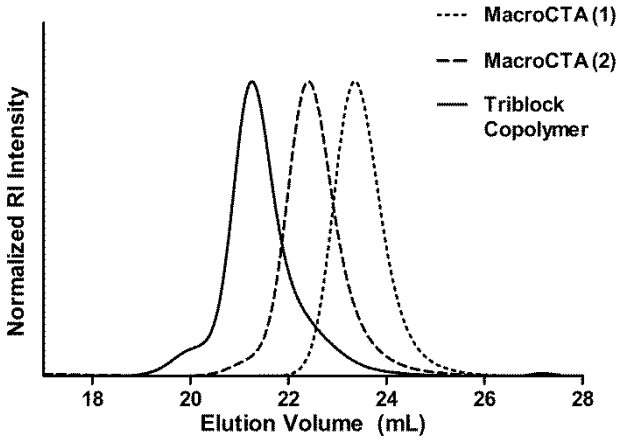

Figure 2.1. Representative molecular weight distributions for intermediate macroCTAs and final triblock copolymer (DPE1) synthesized via RAFT polymerization.

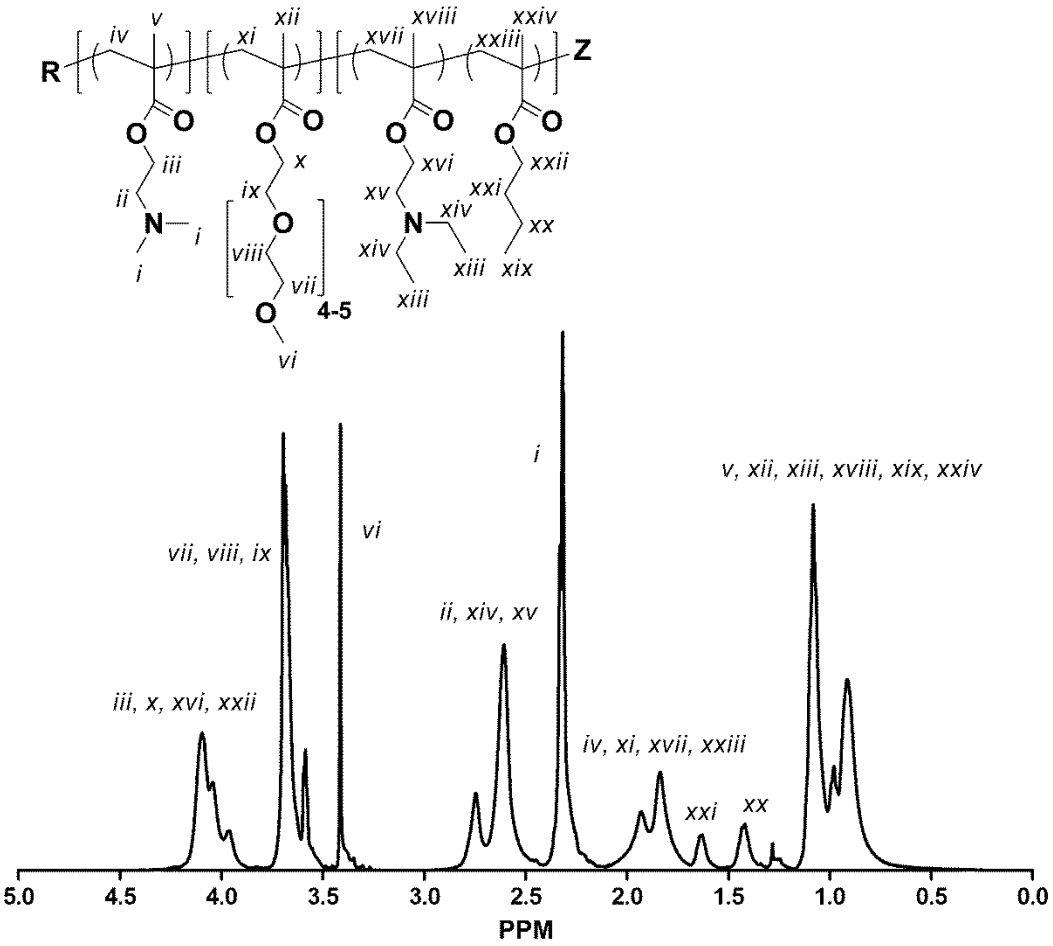

Figure 2.2. Representative ^{1}H-NMR ($CDCl_3$) spectrum of a triblock copolymer (DPE1). Monomer compositions were determined by integration of peaks i, vi, xxi, and (iii, x, xvi, xxii).

3.2. DLS characterization of polymer micelles

Polymers were further characterized by DLS for particle sizing analysis (**Table 2.2**). Molecularly dissolved polymers in solution formed particles 22-36 nm in diameter, indicative of self-assembly into micelles. This behavior is consistent with previous observations in a similar diblock copolymer system [72]. Overall, polymer architecture did not appear to significantly influence polymer micelle formation, although micelle sizes for polymers in the D-P-E configuration appeared to increase slightly with increasing PEGMA block size.

Table 2.2. DLS measurements of polymer micelle sizes.

Polymer	Polymer micelle diameter (nm)
DE	25 ± 2.4
DPE1	29 ± 3.1
DPE2	32 ± 3.9
DPE3	36 ± 3.9
PDE	33 ± 5.5
PED	22 ± 2.9

Diameters are calculated from the intensity size distribution ± standard deviation calculated from the PDI.

3.3. pH-dependent hemolysis activity

The ability of the polymers to disrupt cellular membranes in a pH-dependent manner was assessed by a hemolysis assay. Polymers were incubated with human red blood cells at pH values selected to mimic the acidifying gradient encountered as endocytosed material is trafficked to endosomal/lysosomal compartments (**Figure 2.3**). All polymers exhibited minimal hemolytic activity under physiological conditions (< 2% hemolysis at pH 7.4), but transitioned sharply to high levels of hemolysis at lower pH values. Comparing the hemolytic activities of PDE, PED, and DPE1 to assess the effect of block order on membrane destabilization activity, at pH 6.2, DPE1 and PDE achieved similar hemolysis levels of 83% and 88%, respectively, while PED exhibited only 52% hemolysis, suggesting that placing in the endosomolytic segment in the center of the polymer chain may interfere with its membrane-disruptive properties. Comparing the hemolysis levels at pH 6.2 exhibited by DE (84%), DPE1 (83%), DPE2 (79%), and DPE3 (103%), increasing the PEGMA block size in the D-P-E configuration did not alter the hemolytic profile, with the exception of DPE3 which generated markedly higher levels of hemolysis than

the other three polymers. This finding suggests that sufficiently large PEGMA block lengths in the D-P-E arrangement may improve the pH-dependent membrane destabilization activity of these polymers.

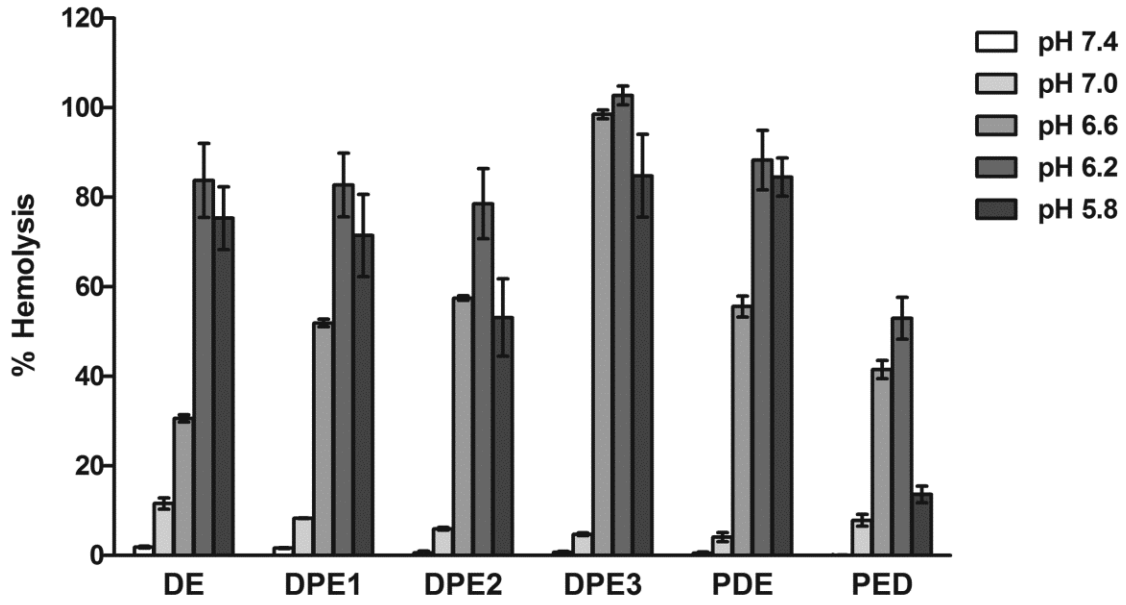

Figure 2.3. Hemolytic activity of polymers at 20 μg/mL mass concentration of the DEAEMA-*co*-BMA block. Activities are normalized relative to a Triton X-100 positive control and DPBS negative control and are from a single representative experiment conducted in triplicate ± standard deviation.

4. Discussion

Here, the synthesis of a series of multifunctional triblock copolymers composed of (1) a DMAEMA block for cationic mRNA condensation, (2) a hydrophilic PEGMA block to provide polyplex stabilization, and (3) a DEAEMA-*co*-BMA block to enable pH-triggered endosomal escape is described. Several aspects of this polymer series represent novel approaches to delivery vector development. First, although multifunctional ABC-type triblock copolymer systems have been previously investigated for pDNA and siRNA transfection, this is the first report of a triblock copolymer developed specifically as an mRNA delivery vector. Second,

although DMAEMA, PEGMA, and DEAEMA-*co*-BMA have all been previously used in the context of intracellular delivery, this particular combination of polymers in a single block copolymer structure has not been previously reported. Third, this is the first study utilizing an ABC-type triblock system that systematically examined all three possible unique block arrangements to determine the optimal architecture for efficient delivery. While some reports on the effect of polymer architecture on polyplex properties and transfection activity are available [116,118,119], block order has typically been overlooked as a potential experimental parameter. In this study, the use of RAFT polymerization techniques enabled the facile synthesis of monodisperse polymers with different block arrangements and sizes.

DLS analysis revealed that all polymers self-assembled into micelle structures in aqueous solution. Manganiello *et al.* previously observed in a similar polymer system that the hydrophobic DEAEMA-*co*-BMA segment is sequestered in the micelle core at physiological pH values, but becomes solvated at endosomal pH values provided that the block composition is ≤ 70% BMA [72]. Furthermore, this micelle to unimer structural transition correlates closely to membrane-disruptive activity. Consistent with this report, the monomer compositions of the DEAEMA-*co*-BMA block for the polymer series ranged from 31-36% BMA, and all polymers demonstrated sharp pH-triggered transitions from inert to hemolytic states. Interestingly, the PED polymer displayed lower levels of peak hemolytic activity compared to DPE1 and PDE, which had equivalent block sizes but differing block configurations. Hypothetically, sequestering the endosomolytic DEAEMA-*co*-BMA in the center of the polymer chain between two relatively hydrophilic blocks may have resulted in steric effects that reduced its ability to

interact with cellular membranes. Additional influences of polymer architecture on delivery performance are further discussed in Chapter 3.

5. Conclusions

A series of multifunctional block copolymers composed of discrete DMAEMA, PEGMA, and DEAEMA-*co*-BMA segments were synthesized by RAFT polymerization. The polymer series encompassed rational iterations on polymer block order and PEGMA block size. All polymers had low polydispersities (PDI $\leq$ 1.14), and molecular weights and compositions close to the targeted values. Polymers were observed to form micelles in aqueous solution and exhibited pH-dependent hemolytic activity indicative of their endosomal escape capabilities. Overall, the synthesized polymers have favorable characteristics for intracellular gene delivery and are a promising platform for investigating the effects of distinct polymer architectures on transfection performance.

Chapter 3

In vitro evaluation of the biological activity of mRNA polyplexes

Abstract

This chapter describes the characterization of mRNA polyplexes formulated with multifunctional block copolymers, and the evaluation of their *in vitro* biological activity. mRNA polyplex properties were analyzed using DLS, zeta potential measurements, and a heparin competitive displacement assay. Polyplex uptake, transfection efficiency, cytotoxicity, and antigen-specific T cell activation were assessed in murine macrophage and dendritic cell lines. mRNA polyplexes formed with polymers that placed the PEGMA block in the center of the polymer chain displayed the greatest stability to heparin displacement, which correlated to high levels of mRNA transfection exceeding that of a commercial liposomal reagent. Polyplex-transfected dendritic cells were shown to be capable of subsequently activating antigen-specific T cells.

1. Introduction

Currently, the most significant barrier to widespread use of nucleic acid-based vaccination is achieving efficient gene delivery to DCs. Reported pDNA transfection levels in DCs using nonviral delivery techniques such as lipofection and electroporation are typically extremely low, with most groups reporting *in vitro* efficiencies ranging from 1-20% [120–123]. In contrast, markedly higher *in vitro* transfection efficiencies in DCs and other APCs have been obtained using mRNA (up to 90%) [28,122–124]. This may be due in part to the nuclear entry barrier for pDNA transfection, which is a non-issue for mRNA-based gene therapies.

Despite the enormous potential of mRNA as an immunotherapeutic agent, research efforts concerning mRNA delivery vehicles have lagged in comparison to pDNA and siRNA, particularly with respect to synthetic polymer carrier development [22,23]. This issue is further complicated by the distinct physiochemical properties of mRNA compared to other nucleic acids. Many groups have observed that mRNA appears to bind more tightly to polycations relative to pDNA and siRNA [88,91,92,94]. This may be a contributing factor to the results obtained in several studies indicating that commonly used cationic gene carriers such as PEI, PLL, and pDMAEMA are unable to mediate high levels of mRNA transfection *in vitro* [87–91]. Preliminary experiments utilizing a diblock copolymer system designed for pDNA delivery [72] also produced disappointingly low mRNA transfection efficiencies (unpublished data).

Taken together, these findings indicate that the polymer design requirements associated with efficient mRNA delivery may differ significantly from the requirements for other nucleic acids. Elucidating the nature of these requirements would facilitate the successful development of mRNA delivery vectors. Here, a series of multifunctional block copolymers with systematic iterations in polymer block order and PEGMA size (previously described in Chapter 2) is used to evaluate the effect of different polymer architectures on *in vitro* mRNA transfection performance. The potential of this system as a platform for mRNA vaccination strategies was evaluated by determining whether polymer-mediated mRNA transfection of DCs can result in the successful presentation the expressed antigen to elicit a T cell response.

2. Experimental methods

2.1. Plasmids and in vitro transcription of mRNA

Plasmid DNA was prepared using the EndoFree Plasmid Mega Kit (Qiagen). Plasmid pGEM4Z-GFP-A64 (a gift from E. Gilboa, University of Miami) encoding eGFP with a synthetic poly-A tail has been previously described [125]. The GFP coding fragment was excised with XbaI and NotI to produce pGEM4Z-A64. The ovalbumin cDNA EcoRI fragment from plasmid pAc-neo-OVA [126] (a gift from M.J. Bevan, University of Washington) was subcloned into the pVAX1 vector (Invitrogen) and amplified by PCR. The PCR primers used added XbaI and NotI sites to the 5' and 3' ends of the cDNA: 5'-GCTCTAGAATGGGCTCCATCGGTGCAGC-3' (forward) and 5'-GCGCGGCCGCTTAAGGGGAAACACATCTGCC-3' (reverse). The product was ligated into pGEM4Z-A64 to produce pGEM4Z-OVA-A64. pGEM4Z-GFP-A64 and pGEM4Z-OVA-A64 were linearized by SpeI and used as templates for *in vitro* transcription using a mMESSAGE mMACHINE T7 Kit (Ambion). The resultant mRNA was purified using a RNeasy MinElute Cleanup Kit (Qiagen).

2.2. Formulation of mRNA-polymer polyplexes and lipoplexes

Polymers were prepared following previously described procedures (Chapter 2). Polyplexes were formed by combining equal volumes of mRNA (0.1 μg/μL in nuclease-free water) and polymer stock solutions for 30 min at room temperature. The theoretical charge ratios (+/-) of the polyplexes were calculated using the mass concentration of the cationic DMAEMA block, assumed to be 50% protonated at pH 7.4. All polyplexes in this study were formed at a theoretical charge ratio of 4:1 unless otherwise specified. Lipoplexes were formed by combining

mRNA and Lipofectamine 2000 (Invitrogen) at a 3:1 v/w Lipofectamine:mRNA ratio in serum and antibiotic-free media in accordance with the manufacturer's protocol.

2.3. Agarose gel electrophoresis

For gel retardation assays, polyplexes were formulated with 0.5 μg mRNA at theoretical charge ratios of 1:1, 2:1, and 4:1 for 30 min at room temperature as described above. Samples were then loaded into a 1.2% w/v agarose gel stained with 1X SYBR Safe (Invitrogen) and run at 100 V for 30 min. For heparin competitive displacement assays, solutions of heparin sodium salt (Sigma) in water were combined with equal volumes of polyplexes formulated at charge ratio 4:1 containing 0.5 μg mRNA and incubated at room temperature for 15 min, followed by gel electrophoresis. For serum protection assays, fetal bovine serum (FBS) was added to polyplexes at a final FBS concentration of 10% and incubated at room temperature for 30 min, followed by gel electrophoresis.

2.4. Characterization of polyplex size and zeta potential

DLS and zeta potential measurements were conducted on a ZetaSizer Nano ZS (Malvern) at a constant scattering angle of 173° at 25 °C. Polyplexes were diluted to 5 μg/mL mRNA in DPBS or water for size and zeta potential measurements, respectively.

2.5. Cell culture

All cell culture media and reagents were obtained from Gibco unless otherwise specified. The RAW 264.7 murine macrophage cell line (ATCC) was maintained in Dulbecco's Modified Eagle

Medium High Glucose containing L-glutamine supplemented with 10% FBS and 1% penicillin-streptomycin. The DC2.4 murine dendritic cell line (a gift from K.L. Rock, University of Massachusetts Medical School) was maintained in RPMI 1640 containing L-glutamine supplemented with 10 mM HEPES, 0.1 mM non-essential amino acids, 55 μM 2-mercaptoethanol, 10% FBS, and 1% penicillin-streptomycin. The B3Z T cell hybridoma (a gift from N. Shastri, University of California, Berkeley) was maintained in RPMI 1640 containing L-glutamine supplemented with 1 mM sodium pyruvate, 55 μM 2-mercaptoethanol, 10% FBS, and 1% penicillin-streptomycin. All cells were cultured at 37 °C and 5% CO_2.

2.6. Polyplex internalization studies

mRNA was labeled with Cy3 using a *Label*IT Tracker Intracellular Nucleic Acid Localization Kit (MirusBio) at a 0.5:1 v/w ratio of *Label*IT Tracker Reagent to mRNA in accordance with the manufacturer's protocol. RAW 264.7 cells were seeded in 24-well plates at 250,000 cells/well in 1 mL complete media and allowed to adhere overnight. Cells were washed with DPBS and the culture medium replaced with polyplexes formulated with Cy3-mRNA in 200 μL serum- and antibiotic-free media. After 2 h, cells were washed and collected by PBS-based cell dissociation buffer (Invitrogen), and resuspended in DPBs containing 2% FBS and 0.01% Trypan blue to quench extracellular fluorescence. 10,000 events, gated by forward and side scatter to exclude cellular debris, were collected per sample and analyzed using FlowJo software (TreeStar) for Cy3 fluorescence.

2.7. In vitro transfection studies

RAW 264.7 or DC2.4 cells were seeded in 24-well plates at 250,000 or 200,000 cells/well, respectively, in 1 mL complete media and allowed to adhere overnight. Cells were washed with DPBS and the culture medium replaced with polyplexes or lipoplexes at 0.25 μg mRNA/well in 200 μL serum- and antibiotic-free media. After 4 h, cells were washed and collected by PBS-based cell dissociation buffer (Invitrogen) or 0.25% trypsin-EDTA, respectively, and resuspended in DPBS containing 2% FBS and 0.2 μg/mL propidium iodide (Invitrogen). To determine GFP expression levels, 10,000 events per sample gated on viable propidium iodide negative cells were acquired on a BD FACScan flow cytometer (BD Biosciences) and analyzed using FlowJo software (TreeStar).

2.8. Transfection studies in the presence of serum

mRNA transfections in RAW 264.7 cells in the presence of serum were carried out as described above, except with the addition of 1% FBS in the transfection medium. pDNA polyplexes were formulated using the same methodologies for mRNA polyplexes using gWiz-GFP (Aldevron). Cell seeding protocols were the same as for mRNA transfection. Cells were then washed with DPBS and the culture medium replaced with polyplexes at 0.25 μg mRNA/well in 200 μL antibiotic-free media containing 10% FBS. After 4 h, the medium was replaced with 500 μL complete medium. After an additional 20 h, cells were collected and analyzed for flow cytometry as described above.

2.9. Fluorescence microscopy

RAW 264.7 cells were seeded at 150,000 cells/well in 400 μL complete media in a Lab-Tek 8-well chambered coverglass (Nunc) and allowed to adhere overnight. The culture medium was replaced with polyplexes or lipoplexes at 150 ng mRNA/well in 150 μL serum- and antibiotic-free media. After 4 h, the medium was replaced with phenol red-free media containing 5 μg/mL Hoechst 33342 (Invitrogen). Cells were imaged on a Zeiss Axio Observer Z1 fluorescence microscope with an ApoTome optical sectioning attachment using a 40x objective.

2.10. Cytotoxicity assay

RAW 264.7 cells were seeded in black 96-well plates at 50,000 cells/well in 200 μL complete media and allowed to adhere overnight. The culture medium was replaced with polyplexes at 50 ng mRNA/well in 40 μL serum- and antibiotic-free media. After 4 h, 60 μL complete media was added to each plate and the cells incubated for an additional 20 h. To determine cell viability based on metabolic activity, alamarBlue reagent (Invitrogen) was added directly to the culture medium at a 1:10 dilution, incubated for 2 h at 37 °C, and fluorescence measurements recorded at 585 nm.

2.11. B3Z T cell activation assay

DC2.4 cells were seeded in U-bottomed 96-well plates at 50,000 cells/well in 100 μL complete media and allowed to adhere overnight. Polyplexes or lipoplexes were added at 50 ng mRNA/well in 100 μL serum- and antibiotic-free media. Control cells were treated with 0.1 μM SIINFEKL peptide (ovalbumin a.a. 257-264, GenScript). After 4 h, cells were washed and co-

cultured with 100,000 B3Z cells/well in 200 μL complete media for 24 h. The media was replaced with 150 μL/well lysis buffer containing 0.1 mM 2-mercaptoethanol, 9 mM $MgCl_2$, 0.1% Triton X-100, and 0.15 mM chlorophenol red β-D-galactyopyranoside in DPBS. After 2 h incubation at 37 °C, absorbance measurements were recorded at 570 nm.

2.12. Statistical methods

ANOVA was used to test for treatment effects and Tukey's test was used for post hoc pairwise comparisons between individual treatment groups.

3. Results

3.1. mRNA polyplex size and zeta potential

All polymers completely condensed mRNA at theoretical charge ratios of 1:1 and higher, as confirmed by an agarose gel retardation assay (**Figure 3.1**). Polyplexes formulated with mRNA were characterized by DLS and zeta potential measurements (**Table 3.1**). When combined with mRNA at a theoretical +/- charge ratio of 4:1, the resultant polyplexes were approximately 86-216 nm in diameter. DPE1 and PDE polyplexes were comparably sized, while PED polyplexes were significantly smaller, suggesting that the P-E-D block architecture is more favorable for compact particle formation. However, comparing mRNA polyplexes formulated from DE, DPE1, DPE2, and DPE3, increasing PEGMA block size was observed to correlate with decreasing particle size, demonstrating that improved mRNA condensation can also be achieved by lengthening the hydrophilic segment in the D-P-E configuration.

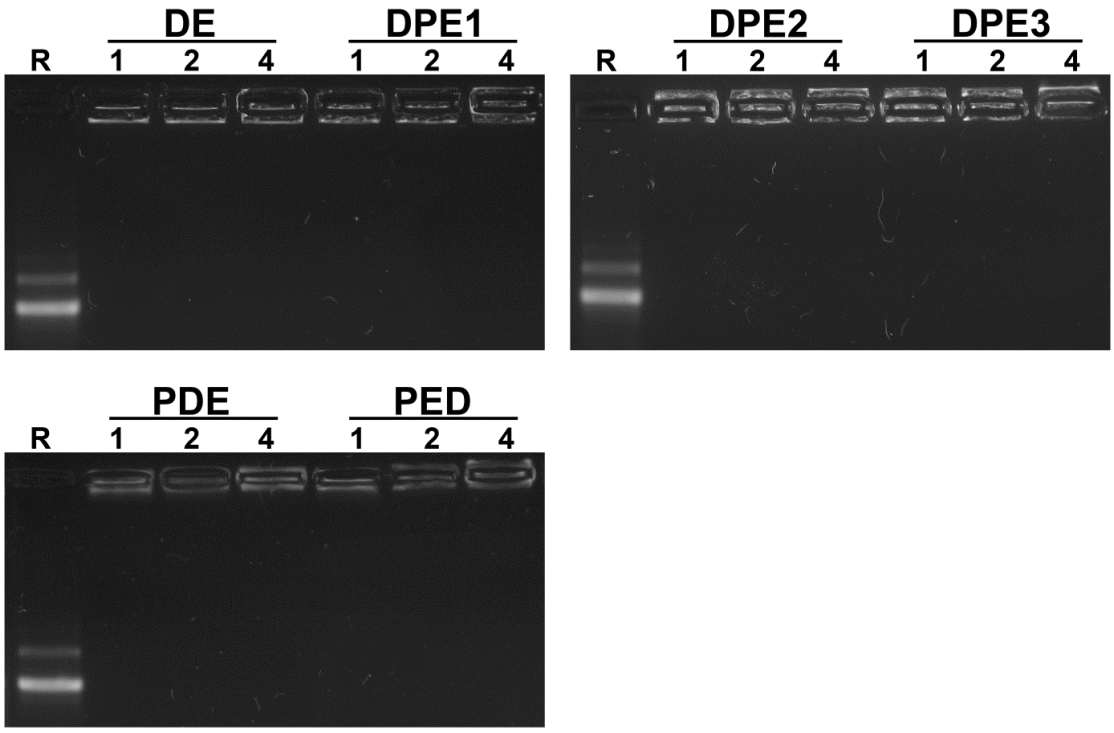

Figure 3.1. Agarose gel retardation assay with mRNA polyplexes. Polyplexes were formulated with mRNA at the indicated theoretical charge ratios (+/-) of 1:1, 2:1, or 4:1 for 30 min prior to agarose gel electrophoresis. R indicates uncomplexed mRNA.

Table 3.1. Particle size and zeta potential measurements of mRNA polyplexes.

Polymer	mRNA polyplex diameter (nm)	mRNA polyplex zeta potential (mV)
DE	201 ± 38	21.0 ± 0.5
DPE1	208 ± 51	20.3 ± 0.7
DPE2	91 ± 18	16.3 ± 1.0
DPE3	86 ± 16	12.4 ± 0.7
PDE	216 ± 66	3.6 ± 0.7
PED	106 ± 30	3.4 ± 0.4

Diameters are calculated from the intensity size distribution ± standard deviation calculated from the polydispersity index (PDI). Zeta potential values are from three experimental runs ± standard deviation.

Comparing PDE, PED and DPE1 to determine the effect of block arrangement on polyplex zeta potential, polyplexes formed with PDE and PED were effectively neutral while DPE1 was still slightly cationic, suggesting that having PEGMA as the middle block of the polymer chain reduces its charge-shielding capability. Comparing DE, DPE1, DPE2, and DPE3 polyplexes, increasing PEGMA size correlated with decreasing zeta potential, demonstrating that improved hydrophilic shielding is achieved with longer PEGMA chains, although complete charge neutralization was not achieved even with the largest PEGMA block (DPE3).

3.2. Polyplex stability

To assess the stability of the mRNA-polymer interaction, a competitive displacement assay was performed in which polyplexes were incubated with increasing concentrations of the polyanion heparin (**Figure 3.2**). Since mRNA in a polyplex does not migrate in an agarose gel, the reappearance of a free mRNA band indicates that the mRNA is no longer complexed. Polyplexes formed with PDE and PED were the least stable, with mRNA displacement beginning to be evident at heparin concentrations of 100 and 150 μg/mL, respectively. In comparison, 250 μg/mL heparin was required to release mRNA from DPE1 polyplexes. Comparing polymer series DE, DPE1, DPE2, and DPE3, polyplexes with longer PEGMA blocks were increasingly resistant to destabilization. Polyplexes formed with DPE3, which had the largest PEGMA block, still retained some mRNA at the highest heparin concentration tested. In summary, the data indicate that the D-P-E configuration provides the greatest polyplex stability, and that this stability is enhanced by increasing the length of the central PEGMA chain.

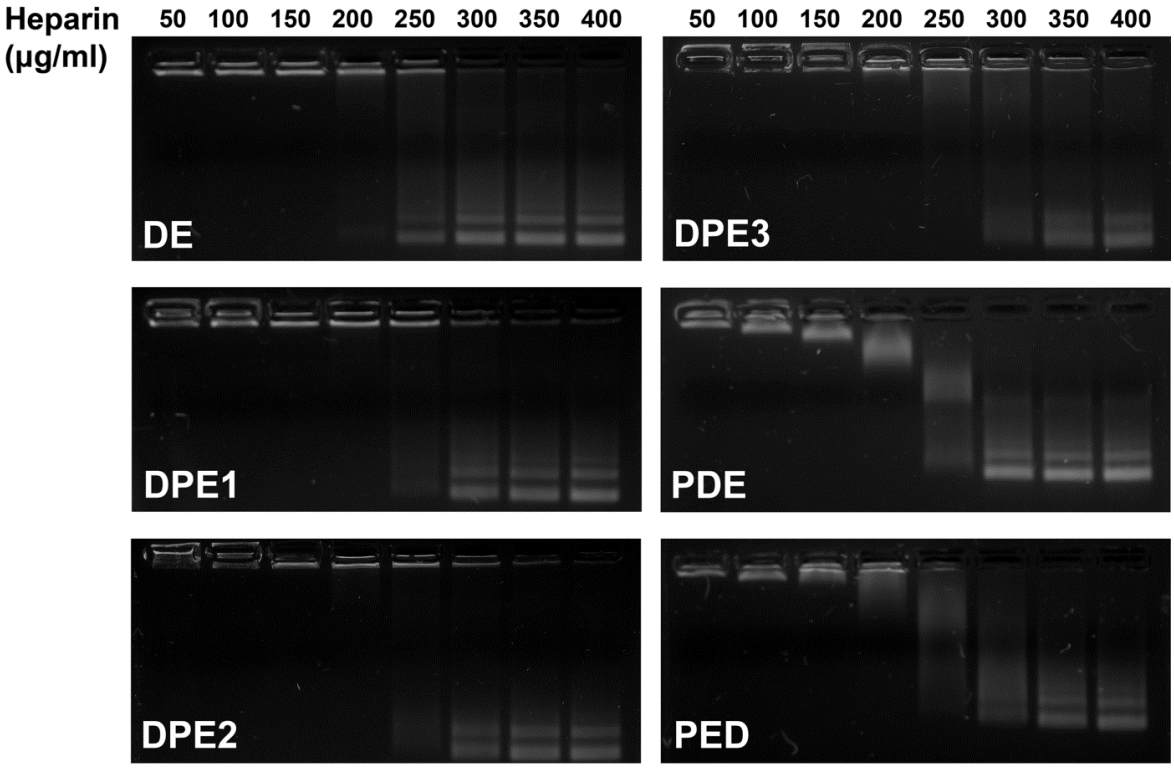

Figure 3.2. mRNA polyplex stability against heparin displacement. Polyplexes were incubated with equal volumes of heparin solutions at the indicated concentrations prior to agarose gel electrophoresis.

3.3. Internalization of Cy3-labeled polyplexes

The *in vitro* internalization of polyplexes was quantified using the RAW 264.7 murine macrophage cell line. Polyplexes formulated with Cy3-labeled mRNA were incubated with cells for 2 h prior to flow cytometric analysis for Cy3 fluorescence indicating polyplex uptake. Extracellular fluorescence originating from membrane-bound polyplexes was quenched using Trypan blue. All mRNA polyplexes exhibited significant uptake by macrophages (**Figure 3.3**). Although the mean cell-associated fluorescence values differed slightly between certain polymer carriers, the overall uptake profiles were very similar, suggesting that polymer architecture did not play a major role in influencing the extent of polyplex internalization. Uptake of naked mRNA was also observed (data not shown), which is consistent with previous reports [127].

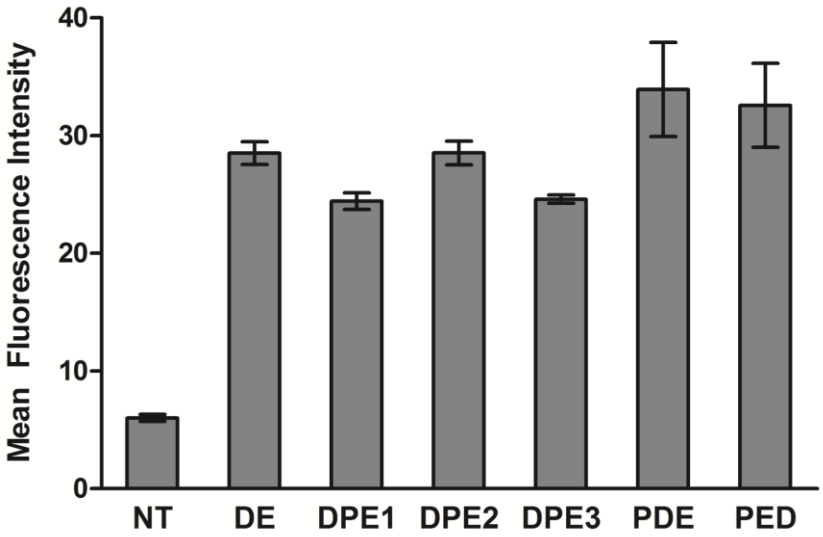

Figure 3.3. mRNA polyplex uptake by RAW 264.7 macrophages. NT indicates untreated cells. Data are from a single experiment conducted in triplicate ± standard deviation. All treatments are significantly different from NT, and PDE and PED are significantly different from DPE1 and DPE3 ($p < 0.05$).

3.4. Evaluation of in vitro mRNA transfection activity

The ability of the polymers to mediate mRNA transfection *in vitro* was evaluated in two murine immune cell lines, RAW 264.7 macrophages (**Figure 3.4.A, C**) and DC2.4 dendritic cells (**Figure 3.4.B**). Cells were incubated with mRNA polyplexes for 4 h prior to analysis for GFP expression by flow cytometry. Lipofectamine 2000 (LF), a commercially available liposomal reagent, was used as a positive control. In both cell lines, PDE and PED polyplexes failed to produce significant mRNA transfection (< 2% GFP+ cells). Polyplexes formed with DE, the diblock copolymer lacking a PEGMA block, generated 8% GFP+ cells, much lower than the efficiency obtained with LF (30%). In contrast, DPE1, DPE2, and DPE3 polyplexes were extremely efficient at transfecting mRNA, with GFP expression levels much higher than LF. In RAW 264.7 cells, the transfection efficiency increased dramatically with increasing PEGMA

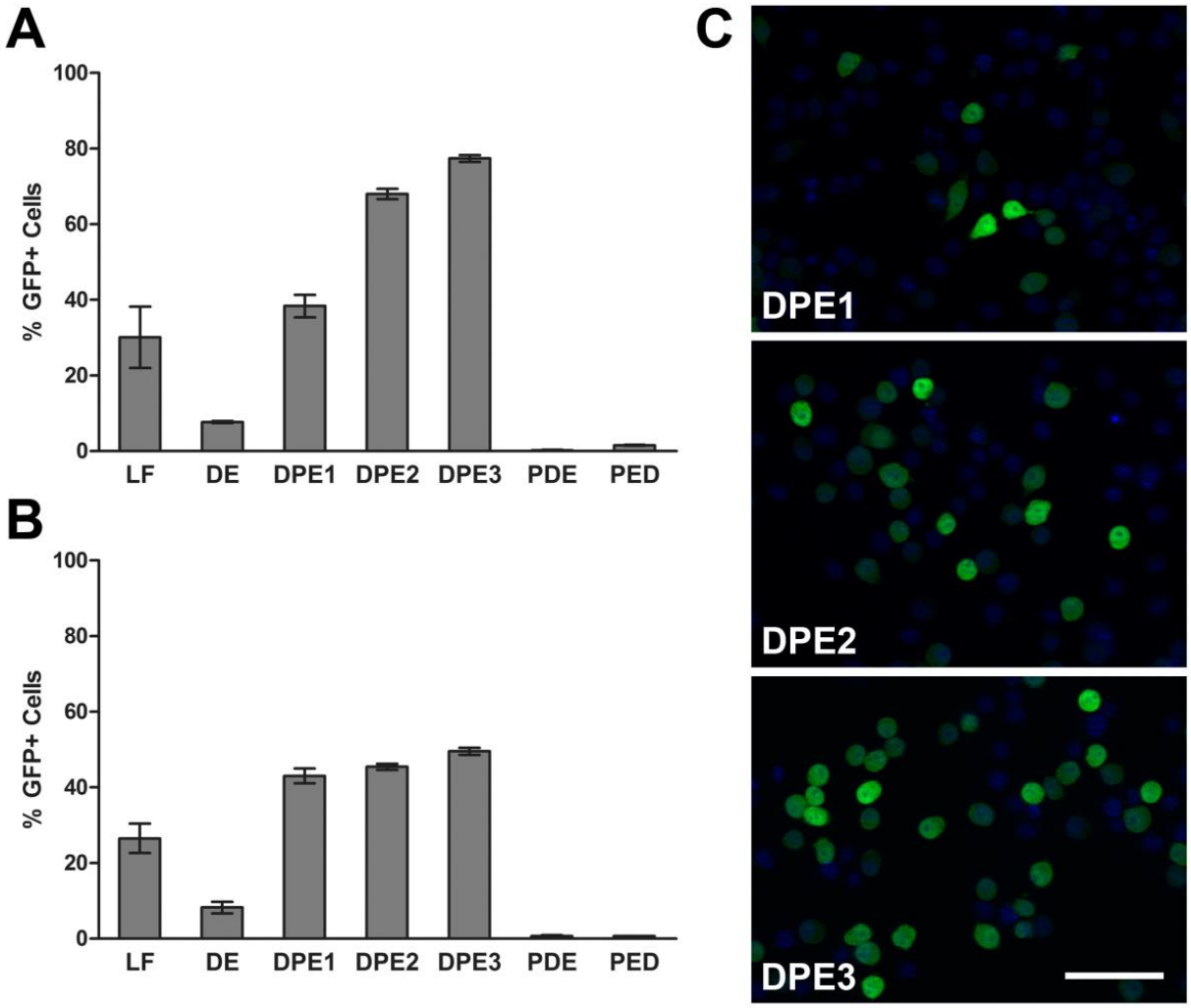

Figure 3.4. *In vitro* transfection efficiencies in (**A**) RAW 264.7 macrophages and (**B**) DC2.4 dendritic cells. Lipofectamine 2000 (LF) was used as a positive control. Data are from a single representative experiment conducted in triplicate ± standard deviation. In (A), DPE2 and DPE3 are significantly different than all other treatments and each other ($p < 0.05$). In (B), DPE1, DPE2, and DPE3 are significantly different than all other treatments, and DPE3 is significantly different than DPE1 ($p < 0.05$). (**C**) Apotome fluorescence microscopy of GFP expression in transfected RAW 264.7 macrophages (blue, Hoechst nuclear stain). Scale bar is 50 μm.

block size: 38% (DPE1) vs. 68% (DPE2) vs. 77% (DPE3). This trend was also observed in DC2.4 cells, but was less pronounced: 43% (DPE1) vs. 45% (DPE2) vs. 50% (DPE3). Overall, these findings demonstrate the importance of polymer architecture in successful mRNA transfection: polymers with the D-P-E arrangement were the most effective for intracellular

mRNA delivery and were capable of mediating transfection levels superior even to LF, while polymers with alternative block arrangements produced very low gene expression.

3.5. Effect of serum on transfection activity

To determine whether mRNA polyplexes were capable of mediating transfection in the presence of serum, a serum protection assay was performed in which polyplexes were incubated with 10% FBS (**Figure 3.5)**. Unprotected mRNA was rapidly degraded, as indicated by the disappearance of the free mRNA band, while no evidence of mRNA decomplexation was observed with any of the polymers.

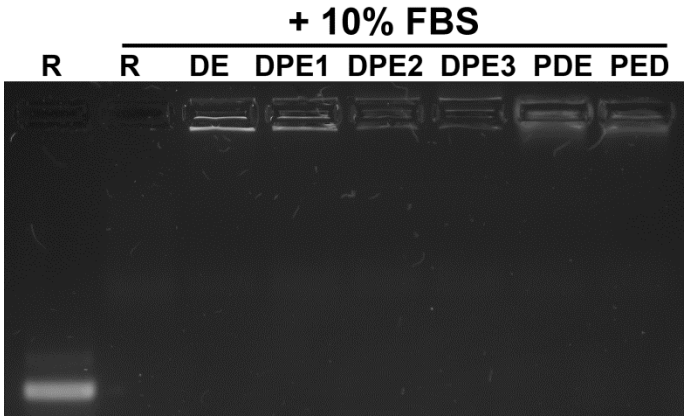

Figure 3.5. Serum protection assay. Polyplexes were incubated with 10% FBS prior to agarose gel electrophoresis. R indicates naked mRNA. The faint high molecular weight band observed in all lanes containing serum is due to non-specific staining of serum components.

Subsequently, an *in vitro* mRNA transfection assay was performed using RAW 264.7 macrophages in the presence or absence of FBS. Surprisingly, as little as 1% FBS in the transfection medium was sufficient to almost completely abolish polyplex transfection activity (2-, 5-, 16-, and 38-fold decreases for DE, DPE1, DPE2, and DPE3 polyplexes, respectively) (**Figure 3.6.A)**. In contrast, pDNA transfection with D-P-E series polyplexes elicited high levels of gene expression even in the presence of 10% FBS (33%, 39% and 49% GFP+ cells with

DPE1, DPE2, and DPE3 polyplexes, respectively) (**Figure 3.6.B**). These findings suggest that mRNA transfection is uniquely inhibited by serum, and that this inhibition does not appear to be caused by the serum protein-mediated unpackaging of polyplexes.

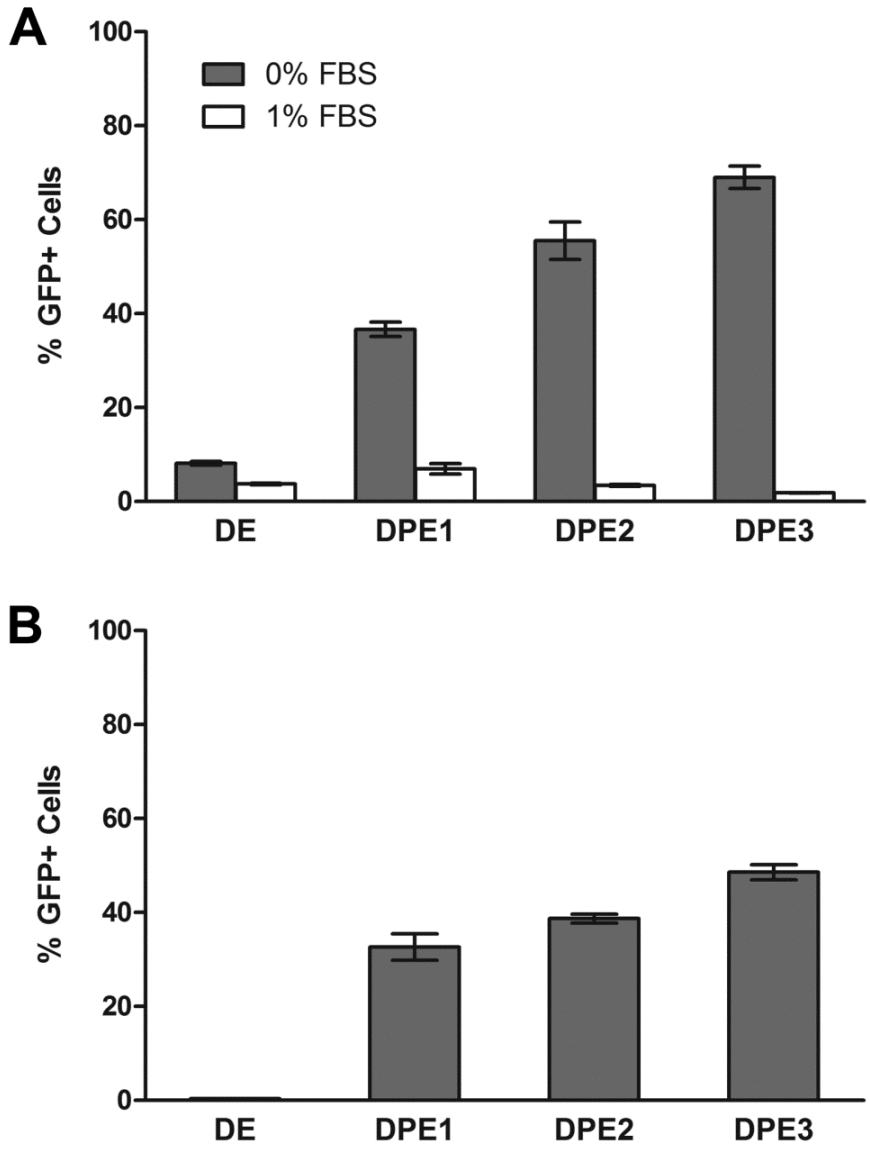

Figure 3.6. *In vitro* transfection efficiencies in RAW 264.7 macrophages in the presence of serum. (**A**) mRNA transfection with 0% or 1% FBS in the transfection medium. (**B**) pDNA transfection with 10% FBS in the transfection medium. Data are from a single experiment conducted in triplicate ± standard deviation

3.6. Polyplex cytotoxicity

The cytotoxicity of the mRNA polyplexes was evaluated by alamarBlue assay in RAW 264.7 macrophages (**Figure 3.7**). Cells were incubated with polyplexes for 24 h, after which cell viability was quantified based on total metabolic activity resulting in reduction of the alamarBlue reagent. All polyplexes exhibited low cytotoxicity (≥ 75% viability), with cytotoxicity generally correlating with increasing transfection activity.

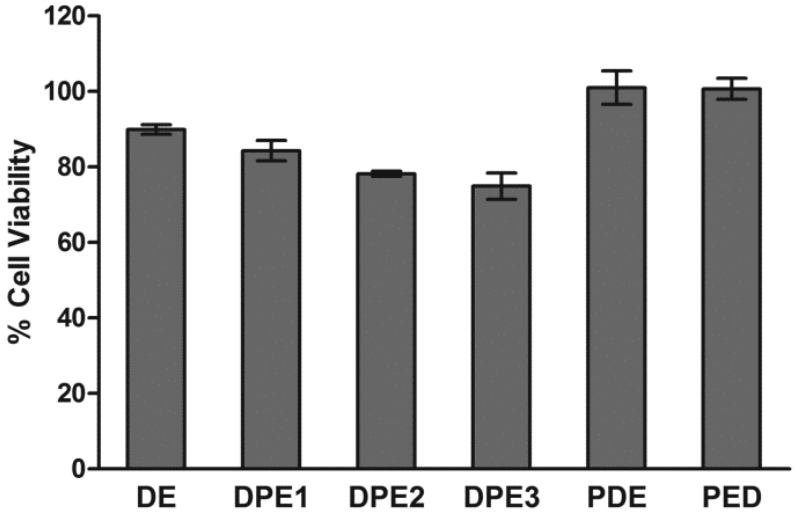

Figure 3.7. *In vitro* cytotoxicity of polyplexes in RAW 264.7 macrophages. Viabilities are normalized relative to untreated cells. Data are from a single representative experiment conducted in triplicate ± standard deviation.

3.7. Antigen presentation assay

To determine whether dendritic cells transfected with mRNA polyplexes could successfully process and present the encoded antigen on MHC molecules, an *in vitro* MHC I antigen presentation assay was performed using the B3Z CD8+ T cell hybridoma (**Figure 3.8**). The B3Z cell line produces β-galactosidase upon recognition of the ovalbumin CD8 epitope (SIINFEKL) presented in the context of MHC I H-2K^b [128]. DC 2.4 cells were transfected with polyplexes

containing ovalbumin mRNA for 4 h, cocultured with B3Z cells for 24 h, and evaluated for antigen presentation by quantifying the overall T cell response via β-galactosidase activity.

All polymers except for PDE and PED generated high levels of T cell activity, outperforming LF. DPE1 in particular produced the highest T cell response, despite having a slightly lower mRNA transfection efficiency than DPE2 and DPE3. Similarly, DE produced less gene expression than LF in the transfection assay, but mediated higher levels of T cell activity. In summary, these findings demonstrate that mRNA transfection mediated by these polymer systems can lead to antigen presentation and subsequent T cell activation, although the level of activation does not necessarily correlate precisely to the efficiency of transfection.

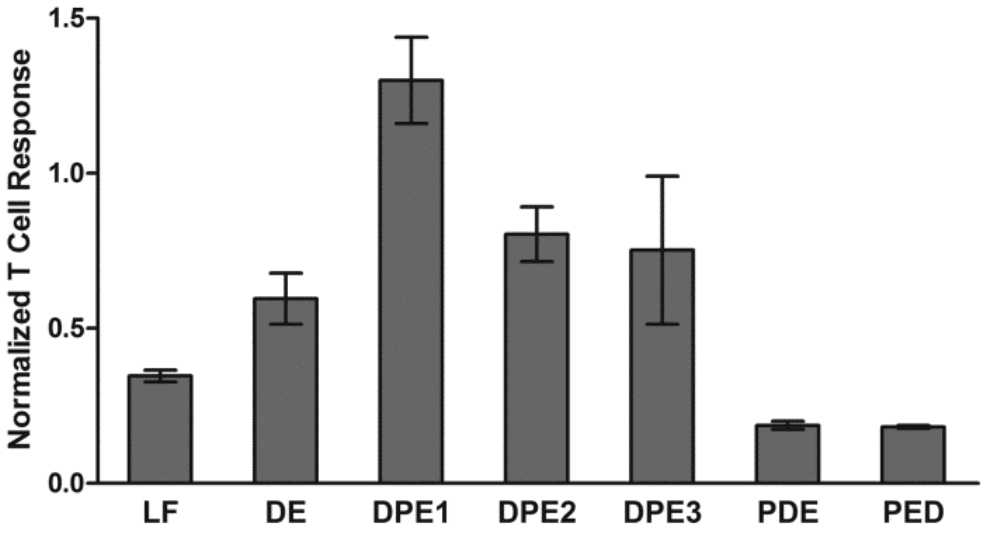

Figure 3.8. B3Z T cell activation by transfected DC2.4 dendritic cells. Responses are normalized relative to cells treated with 0.1 μM SIINFEKL peptide as a positive control and are from a single representative experiment conducted in triplicate ± standard deviation. DPE1, DPE2, and DPE3 are significantly different than LF, and DPE1 is significantly different than all other treatments ($p < 0.05$).

4. Discussion

Typically, triblock copolymer architectures incorporating a hydrophilic segment place this block at the chain end. Accordingly, two of the polymers in this study, PDE and PED, were synthesized with PEGMA segments at one end and either DMAEMA or DEAEMA-*co*-BMA segments at the other. A third polymer, DPE1, was synthesized with the same block lengths as PDE and PED, but placed the PEGMA segment in the middle of the polymer chain instead. Intriguingly, of these three polymers, only DPE1 was capable of mediating mRNA transfection and antigen presentation *in vitro*. To further explore this phenomenon, the effect of PEGMA block size was investigated by synthesizing a series of triblock copolymers in the D-P-E configuration with increasing PEGMA length (DPE1, DPE2, DPE3), as well as a diblock copolymer lacking PEGMA (DE). Transfection studies demonstrated that delivery efficacy improved significantly with increasing PEGMA block size, though the magnitude of the difference was dependent on cell type. The most efficient polymers were able to surpass a commercial liposomal reagent, Lipofectamine 2000, in mRNA transfection activity.

Heparin displacement studies suggested that the differences in mRNA transfection were potentially linked to polyplex stability: the most stable polyplexes were also those that exhibited the highest transfection efficiencies. Destabilization of polyplexes by anionic compounds such as serum proteins, extracellular matrix components, and cell surface glycosaminoglycans constitutes a significant barrier to intracellular gene delivery [64,77,129,130]. While PEGylation improves polyplex stability by creating a hydration shell that masks excess cationic charges [26,64,77], hydrophilic polymers may also interfere with nucleic acid condensation [131,132]. Of the six polymer systems investigated in this report, polyplexes formulated with PDE and PED

were also the least stable to heparin displacement, despite having near-neutral zeta potentials indicative of complete hydrophilic shielding. In contrast, polymers in the D-E and D-P-E arrangements exhibited improved stability, with longer PEGMA block lengths conferring stronger mRNA binding and reduced cationic surface charge. The D-P-E polymer architecture in particular appeared to achieve an optimal balance between charge shielding and polyplex stability that translated into highly efficient mRNA transfection.

While Üzgün *et al.* also concluded that improved mRNA binding led to improved transfection [91], other groups have demonstrated that highly stable mRNA-polymer interactions can be detrimental to transfection, presumably due to the inability of these vehicles to release mRNA in the cytosol [87,88,94]. These findings are not necessarily inconsistent, given the structural and compositional differences between the polymer systems used in these various studies. Taken together, it is clear that polyplex stability is an important factor that needs to be carefully modulated in order to achieve optimal mRNA delivery.

To determine whether efficient mRNA transfection translated to successful antigen presentation and subsequent T cell activation, DC2.4 cells transfected with mRNA polyplexes were cocultured with ovalbumin-specific CD8+ T cells. All polymers except for PDE and PED generated T cell responses that surpassed those attained by Lipofectamine 2000. Surprisingly, polymers DE and DPE1 produced greater T cell activation than might be expected from their relative transfection efficiencies. Although the underlying reason for these discrepancies remains to be elucidated, potential explanations include differences in transfection activity when

using ovalbumin mRNA versus GFP mRNA, or changes in antigen processing pathways triggered by cell-polymer interactions.

5. Conclusions

A series of multifunctional block copolymers composed of DMAEMA, PEGMA, and DEAEMA-*co*-BMA were evaluated for their ability to facilitate intracellular mRNA delivery. Polymers exhibited favorable size, charge, internalization profiles, and biocompatibility when complexed with mRNA. The D-P-E architecture with the PEGMA block in the center of the polymer chain demonstrated enhanced polyplex stability against heparin displacement relative to other configurations, with longer PEGMA block lengths enhancing mRNA binding. This system achieved superior mRNA transfection efficiencies in two immune cell lines compared to a commercial liposomal reagent, Lipofectamine 2000. Transfected dendritic cells were shown to be capable of subsequently activating antigen-specific T cells, demonstrating the potential of these multifunctional block copolymers for mRNA-based vaccination strategies.

Chapter 4

Evaluation of mRNA polyplexes for *in vivo* gene delivery

Abstract

This chapter describes studies performed in mouse models to evaluate the efficacy of mRNA polyplexes for *in vivo* delivery. A luciferase mRNA reporter vector was constructed and used in conjunction with live animal imaging to determine the extent of polyplex-mediated gene expression following subcutaneous administration. *In vivo* polyplex tissue distribution and trafficking to draining lymph node DCs were characterized using fluorescently-labeled mRNA. Contrary to *in vitro* observations, naked mRNA produced superior *in vivo* transfection compared to mRNA polyplexes. While local tissue distribution studies suggested that delivery mode and vehicle characteristics affected mRNA trafficking *in vivo*, neither naked mRNA nor mRNA polyplexes were observed in DCs in the draining lymph nodes.

1. Introduction

One of the primary issues confounding the development of synthetic gene delivery vehicles is the poor correlation of *in vitro* transfection results with *in vivo* efficacy. This discrepancy may be related to the cationic nature of many lipids and polymers used in *in vitro* gene delivery. A recent study by van den Berg *et al*. compared the expression of naked pDNA, pDNA lipoplexes, and pDNA polyplexes, the latter two bearing cationic surface charges [133]. In an *in vitro* assay, polyplexes and lipoplexes exhibited 26-fold and 900-fold increases in gene expression compared to naked pDNA, respectively. However, when administered by intradermal tattooing to *ex vivo*

human skin and *in vivo* murine skin, lipoplexes and polyplexes yielded extremely low levels of gene expression, in contrast to the robust expression obtained with naked pDNA. In accordance with these results, intradermal vaccination with lipoplexes and polyplexes also failed to elicit detectable levels of antigen-specific immune responses. PEGylation of lipoplexes and polyplexes restored *in vivo* transfection activity and enabled the induction of antigen-specific T cell responses, despite lower transfection efficiencies *in vitro* compared to unPEGylated carriers. Similar results were obtained by Üzgün *et al.* using pDNA polyplexes formulated with PEI or a copolymer of DMAEMA and oligo(ethylene glycol) methyl ether methacryate (p(DMAEMA-*co*-OEGMA)) [134]. While PEI outperformed p(DMAEMA-*co*-OEGMA) by more than 10-fold *in vitro*, intratracheal administration of p(DMAEMA-*co*-OEGMA) polyplexes resulted in a 7-fold increase in gene expression compared to PEI polyplexes.

Taken together, these findings suggest that shielding of cationic surface charges is crucial for efficient *in vivo* gene delivery. The cationic nature of many synthetic delivery vehicles has been associated with toxicity, aggregation, and polyplex instability *in vivo* [63], and may contribute to poor *in vivo* transfection performance. Previous studies have demonstrated that negatively charged biomacromolecules such as serum proteins, extracellular matrix (ECM) components, and cell-surface glycosaminoglycans can interact with and destabilize polyplexes, leading to premature extracellular unpackaging [64,77,129,130]. Shielding excessive cationic charge through the use of PEG and other hydrophilic steric stabilizers may mitigate these adverse effects.

Additionally, the diffusivity of cationic vehicles *in vivo* may be limited due to electrostatic interactions with the ECM, or also by the formation of large aggregates caused by polyplex instability. This has implications for the accessibility of polyplexes to resident DCs and other APCs. Palumbo *et al*. investigated pDNA polyplexes formulated with PEI, linear poly(2-aminoethyl methacrylate) (PAEM), and PEGylated PAEM (PEG-*b*-PAEMA) [135]. PEI and PAEM polyplexes rapidly formed large aggregates in media formulated to mimic the *in vivo* environment, while PEG-PAEM polyplexes remained stable. Upon intradermal administration, PEG-PAEM polyplexes were observed to be more widely distributed from the injection site than PEI and PAEM polyplexes. Furthermore, DC colocalization was significantly higher with PEG-PAEM compared to PEI and PAEM polyplexes. In the latter case, DC colocalization was limited to the edge of the aggregates, suggesting that DCs were unable to infiltrate into the dense polyplex clumps.

While these studies begin to elucidate critical design parameters for successful *in vivo* gene transfection, systematic studies of the effect of vehicle characteristics on *in vivo* delivery efficacy are still needed, particularly with respect to mRNA. Here, studies assessing a series of block copolymer architectures (Chapters 2 and 3) for *in vivo* mRNA delivery are described. Polyplexes were formulated using polymer micelles with varying PEGMA content and cationic surface charge, then evaluated in mouse models for transfection efficacy, local tissue distribution, and trafficking to lymph node DCs.

2. Experimental methods

2.1. Plasmids and in vitro transcription of mRNA

The construction of pGEM4Z-A64 has been previously described (Chapter 3). Plasmid DNA was purified using the EndoFree Plasmid Mega Kit (Qiagen). The luciferase cDNA from pCMV-Luciferase (Elim Biopharmaceuticals) was amplified by PCR using primers that added flanking PstI and NotI restriction sites to the 5' and 3' ends of the cDNA, respectively: 5'-GCTCTGCAGGGTACTGTTGGT-3' (forward) and 5'-GCTGCGGCCGCTTACAATTTG-3' (reverse). The PCR product was ligated into pGEM4Z-A64 to produce pGEM4Z-LUC-A64. pGEM4Z-LUC-A64 was linearized by SpeI and used as a template for *in vitro* transcription using a mMESSAGE mMACHINE T7 Kit (Ambion). The resultant mRNA was purified using a RNeasy MinElute Cleanup Kit (Qiagen).

2.2. Formulation of mRNA-polymer polyplexes

Polymers were prepared following previously described procedures (Chapter 2) in DPBS, for *in vitro* studies, or in HEPES-buffered glucose (HBG, 20 mM HEPE, 5% w/v glucose, pH 7.4), for *in vivo* studies. Polyplexes were formed by combining equal volumes of mRNA (0.1 μg/μL in nuclease-free water) and polymer stock solutions for 30 min at room temperature. The theoretical charge ratios (+/-) of the polyplexes were calculated using the mass concentration of the cationic DMAEMA block, assumed to be 50% protonated at pH 7.4. All polyplexes in this study were formed at a theoretical charge ratio of 4:1 unless otherwise specified. As controls, some mRNA polyplexes were formulated with in vivo-jetPEI (Polyplus) in accordance with the manufacturer's protocols at an N/P ratio of 8.

2.3. Cell culture

All cell culture media and reagents were obtained from Gibco unless otherwise specified. The RAW 264.7 murine macrophage cell line (ATCC) were maintained in Dulbecco's Modified Eagle Medium High Glucose containing L-glutamine supplemented with 10% FBS and 1% penicillin-streptomycin.

2.4. In vitro luciferase transfection assay

RAW 264.7 cells were seeded in 24-well plates at 250,000 cells/well in 1 mL complete media and allowed to adhere overnight. Cells were washed with DPBS and the culture medium replaced with polyplexes at 0.25 μg mRNA/well in 200 μL serum- and antibiotic-free media. After 4 h, cells were washed and lysed with 150 μL Glo Lysis Buffer (Promega) for 5 min. 100 μL of lysate were assayed for bioluminescence signal using a Bright-Glo Luciferase Assay Kit (Promega) in accordance with the manufacturer's protocol. Luminescence values were normalized to the total cellular protein per well as determined by a BCA assay kit (Pierce).

2.5. In vivo luciferase transfection and bioluminescence imaging

Female BALB/c mice 6 to 8 weeks old (Jackson Laboratories) were maintained under specific pathogen-free conditions and in accordance with University of Washington IACUC protocols. Uncomplexed mRNA or polyplexes containing 10 μg mRNA were administered via a single subcutaneous injection of 200 μL volume in the lower right abdominal quadrant. To assess *in vivo* luciferase gene expression, mice were injected intraperitoneally with 150 mg/kg D-luciferin potassium salt (15 mg/ml in DPBS, Caliper), anesthesized with isoflurane, and imaged for

bioluminescence using a Xenogen IVIS200 Spectrum Imager. Luciferase expression was quantified based on total luminescence signal normalized per area using Living Image software (Caliper).

2.6. In vivo trafficking of fluorescent polyplexes

mRNA was labeled with Cy5 using a *Label*IT Tracker Intracellular Nucleic Acid Localization Kit (MirusBio) at a 0.5:1 v/w ratio of *Label*IT Tracker Reagent to mRNA in accordance with the manufacturer's protocol. Uncomplexed mRNA or polyplexes containing 10 μg Cy5-mRNA were administered via a single subcutaneous injection of 200 μL volume in the lower right abdominal quadrant of 6- to 8-week-old female BALB/c mice. For fluorescence imaging, mice were anesthesized with isoflurane and imaged using a Xenogen IVIS200. Image analysis was performed using Living Image software.

2.7. Polyplex trafficking to draining lymph nodes

Cy5-labeled polyplexes or mRNA were prepared and administered via subcutaneous injection as described above to 6- to 8-week-old female C57BL/6 mice. Animals were euthanized by CO_2 at specified time points and the inguinal lymph nodes were isolated. Lymph nodes were digested with 0.34 mg/mL Liberase TL and 2 mg/mL DNaseI (Roche), filtered through a 40 μm cell strainer, and incubated for 5 min in ACK buffer to lyse erythrocytes. Cell suspensions were incubated with rat anti-mouse CD16/32 antibody (BD Biosciences) to block Fc receptors, then stained with Pacific Blue-anti-CD11c (BioLegend) and PE-anti-I-Ab (BD Biosciences). Approximately 1 million single cell events per sample were collected using a BD FACSCanto II and analyzed using FlowJo software (TreeStar).

2.8. Statistical methods

ANOVA was used to test for treatment effects and Tukey's test was used for post hoc pairwise comparisons between individual treatment groups.

3. Results

3.1. Evaluation of in vitro luciferase transfection

An *in vitro* transfection assay in RAW 264.7 macrophages was used to confirm the functionality of the luciferase mRNA reporter construct. Cells were incubated with mRNA polyplexes for 4 h prior to the analysis of gene expression by bioluminescence signal. The relative expression levels followed trends similar to those observed in the GFP transfection assays described in Chapter 3, with the DPE1, DPE2, and DPE3 polyplexes generating the highest amounts of luciferase expression (**Figure 4.1**). Uncomplexed mRNA performed poorly in the *in vitro* transfection assay, with expression levels four orders of magnitude lower than the DPE series polymers and roughly comparable to untreated negative controls (data not shown).

3.2. In vivo gene expression

The ability of mRNA polyplexes to mediate transfection *in vivo* was evaluated using a mouse model. Polyplexes formulated with the luciferase mRNA reporter construct were administered via subcutaneous injection, and bioluminescence imaging was used to determine the extent of local gene expression at specified time points.

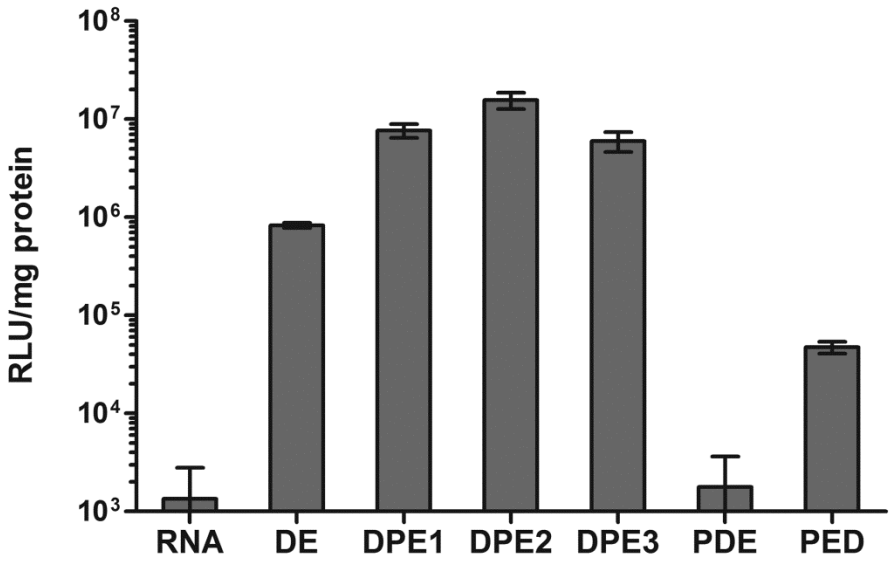

Figure 4.1. *In vitro* transfection of RAW 264.7 macrophages. Data are presented as relative luminescence units (RLU) normalized to total cellular protein and are from a single representative experiment conducted in triplicate ± standard deviation.

Uncomplexed mRNA produced the highest levels of luciferase expression, while the PDE, PED, and DPE3 polyplexes generated low to undetectable bioluminescence signals (**Figure 4.2**). Transfection mediated by naked mRNA was transient, with luciferase expression peaking at approximately 8 h post-injection and undetectable by 96 h. Control polyplexes formulated with jetPEI, a polymer-based reagent, also failed to mediate transfection *in vivo*. Similar negative results were observed for DE, DPE1, and DPE2 polyplexes (data not shown). Overall, these results demonstrate that naked mRNA is superior to mRNA polyplexes for *in vivo* transfection of local tissue following subcutaneous injection. Intriguingly, this finding contradicts observations from *in vitro* transfection studies, in which naked mRNA consistently performed poorly compared to mRNA polyplexes.

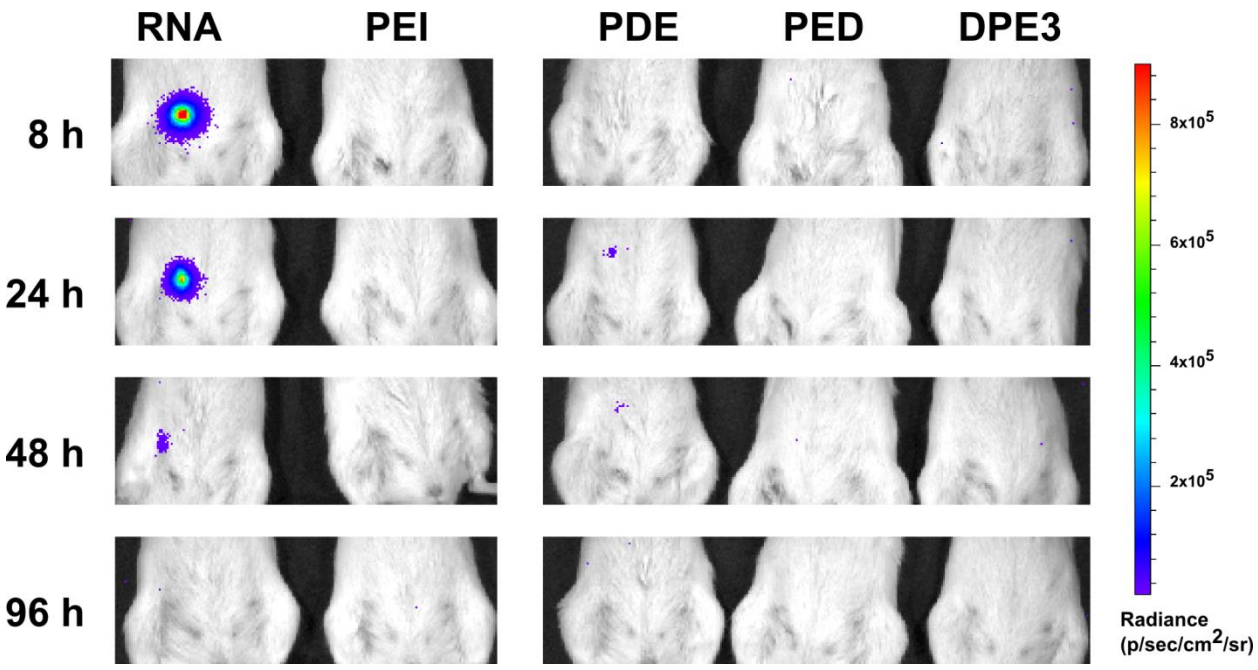

Figure 4.2. *In vivo* bioluminescence imaging of luciferase expression. Uncomplexed mRNA, mRNA polyplexes, and JetPEI polyplexes (PEI) were administered via subcutaneous injection at t = 0 h. Mice were imaged for bioluminescence indicative of luciferase gene expression at the indicated time points.

3.3. In vivo polyplex trafficking

To assess the fate of polyplexes *in vivo*, mice were given subcutaneous injections of Cy5-labeled mRNA and live animal imaging was used to track the distribution of fluorescence over time. A preliminary study screening the entire block copolymer series indicated that naked mRNA was cleared from the injection site more rapidly than mRNA in polyplexes and that neutral polyplexes (PDE, PED) appeared to dissipate more rapidly than cationic polyplexes (DE, DPE1, DPE2, DPE3) (**Figure 4.3**).

In order to further investigate this phenomenon, a second study with higher animal numbers was performed to compare the trafficking of naked mRNA, highly cationic DE polyplexes (zeta

potential 21.0 mV), and slightly cationic DPE3 polyplexes (zeta potential 12.4 mV) (**Figure 4.4**). The results were consistent with the preliminary data: naked mRNA was eliminated more quickly from the injection site than mRNA in polyplexes and was not longer observable at 4 h post-injection. Comparing the two polyplexes, the less cationic DPE3 polyplexes took 24 h to be cleared, while the fluorescence signals from the highly cationic DE polyplexes were still detectable at 48 h. Based on these findings, it can be concluded that the trafficking profile of mRNA following subcutaneous injection is contingent upon the mode of delivery (naked versus complexed), as well as the physiochemical characteristics of the delivery vehicle.

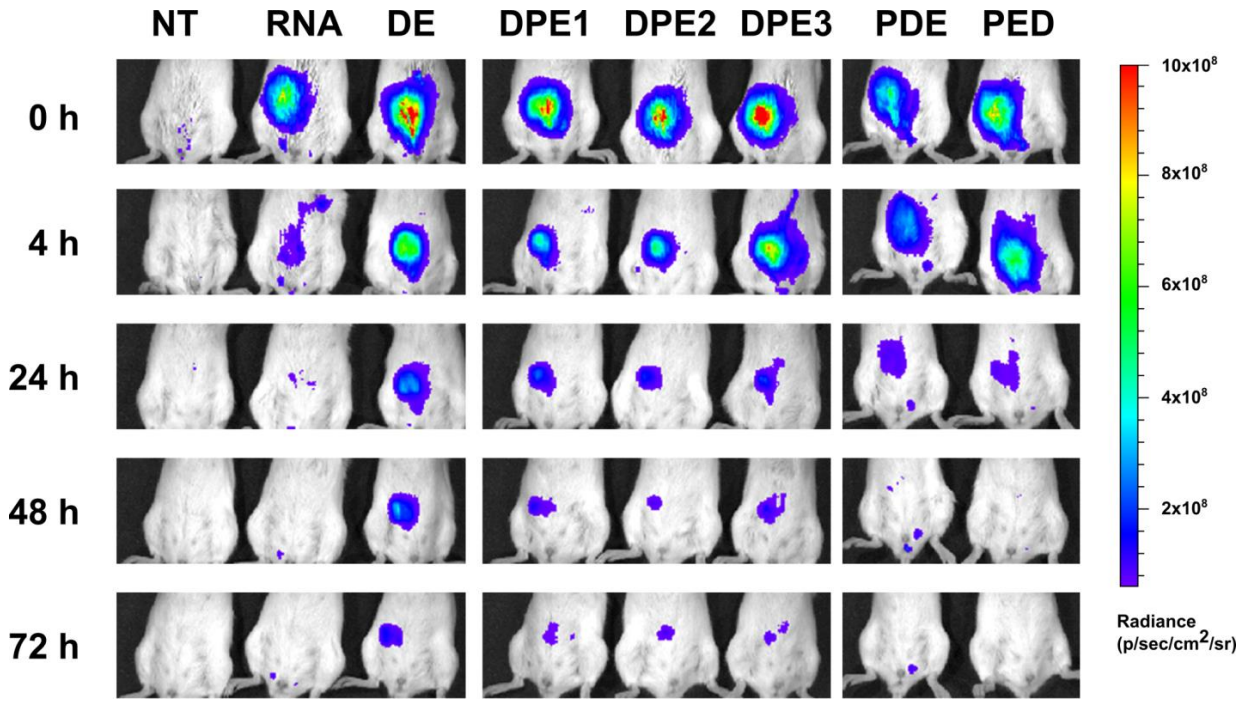

Figure 4.3. Preliminary screen of *in vivo* trafficking of mRNA polyplexes. Polyplexes were formulated with Cy5-labeled mRNA and administered via subcutaneous injection at t = 0 h. Control animals received no treatment (NT) or naked mRNA. Mice were imaged at the specified time points for Cy5 fluorescence.

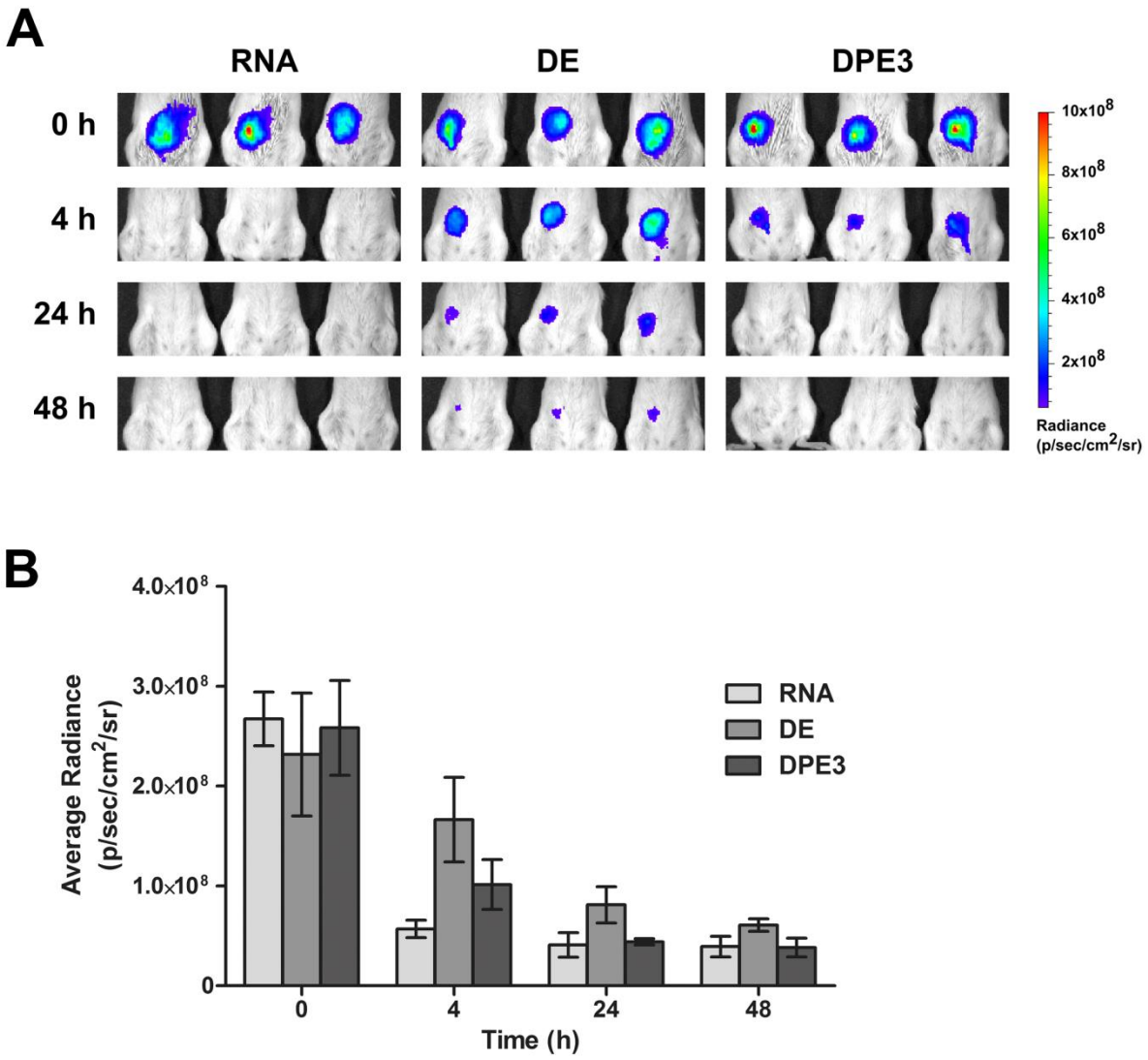

Figure 4.4. *In vivo* trafficking of mRNA polyplexes. Polyplexes were formulated with Cy5-labeled mRNA and administered via subcutaneous injection at t = 0 h (n = 3 mice per group). (**A**) Distributions of fluorescent mRNA at the specified time points post-injection. (**B**) Temporal evolution of average Cy5 fluorescence intensities at the local injection site. DE varies significantly from RNA at t = 4 h, and from both RNA and DPE3 at t = 24 h ($p < 0.05$). Data are from a single experiment ± standard deviation.

3.4. Polyplex trafficking to DCs in draining lymph nodes

To determine whether mRNA polyplexes were being trafficked to the draining lymph nodes, polyplexes were formulated with Cy5-labeled mRNA, administered via subcutaneous injection,

and the inguinal lymph nodes isolated at subsequent time points. The CD11c+ MHCII+ DC population, representing roughly 1-2% of the total lymph node cell population (data not shown), was analyzed for Cy5 fluorescence indicative of mRNA uptake. At 48 h post-injection, uptake frequencies for naked mRNA, DE polyplexes, and DPE3 polyplexes were all extremely low (≤ 2% Cy5+ cells) and were comparable to background fluorescence levels observed in animals treated with HBG only as negative controls (**Figure 4.5**).

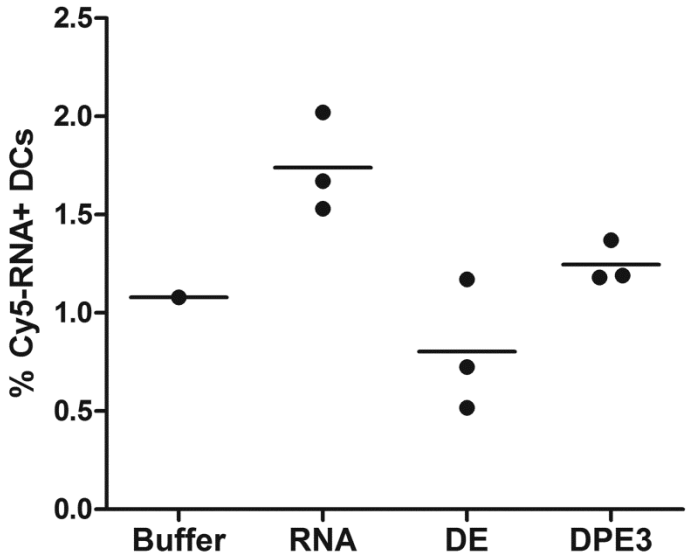

Figure 4.5. *In vivo* uptake of mRNA polyplexes by lymph node DCs. Polyplexes were formulated with Cy5-labeled mRNA and administered via subcutaneous injection (n = 1-3 mice per group). Control animals received injections of HBG only (Buffer). Inguinal lymph nodes were isolated after 48 h and the percentage of CD11c+ MHCII+ DCs demonstrating Cy5-mRNA uptake determined by flow cytometric analysis.

Similar results were obtained with other polyplexes, and at 12 h and 24 h post-injection (data not shown). Overall, the evidence indicates that neither naked mRNA nor mRNA polyplexes appear to be trafficked to the DC population in draining lymph nodes following subcutaneous injection.

4. Discussion

Disappointingly, despite previous findings demonstrating successful *in vitro* mRNA transfection using the polymer series described in this work, none of these polymers achieved satisfactory mRNA delivery *in vivo*. mRNA polyplexes failed to mediate any observable *in vivo* transfection, while delivery of naked mRNA was able to generate transient expression at the injection site. These results stand in contradiction to the *in vitro* data, which consistently demonstrated that polyplexes were superior to naked mRNA for transfection.

As discussed in the Chapter Introduction, these findings are not necessarily unusual, given previous reports of such discrepancies between *in vitro* and *in vivo* delivery efficacies for naked and complexed pDNA. However, while van den Berg *et al*. were able to restore *in vivo* pDNA activity by PEGylation of their cationic delivery vehicles [133], no gene expression was observed in this study even with polymers incorporating PEGMA segments and exhibiting reduced cationic surface charges. Polymer vehicle characteristics did appear to influence polyplex trafficking: shielded polyplexes were cleared more rapidly than cationic polyplexes following subcutaneous injection. The prolonged retention of cationic polyplexes at the injection site suggested the formation of polymer "depots," or aggregates that could prevent cells from accessing and taking up mRNA for transfection [135]. However, since the differences in polyplex tissue distribution did not translate to detectable changes in gene transfection, the significance of these results for delivery vehicle design remains ambiguous. It appears that the reduction of polyplex charge by incorporation of PEGMA is not sufficient to guarantee successful *in vivo* mRNA transfection, and that future studies will need to focus on other design parameters.

A recent report suggests that delivery route may also be an important factor for successful *in vivo* mRNA delivery [136]. Phua *et al.* found that nanoparticulate mRNA formulated from a commercial reagent successfully transfected DCs *in vitro*, while naked mRNA failed to produce any observable gene expression. The opposite trend was observed following subcutaneous administration in mice, in which naked mRNA generated higher and more prolonged levels of gene expression compared to mRNA nanoparticles. Intriguingly, this pattern only held true for the subcutaneous route: when mRNA was delivered via intravenous or intranasal administration, mRNA nanoparticles outperformed naked mRNA by a significant margin. These findings are corroborated by Su *et al.*, who also reported the superiority of nanoparticulate mRNA compared to naked nucleic acid for intranasal delivery [95]. Based on these results, it appears that subcutaneous sites may not be optimal for polymer-based mRNA delivery. Cellular uptake of naked mRNA versus mRNA nanoparticles occurs through distinct pathways [137], and it is possible that the uptake mechanisms for polyplex-based systems could be relatively inefficient in subcutaneous tissue.

For vaccines, the choice of delivery route must also take into consideration the accessibility of the vaccine particles by DCs. Initiation of an adaptive immune response requires the interaction of antigen-loaded DCs with T cells residing in secondary lymphoid organs such as the lymph nodes [138]. Vaccines can accomplish this by (1) targeting DCs already resident in the lymph nodes or (2) targeting DCs in peripheral tissues that subsequently migrate to the lymph nodes [21,139,140]. Particle size has been demonstrated to strongly influence the mode of lymph node trafficking, with smaller particles (< 100 nm) capable of passive drainage to lymph nodes, and

larger particles relying upon capture by peripheral DCs [141–143]. Based on the size range of the mRNA polyplexes (86-216 nm), trafficking to lymph nodes would be expected to occur primarily via uptake by DCs in the skin. However, no mRNA uptake was observed in lymph node DCs with either naked or polyplex mRNA at any of the time points examined in this study.

Overall, these findings demonstrate that significant improvements to the block copolymer platform are needed in order to achieve efficacious *in vivo* delivery of mRNA vaccines. Recommendations for future studies are to (1) redesign the current polymer carrier platform to improve transfection efficacy and targeting to lymph node DCs, and (2) investigate alternative delivery routes, such as intranasal administration, which have proven more amenable than subcutaneous injection for nanoparticle-mediated mRNA delivery.

5. Conclusions

A series of multifunctional block copolymers encompassing varying compositions of DMAEMA, PEGMA, and DEAEMA-*co*-BMA were evaluated for their ability to facilitate mRNA delivery *in vivo*. While mRNA polyplexes outperformed naked mRNA in transfection assays *in vitro*, they did not generate satisfactory transfection following subcutaneous administration in mice, with naked mRNA producing superior levels of gene expression. However, neither naked mRNA nor polyplexes were observed in DCs in the draining lymph nodes. These findings suggest that further improvements in polymer design are needed not only to improve the efficiency of polymer-mediated *in vivo* mRNA transfection, but also to enhance trafficking of mRNA vaccines to DCs.

Chapter 5

Evaluation of glycopolymer micelles for *in vivo* delivery of pDNA vaccines

Matthew J. Manganiello contributed equally to this work.

Abstract

This chapter describes studies performed to evaluate glycopolymer micelles for *in vivo* pDNA delivery. A series of diblock copolymer micelles containing a pH-responsive DEAEMA-*co*-BMA core were synthesized via RAFT polymerization. To assess the effectiveness of glycotargeting for pDNA vaccine delivery, the following micelle corona compositions were investigated: (1) varying molar ratios (0-100%) of mannose ethyl methacrylate (ManEMA) copolymerized with DMAEMA, (2) galactose ethyl methacrylate (GalEMA), and (3) PEGMA. DLS studies indicated that all polymers condensed pDNA into 87-200 nm polyplexes, with zeta potentials of the polyplexes varying based on the corona composition: micelles with high DMAEMA content generated positive zeta potentials, purely glycosylated micelles were near neutral, and PEGMA micelles were slightly negative. ManEMA, GalEMA, and PEGMA polyplexes produced gene expression following subcutaneous administration in mice, while cationic polyplexes failed to generate any observable *in vivo* transfection. ManEMA and GalEMA polyplexes demonstrated superior trafficking to lymph node DCs (13.7% and 10.2% pDNA+ cells, respectively) compared to other polyplexes and free pDNA, demonstrating the potential of RAFT-based glycopolymer micelles for enhancing *in vivo* delivery of pDNA vaccines.

1. Introduction

pDNA vaccination is a promising strategy for combating a wide variety of diseases and pathogens, as it is safe, versatile, and capable of eliciting cellular and humoral immunity [3,144]. However, the low immunogenicity of pDNA vaccines in humans remains a major barrier to the clinical utility of this technology [17]. One approach to improving vaccine potency is the usage of synthetic carriers, most commonly polymers, liposomes, or micro/nanoparticles [20], to enhance vaccine delivery to DCs. As professional APCs, DCs are an ideal target for vaccination applications due to their critical role in the initiation of adaptive immunity. Immature DCs survey peripheral tissues for pathogens and, upon capturing foreign antigens, undergo maturation and migrate to the lymph nodes for antigen presentation to T cells [145]. Vaccine delivery strategies typically target antigens to peripheral DCs located in tissues such as the skin, but have also directly targeted DCs resident in lymph nodes [139,143].

Mannose-functionalized carriers have been the subject of much research interest owing to their ability to target DCs via the macrophage mannose receptor (MMR) [146,147]. The MMR is an endocytic C-type lectin receptor expressed by DC subsets and macrophages [147,148]. In DCs, the MMR functions as an antigen uptake receptor, enhancing the processing and presentation of mannosylated antigens [149–151]. For pDNA vaccination applications, the immunostimulatory potential of mannose glycotargeting has been demonstrated in a variety of carrier systems, including mannose- and mannan-modified liposomes [152–154], polymers [155–158], nanoparticles [159], and microspheres [160].

While the affinity between a single carbohydrate recognition domain (CRD) of a C-type lectin receptor and a simple monosaccharide is relatively weak [161], natural glycan-lectin interactions frequently involve multivalent binding between more complex polysaccharide structures and multiple CRDs, thus increasing the overall avidity [162]. Synthetically, multivalency can be achieved through the polymerization of monomers incorporating pendent monosaccharides to generate a glycopolymer chain. Controlled free radical polymerization techniques such as RAFT offer precise control of polymer architectures and have been widely used for the development of gene delivery vectors [80,85]. Lowe *et al.* described the first RAFT polymerization of a glycomonomer, 2-methacryloxyethyl glucoside [163]. A wide variety of RAFT glycopolymer architectures have been reported since, including micelles [164,165], stars [166], and block copolymers [167,168]. Recently, Obata *et al.* developed copolymers of ManEMA and DMAEMA, and demonstrated that these systems exhibited both carbohydrate-specific lectin binding and pDNA condensing capabilities [169]. However, studies assessing the *in vivo* performance of RAFT glycopolymers for gene delivery applications remain scarce.

Here, the development and *in vivo* evaluation of mannose-functionalized glycopolymer micelles prepared using RAFT synthesis is described. These micelles are based upon a previously reported diblock copolymer pDNA delivery vector utilizing a pH-responsive copolymer of DEAEMA and BMA (DEAEMA-*co*-BMA) in the micelle core to facilitate escape from endolysosomal entrapment [72]. To assess the effect of mannosylation on pDNA delivery characteristics, the micelle series was designed with varying ManEMA and DMAEMA content in the micelle corona. Micelles incorporating GalEMA or PEGMA in the corona were also

investigated, in order to provide comparisons with untargeted glycopolymer micelles and untargeted hydrophilic micelles, respectively.

2. Experimental methods

2.1. Materials

Chemicals were supplied by Sigma-Aldrich unless otherwise specified. 2,2′-azobis(4-methoxy-2,4-dimethyl valeronitrile) (V-70) and 1,1'-azobis(cyclohexane-1-carbonitrile) (V-40) were obtained from Wako Chemicals. Spectra/Por 7 standard regenerated cellulose dialysis tubing was obtained from Spectrum Labs and Amicon Ultra centrifugal filters were obtained from EMD Millipore. 4-cyano-4-(ethylsulfanylthiocarbonyl) sulfanylvpentanoic acid (ECT) was synthesized as previously described [71]. 2,2-azobisisobutyronitrile (AIBN) was recrystallized from methanol. 4-cyanopentanoic acid dithiobenzoate (CTP) and 4,4-azobis(4-cyanopentanoic acid) (V-501) were used as received. Dimethylaminoethyl methacrylate (DMAEMA), diethylaminoethyl methacrylate (DEAEMA), and butyl methacrylate (BMA) were distilled prior to use. Acetylated mannose ethyl methylacrylate (AcManEMA) and acetylated galactose ethyl methacrylate (AcGalEMA) were synthesized according to previous methods [170]. Poly(ethylene glycol) methyl ether methacrylate (PEGMA, average M_n = 300 g/mol) was passed through a basic alumina column prior to use.

2.2. Synthesis of poly(DEAEMA-co-BMA) macro chain transfer agent

The RAFT copolymerization of DEAEMA and BMA was conducted in dioxane (50 wt% monomer) at 90 °C under a nitrogen atmosphere for 6 h using ECT and V40 as the chain transfer

agent (CTA) and radical initiator, respectively. The initial monomer to CTA molar ratio ($[M]_0/[CTA]_0$) was 100:1, CTA to initiator molar ratio ($[CTA]_0/[I]_0$) was 20:1, and molar feed ratio of DEAEMA:BMA was 3:2 (40 mol% BMA). The resultant polymer, termed EB40 macroCTA, was isolated by dialysis against methanol with 1000 MWCO tubing followed by rotary evaporation and drying overnight in vacuo to remove residual solvent.

2.3. Diblock copolymerization of DMAEMA and AcManEMA, AcGalEMA from EB40 macroCTA

DMAEMA and AcManEMA were copolymerized from an EB40 macroCTA in which the initial molar feed of AcManEMA was 0, 25, 50, 75, or 100%, to generate polymers 0% Man, 25% Man, 50% Man, 75% Man, and 100% Man, respectively. AcGalEMA was polymerized from an EB40 macroCTA to generate polymer Gal. Each polymerization was conducted in dioxane at 40 wt% monomer for 18 h at 30 °C using V70 as the primary radical source. The $[M]_0/[CTA]_0$ and $[CTA]_0/[I]_0$ ratios were 65:1 and 20:1, respectively. The resultant diblock copolymers were isolated by precipitation into cold hexanes and dried overnight in vacuo.

2.4. Saponification of glycopolymers

To display native pendent glycomoieties on the glycopolymers, protective acetyl groups were removed via base-catalyzed hydrolysis. The glycopolymers (0-100% Man, Gal) were separately added to a solution of 1 wt% sodium methoxide in anhydrous methanol at a copolymer concentration of 50 mg/mL. After 1 hour incubation at room temperature, the solutions were neutralized with acetic acid to a pH of ~7 and dialyzed against deionized water using 1000 MWCO tubing. The solutions were then lyophilized to obtain the final diblock copolymers. Aqueous stocks of the deprotected diblock copolymers were formulated from the lyophilized

material at 2 mg/mL in 1X pH 7.4 Dulbecco's phosphate-buffered saline (DPBS). The copolymers were pre-dissolved at 40 mg/mL in methanol prior to addition into buffer to promote micelle formation. For *in vivo* studies, copolymer stocks were buffer exchanged into HEPES buffered glucose (HBG; 20 mM HEPES, 5% (w/v) glucose, pH 7.4) via centrifugal filtration with a 3000 MWCO.

2.5. Synthesis of poly(PEGMA) macro chain transfer agent

The synthesis of PEGMA-containing block copolymers was conducted as previously described (Chapter 2) [171]. The RAFT polymerization of PEGMA was conducted in dioxane (10 wt% monomer) at 60 °C under a nitrogen atmosphere for 18 h using CTP and AIBN as the CTA and radical initiator, respectively. The $[M]_0/[CTA]_0$ and $[CTA]_0/[I]_0$ ratios were 130:1 and 10:1, respectively. The resultant polymer, termed pPEGMA macroCTA, was isolated by precipitation into pentane (x5) and dried.

2.6. Diblock copolymerization of DEAEMA and BMA from pPEGMA macroCTA

DEAEMA and BMA were copolymerized from a pPEGMA macroCTA in dioxane at 40 wt% monomer for 18 h at 60 °C using V501 as the radical initiator. The $[M]_0/[CTA]_0$ and $[CTA]_0/[I]_0$ ratios were 100:1 and 4:1, respectively. The resultant polymer, termed PEG, was isolated by precipitation into pentane and dried. Dried polymers were then dissolved into ethanol followed by addition into DPBS (10 vol% ethanol, 8-12 mg/mL polymer), purified by chromatographic separation via a PD-10 desalting column (GE Healthcare), and lyophilized. Polymer stock solutions were prepared by redissolving lyophilized polymers into ethanol followed by addition into HBG or DPBS (2 vol% ethanol, 2 mg/mL polymer).

2.7. Gel permeation chromatography

GPC was used to determine molecular weights and polydispersities (M_w/M_n, PDI) of the macroCTA and diblock copolymers. SEC Tosoh TSK-GEL R-3000 and R-4000 columns were connected in series to a Agilent 1200 series, refractometer Optilab-rEX and triple-angle static light scattering detector Wyatt miniDAWN TREOS. HPLC-grade DMF containing 0.1 wt.% LiBr at 60 °C was used as the mobile phase at a flow rate of 1 ml/min. The molecular weights of each polymer were determined using a multi-detector calibration based on dn/dc values calculated separately for copolymer composition assuming 100% mass recovery.

2.8. ^{1}H-NMR spectroscopy

The ^{1}H-NMR spectra of all dried macroCTA intermediates and final lyophilized polymers were acquired using a Bruker AV 500 at 25 °C with polymer dissolved at 10-20 mg/mL in $CDCl_3$ (PEG) or CD_3OD (0-100% Man, Gal).

2.9. Hemolysis assay

The potential for the diblock copolymers to disrupt endosomal membranes was assessed by a hemolysis assay as previously described [117]. Briefly, polymers (20 µg/mL) were incubated with erythrocytes in 100 mM sodium phosphate buffers (supplemented with 150 mM NaCl) of varying pH values (7.4, 7.0, 6.6, 6.2, and 5.8) intended to mimic the acidifying pH gradient to which endocytosed material is exposed. The extent of cell lysis (i.e. hemolytic activity) was determined by detecting released hemoglobin via absorbance measurements at 492 nm.

2.10. Concanavalin A (ConA) agglutination assay

A stock solution of ConA was prepared in HEPES buffered saline supplemented with $MgCl_2$ and $CaCl_2$. Glycopolymers were added to diluted ConA to obtain the following final concentrations: [ConA] = 100 μg/mL and [polymer] = 50 μg/mL. The mixture was quickly vortexed and the solution turbidity quantified by absorbance measurements at 350 nm at 0.1 Hz intervals.

2.11. Formation of diblock copolymer/pDNA polyplexes and lipoplexes

gWiz-GFP and pCMV-luciferase plasmids were obtained from Aldevron and Elim Biopharm, respectively. Diblock copolymer/pDNA polyplexes were prepared by first diluting pDNA to 0.1 mg/mL in DPBS (for *in vitro* studies) or HBG (for *in vivo* studies), followed by addition of the diblock copolymers with a minimum incubation time of 20 min at room temperature. The total formulation volume was 20 μL per 1 μg pDNA. Polyplexes were formulated at a fixed weight ratio of polymer:DNA of 9:1. Lipoplexes were formed by combining pDNA with Lipofectamine 2000 (LF, Invitrogen) at a 3:1 v/w LF:DNA ratio in serum-free media in accordance with the manufacturer's protocol.

2.12. Dynamic light scattering and zeta potential measurements

The sizes of free diblock copolymer micelles and copolymer/pDNA polyplexes in DPBS were determined by DLS measurements using a Malvern Zetasizer Nano ZS. Free copolymer measurements were performed at a polymer concentration of 200 μg/mL while polyplexes were analyzed at a pDNA concentration of 5 μg/mL. Free copolymer mean diameters are reported as the number average ± peak half-width while polyplex mean diameters are reported as the Z-

average ± standard deviation. For zeta potential measurements, polyplexes were diluted into water to achieve a final pDNA concentration of 5 μg/mL.

2.13. In vitro transfection

All cell culture reagents were obtained from Invitrogen unless otherwise specified. RAW 264.7 (murine leukaemic monocyte macrophage cell line) (ATCC) cells were maintained in Dulbecco's Modified Eagle Medium (DMEM) High Glucose containing L-glutamine supplemented with 1% penicillin-streptomycin and 10% fetal bovine serum (FBS) at 37 °C and 5% CO_2. RAW 264.7 cells were seeded in 24-well plates at 1 x 10^5 cells/well in 0.5 mL media and cultured for 18 h to approximately 50% confluency. Polyplexes and lipoplexes were formulated as described above using GFP pDNA, and added to the cells at 1 μg pDNA/well. Cell media was added to each well to obtain a total volume 1 mL/well and the poly/lipoplexes were allowed to incubate for 24 h. After this time, the cells were washed once with DPBS and then lysed with 300 μL RIPA lysis buffer (Pierce) for 1 h at 4 °C. Lysates were transferred to a black 96-well plate (150 μL/well) and fluorescence intensity was measured at excitation and emission wavelengths of 470 and 510 nm, respectively.

2.14. Bone marrow-derived dendritic cells

All animal protocols were approved by the University of Washington Institutional Animal Care and Use Committee. Murine bone marrow-derived dendritic cells (BMDCs) were obtained by euthanizing 6-8 week-old female C57BL/6 mice (Jackson Laboratories) with CO_2 and collecting the femurs and tibiae. The bone marrow was flushed out with complete media (RPMI 1640 supplemented with 10% FBS, 2 mM L-glutamine, 10 mM HEPES, 1 mM sodium pyruvate, 0.1

mM nonessential amino acids, 55 μM beta-mercaptoethanol, and 1% penicillin-streptomycin) and filtered through a 70 μm cell strainer. Cells were resuspended in ACK buffer to lyse erythrocytes for 5 min, washed, and cultured in Petri dishes in 10 mL complete media containing 20 ng/mL granulocyte macrophage colony-stimulating factor (GM-CSF, Peprotech, Rocky Hill, NJ). 10 mL fresh media containing 20 ng/mL GM-CSF was added on Day 3, and media was changed on Day 5. On Day 7, media was exchanged with fresh media containing 10 ng/mL GM-CSF.

2.15. In vitro BMDC maturation assay

BMDCs were collected on Day 8 using PBS-based cell dissociation buffer, seeded into non-tissue culture treated 24-well plates at 2.5 x 10^5 cells/well in 1 mL complete media with 10 ng/mL GM-CSF, and cultured overnight. Polyplexes and free pDNA were then added at a final concentration of 1 μg pDNA per well. Free polymer micelles were added at equivalent polymer concentrations as the polyplexes. As a positive control, lipopolysaccharides from *E. coli* (LPS, Sigma-Aldrich) were added at 100 ng/mL. After 24 h, cells were collected, incubated with rat anti-mouse CD16/32 antibody to block Fc receptors, and stained with APC-anti-CD11c, FITC-anti-CD80, and PE-Cy7-anti-CD86 (BD Biosciences). Samples were analyzed on a BD FacsCanto II.

2.16. In vivo transfection

Polyplexes were formulated with 5 μg luciferase pDNA as described above, and diluted to a final volume of 200 μL in HBG. Treatments were administered to 6-8 week-old female BALB/c mice (Jackson Laboratories) by subcutaneous injection in the lower right abdominal quadrant. At 24 h

post-injection, mice were injected intraperitoneally with luciferin (PerkinElmer) in DPBS at 150 mg/kg, anesthetized with isoflurane, and imaged for bioluminescence using a IVIS200 system (Xenogen Corp). Image analysis was performed using Living Image software (Caliper Life Sciences).

2.17. Polyplex trafficking to draining lymph nodes

pDNA was labeled with Cy5 using a *Label*IT Tracker™ Intracellular Nucleic Acid Localization Kit, Cy™5 (Mirus Bio) in accordance with manufacturer's protocol. Polyplexes were formulated with 5 μg Cy5-pDNA, diluted to a total volume of 200 μL, and administered to 6-8 week-old female C57BL/6 mice (Jackson Laboratories) by subcutaneous injection in the lower right abdominal quadrant. Animals were euthanized by CO_2 24 h post-injection and the inguinal lymph nodes were isolated. Lymph nodes were digested with 0.34 mg/mL Liberase TL and 2 mg/mL DNaseI (Roche), filtered through a 40 μm cell strainer, and incubated for 5 min in ACK buffer to lyse erythrocytes. Cell solutions were incubated with rat anti-mouse CD16/32 antibody (BD Biosciences) to block Fc receptors, then stained with Pacific Blue-anti-CD11c (BioLegend) and PE-anti-I-Ab (BD Biosciences). Samples were analyzed using a BD FACSCanto II.

2.18. Immunizations

6-8 week-old female C57BL/6J mice were immunized with polyplexes containing 20 μg of ovalbumin pDNA via two subcutaneous injections on day 0, 7, and 14. Blood samples were collected on day 20 via submandibular bleeding. Mice were sacrificed on day 28 by CO_2 euthanasia and the spleens removed. Splenocytes were isolated by homogenizing the spleen, passing the cell suspension through two 100 μm cell strainers, and incubating with ACK lysis

buffer for 5 min to lyse red blood cells. Isolated splenocytes were cultured in RPMI 1640 with 2 mM L-glutamine supplemented with 55 μM 2-mercaptoethanol, 10% heat-inactivated FBS, and 1% penicillin-streptomycin.

2.19. Intracellular cytokine (ICC) staining and flow cytometry

All materials for the ICC staining procedure were obtained from BD Biosciences unless otherwise stated. Isolated splenocytes were seeded in U-bottomed 96-well plates at 2 x 10^6 cells/well in 100 μL media. Cells were stimulated with 20 μg/mL each of ovalbumin CD4 and CD8 peptide epitopes (Genscript) for 1 h, then treated with 0.2 μL/well GolgiStop for 8 h at 37 °C to inhibit cytokine secretion. Cells were then washed, blocked with Fc Block for 15 min at 4 °C, then stained for surface marker expression with AlexaFluor 488 anti-CD8 and PerCP-Cy5.5 anti-CD4 for 30 min at 4 °C. Cells were then washed, fixed using BD CytoFix/CytoPerm for 20 min at 4 °C, then stained with APC anti-IFN-γ for 30 min at 4 °C. Cells were then resuspended in DPBS containing 2% FBS and analyzed on a FACScanto flow cytometer with 400,000 singlet events collected per sample.

2.20. Enzyme-linked immunosorbent assay (ELISA)

Submandibular blood samples were centrifuged for 5 min at 2500g and plasma aliquots collected for storage at -80 °C. 96-well Maxisorp plates (Nunc) were coated with 100 μL/well of 1 μg/mL ovalbumin (Sigma) in DPBS and incubated overnight at 4 °C. Plates were then washed and blocked with 1% BSA in DPBS for 1 h at 37 °C. Diluted plasma samples and anti-ovalbumin IgG1 standards (Sigma) were added to the plates and incubated for 1 h at 37 °C. The secondary antibody, horseradish peroxidase-conjugated goat anti-mouse IgG (Biolegend) was added at a

1:2000 dilution and incubated for 30 min at 37 °C. Plates were developed for 10 min using TMB 2-component peroxidase substrate (Thermo Scientific), with 2 M H_2SO_4 as the stop solution, and analyzed for absorbance at 450 nm.

2.21. Statistical Analysis

ANOVA was used to test for treatment effects, and Tukey's test was used for post hoc pairwise comparisons between individual treatment groups.

3. Results

3.1. Polymer synthesis and characterization

A series of mannosylated diblock copolymers was synthesized via RAFT using the methodology outlined in **Scheme 5.1**. These glycopolymers consisted of two discrete functional segments: (1) a DC-targeting block composed of varying monomer feed ratios of DMAEMA and AcManEMA (0%, 25%, 50%, 75%, and 100%), and (2) an endosomolytic block composed of a copolymer of DEAEMA and BMA (**Table 5.1**). The monomer feed ratio of the DEAEMA-*co*-BMA was 40% BMA, in accordance with previous work demonstrating that this composition is optimal for cytosolic delivery and pDNA transfection of APCs [72]. As a non-targeted glycopolymer control, a galactosylated diblock copolymer was also prepared in a similar fashion using AcGalEMA as the first block. A PEGylated diblock copolymer substituting PEGMA as the first block was synthesized as an additional non-targeted control using previously described protocols (Chapter 2).

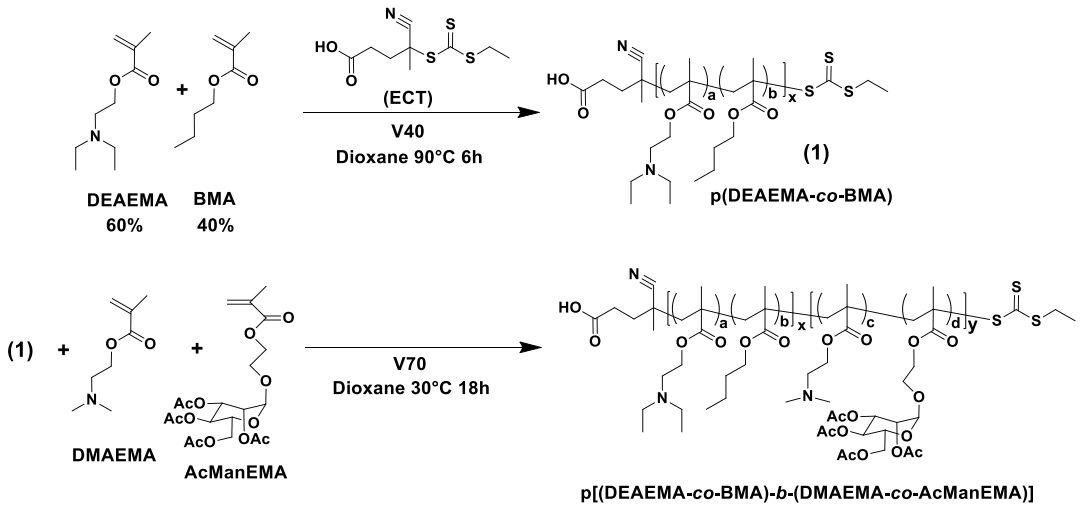

Scheme 5.1. Representative RAFT-mediated synthesis of glycopolymer micelles. Polymers consisted of an endosomolytic block (DEAEMA-*co*-BMA), which acted as a macroCTA for the copolymerization of DMAEMA and AcManEMA at varying molar feed ratios. AcGalEMA glycopolymer synthesis followed the same scheme with the omission of DMAEMA.

Table 5.1. Molecular weights, polydispersities, and monomer compositions for diblock copolymer designs.

Polymer	1st block M_n[a,c] (g/mol)	2nd block M_n[b,c] (g/mol)	Total M_n[d] (g/mol)	PDI[c] (M_w/M_n)	Theoretical[e] % ManEMA 1st block	Experimental[f] % ManEMA 1st block
0% Man	11700	15600	27300	1.09	0	0
25% Man	10700	15600	26300	1.11	25	29
50% Man	12800	15600	28400	1.19	50	57
75% Man	18400	15600	34000	1.14	75	79
100% Man	22000	15600	37600	1.27	100	100
Gal	19600	15600	35200	1.14	--	--
PEG	19600	12300	31900	1.09	--	--

[a] 1st block is ManEMA-*co*-DMAEMA (0-100% Man), GalEMA (Gal), or PEGMA (PEG)
[b] 2nd block is DEAEMA-*co*-BMA, with 43% BMA (0-100% Man, Gal) or 47% BMA (PEG), as determined by ^{1}H-NMR spectroscopy
[c] As determined by GPC
[d] For 0-100% Man and Gal, represents molecular weight estimation following saponification based upon complete removal of acetyl groups
[e] Calculated molar feed ratio
[f] As determined by ^{1}H-NMR spectroscopy

All polymers exhibited unimodal molecular weight distributions with low polydispersities (PDI ≤ 1.27) (**Figure 5.1)**. For the mannosylated glycopolymer series, NMR analysis demonstrated that the final monomer incorporation of AcManEMA and DMAEMA was close to the initial feed ratios (**Figure 5.2**). The protective acetyl groups were subsequently removed via base-catalyzed hydrolysis under Zemplén conditions to yield glycopolymers with the native sugar conformation (**Figure 5.3**).

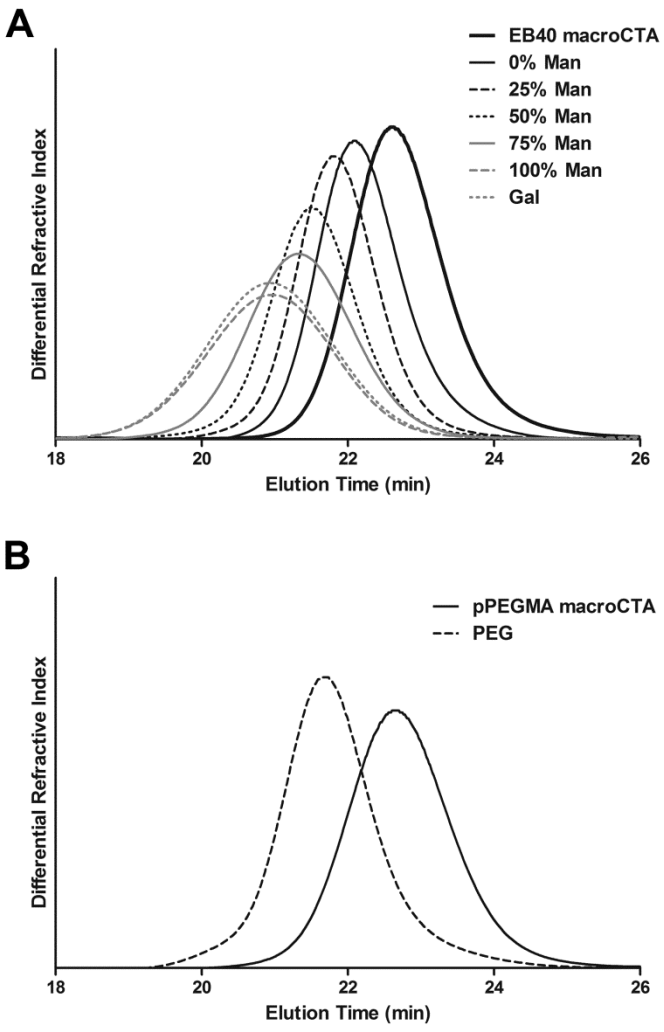

Figure 5.1. Molecular weight distributions obtained by GPC for (A) acetylated mannose and galactose glycopolymer series and (B) PEGylated polymer.

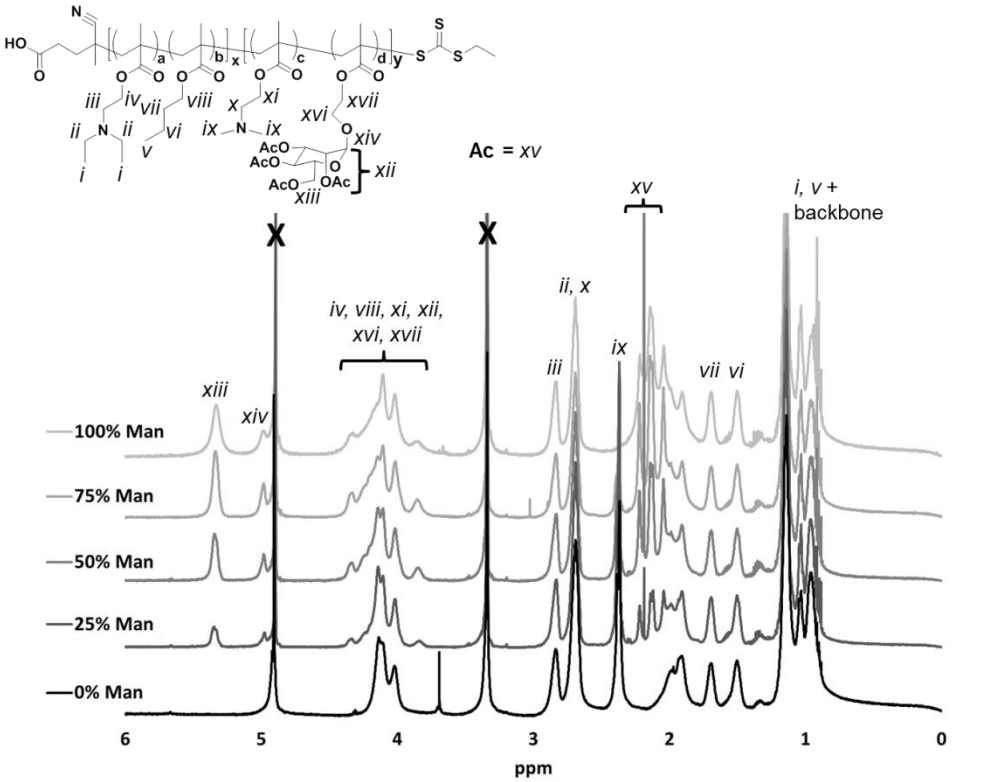

Figure 5.2. ^{1}H-NMR (CD_3OD) spectra of mannosylated glycopolymer series prior to saponification for removal of protective acetyl groups.

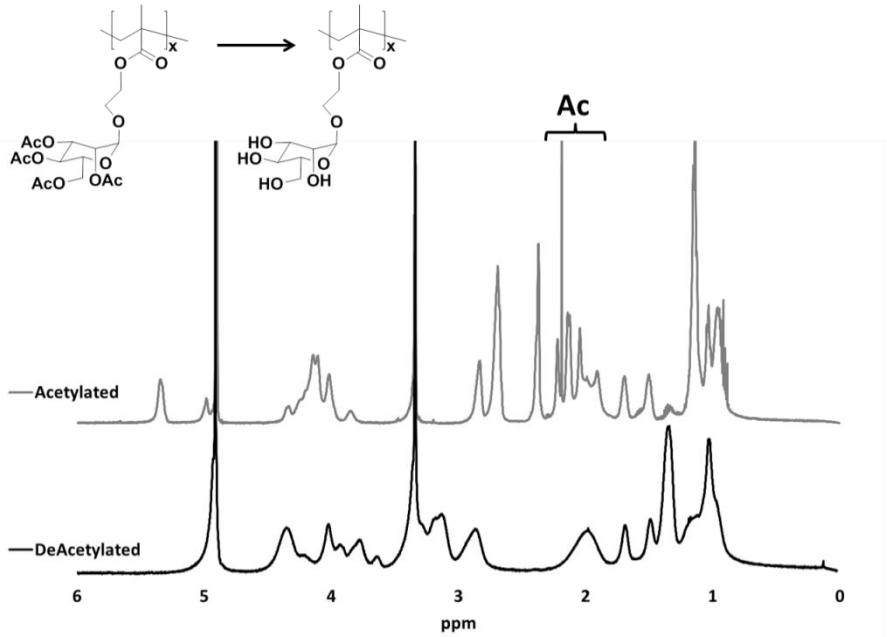

Figure 5.3. Representative ^{1}H-NMR (CD_3OD) spectra of acetylated and deacetylated diblock glycopolymer (50% Man).

3.2. Characterization of polymer micelles

Based on a previous report of a similar diblock copolymer series [72], it was hypothesized that the polymers would organize into micelles in aqueous solution, with the hydrophobic DEAEMA-*co*-BMA segment sequestered in the micelle core. This hypothesis was supported by DLS analysis indicating that polymers in DPBS formed 12-17 nm particles, a size range consistent with micellar organization (**Table 5.2**). Subsequently, a hemolysis assay was performed to confirm that these micelles exhibited the ability to disrupt cell membranes under endolysosomal pH conditions (**Figure 5.4**). As expected, all polymers were inert under physiological conditions (pH 7.4, 7.0), but transitioned sharply to high levels of hemolytic activity under acidic conditions (pH 6.6, 6.2, 5.8). These findings confirm that modification of the micelle corona with mannose, galactose, or PEG does not affect the pH-response of the endosomolytic micelle core.

Table 5.2. Particle sizes and zeta potential measurements of free polymer micelles and pDNA polyplexes.

Polymer	Polymer Micelle Diameter[a] (nm)	pDNA Polyplex Diameter[b] (nm)	Zeta Potential[c] (mV)
0% Man	17 ± 2	190 ± 5	28 ± 2
25% Man	12 ± 2	200 ± 20	22 ± 3
50% Man	13 ± 2	140 ± 10	16 ± 3
75% Man	13 ± 2	140 ± 10	10 ± 2
100% Man	15 ± 2	140 ± 5	-1 ± 2
Gal	13 ± 2	130 ± 30	-1 ± 3
PEG	15 ± 4	87 ± 17	-11 ± 1

[a] Diameter calculated from number size distribution ± peak half-width
[b] Z-average diameter ± standard deviation
[c] Three experimental runs ± standard deviation

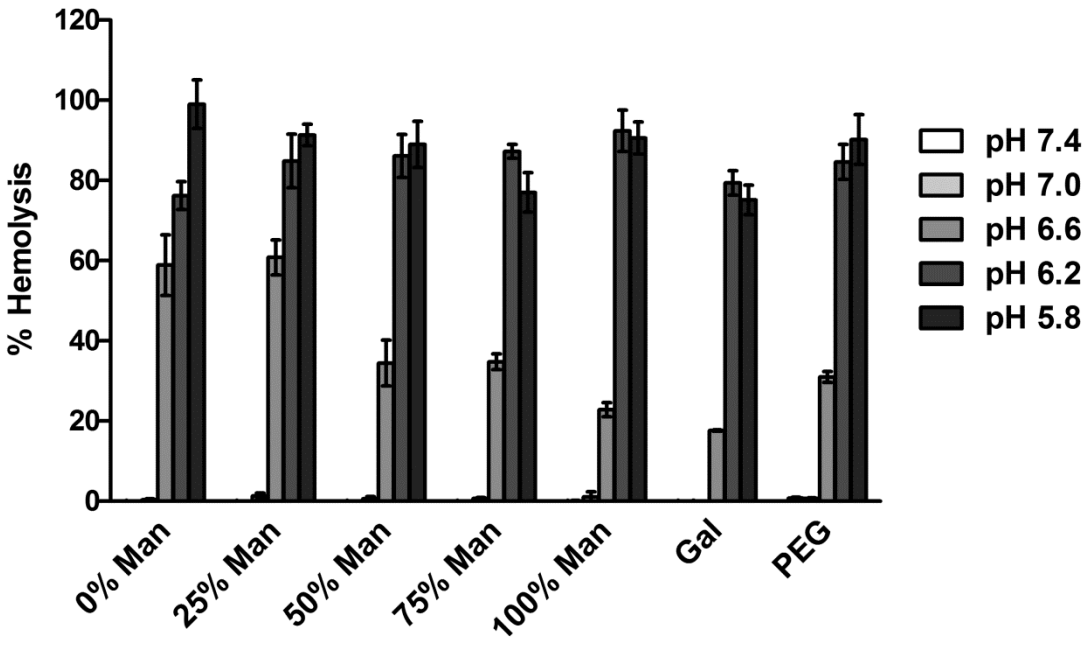

Figure 5.4. Hemolytic activity of polymer micelles. Polymer micelles (20 μg/mL) were incubated with red blood cells at the indicated pH values for 1 h at 37 °C. Hemolytic activities were quantified based on absorbance measurements for hemoglobin release, and are normalized relative to a 1% Triton X-100 positive control. Data are from a single experiment conducted in triplicate ± standard deviation.

3.3. Lectin binding activity by mannosylated glycopolymers

To confirm that the mannosylated glycopolymer series demonstrated lectin-binding capabilities, an agglutination assay was performed using concanavalin A (ConA), a tetrameric lectin recognizing mannose [172]. All polymers incorporating ManEMA (25-100% Man) exhibited binding to ConA, as indicated by an increase in solution turbidity, with higher ManEMA content correlating to a greater degree of agglutination (**Figure 5.5**). Neither 0% Man nor Gal, which contained DMAEMA and GalEMA in their micelle coronas, respectively, demonstrated any binding activity (data not shown for Gal). These results confirm that the mannosylated glycopolymers are uniquely capable of binding mannose-specific lectins.

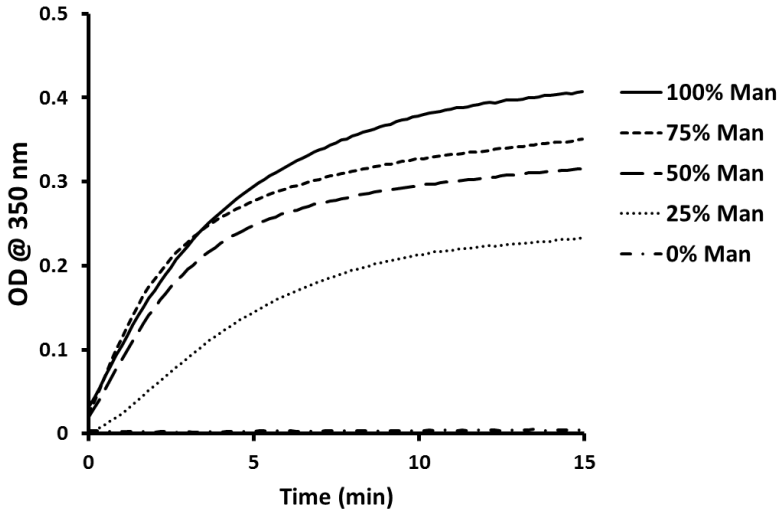

Figure 5.5. Time-dependent agglutination of ConA mediated by mannosylated glycopolymers. Solutions of ConA (100 μg/mL) and glycopolymers (50 μg/mL) were combined, and agglutination activity quantified based on changes in absorbance at 350 nm.

3.4. Characterization of pDNA polyplexes

pDNA polyplexes were formulated by combining polymers with pDNA at a fixed weight ratio (9:1 polymer:pDNA). DLS analysis confirmed that all polymers were capable of condensing pDNA into particulate polyplexes ranging from 87-200 nm in diameter (**Table 5.2**). This result was further validated by a gel retardation assay demonstrating complete retention of pDNA by 0% and 100% Man at this polymer:pDNA ratio (data not shown). Interestingly, polyplex formation was observed in polymers lacking DMAEMA in the micelle corona (100% Man, Gal, PEG), suggesting that the tertiary amines from DEAEMA in the micelle core are also available for pDNA complexation. These DEAEMA groups do not appear to contribute to polyplex surface charge, as zeta potential measurements were positive only for polymers containing DMAEMA (0-75% Man). The zeta potential decreased with increasing ManEMA incorporation, while polymers completely lacking DMAEMA were neutral (100% Man, Gal) or slightly anionic (PEG).

3.5. In vitro transfection and BMDC maturation

An *in vitro* pDNA transfection assay was performed using RAW 264.7 murine macrophages. pDNA polyplexes formulated from mannosylated glycopolymers were incubated with cells for 24 h prior to analysis of cell lysates for GFP fluorescence. While 0% Man polyplexes mediated successful GFP transfection comparable to the Lipofectamine 2000 (LF) positive control, glycopolymers with higher ManEMA incorporation performed poorly, with 50% Man, 75% Man, and 100% Man not differing significantly from the negative control (**Figure 5.6**). Overall, these results indicate that for *in vitro* gene delivery, DMAEMA plays a critical role that cannot be replicated by the potential glycotargeting effects of ManEMA.

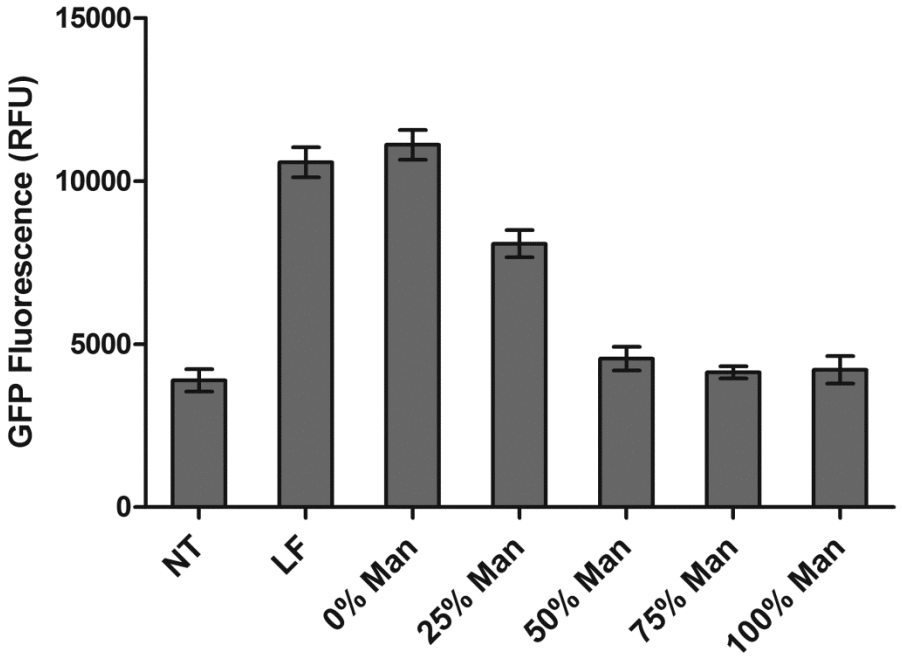

Figure 5.6. *In vitro* transfection of RAW 264.7 macrophages mediated by pDNA polyplexes. Cells were treated with pDNA polyplexes for 24 h, then lysed and analyzed for total GFP fluorescence. Cells receiving no treatment (NT) and treatment with Lipofectamine 2000 (LF) were used as negative and positive controls, respectively. 0% Man and 25% Man are significantly different from NT ($p < 0.05$). Data are from a single experiment conducted in triplicate ± standard deviation.

To determine whether the polymers developed in this study could induce DC maturation, murine BMDCs were cultured for 24 h in the presence of polymer micelles or pDNA polyplexes, then analyzed for the expression of CD80 and CD86. Expression levels for polymer-treated cells were comparable to untreated negative controls, indicating that none of the polymers stimulated BMDC maturation (**Figure 5.7A**, **B**).

3.6. In vivo transfection

To evaluate the efficacy of polymers for *in vivo* gene delivery, luciferase pDNA was administered to mice via subcutaneous injection in polyplexes or as free pDNA. 24 h post-injection, live animal imaging was used to assess the extent of luciferase expression. Luciferase activity was observed at the injection site for animals treated with free pDNA, 100% Man, Gal, and PEG, while no signal was observed in animals treated with 0% Man and 50% Man (**Figure 5.8A**). Transfection levels were highly variable between individual animals in the free pDNA, 100% Man, and Gal groups, such that the only significant differences ($p < 0.05$) observed were between free pDNA and the mannosylated polyplexes (**Figure 5.8B**). These findings suggest that a cationic surface charge is detrimental for *in vivo* gene delivery, as polyplexes formed from 0% Man and 50% Man, both of which had positive zeta potentials due to incorporation of DMAEMA, failed to generate any detectable gene expression. 100% Man, Gal, and PEG polyplexes, which were neutral or anionic, successfully mediated *in vivo* transfection, although the mean luminescence signal from these groups was lower than the mean signal produced by free pDNA.

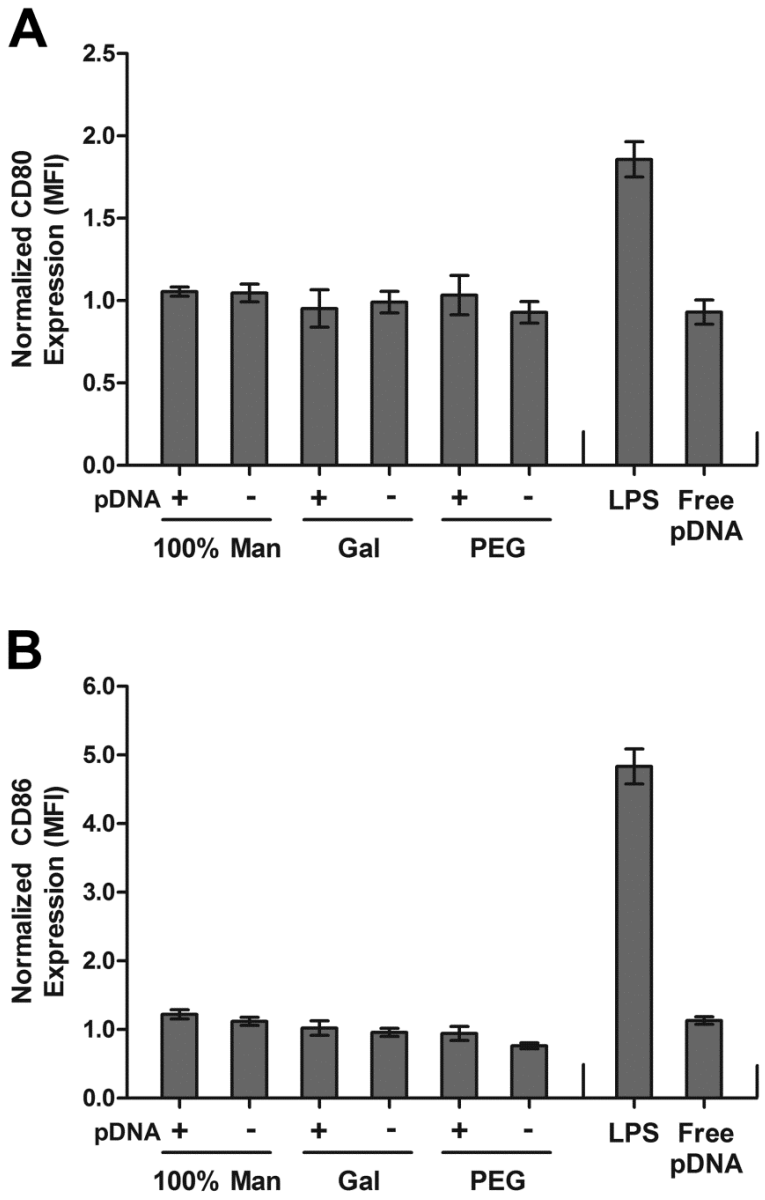

Figure 5.7. *In vitro* BMDC maturation assay. Polymer micelles (pDNA-) or polyplexes (pDNA+) were incubated with BMDCs for 24 h. Cells were analyzed by flow cytometry for expression of (A) CD80 and (B) CD86 as markers for DC maturation. Lipopolysaccharide (LPS, 100 ng/mL) was used as a positive control. Data are normalized to untreated negative controls and are from a single experiment conducted in triplicate ± standard deviation.

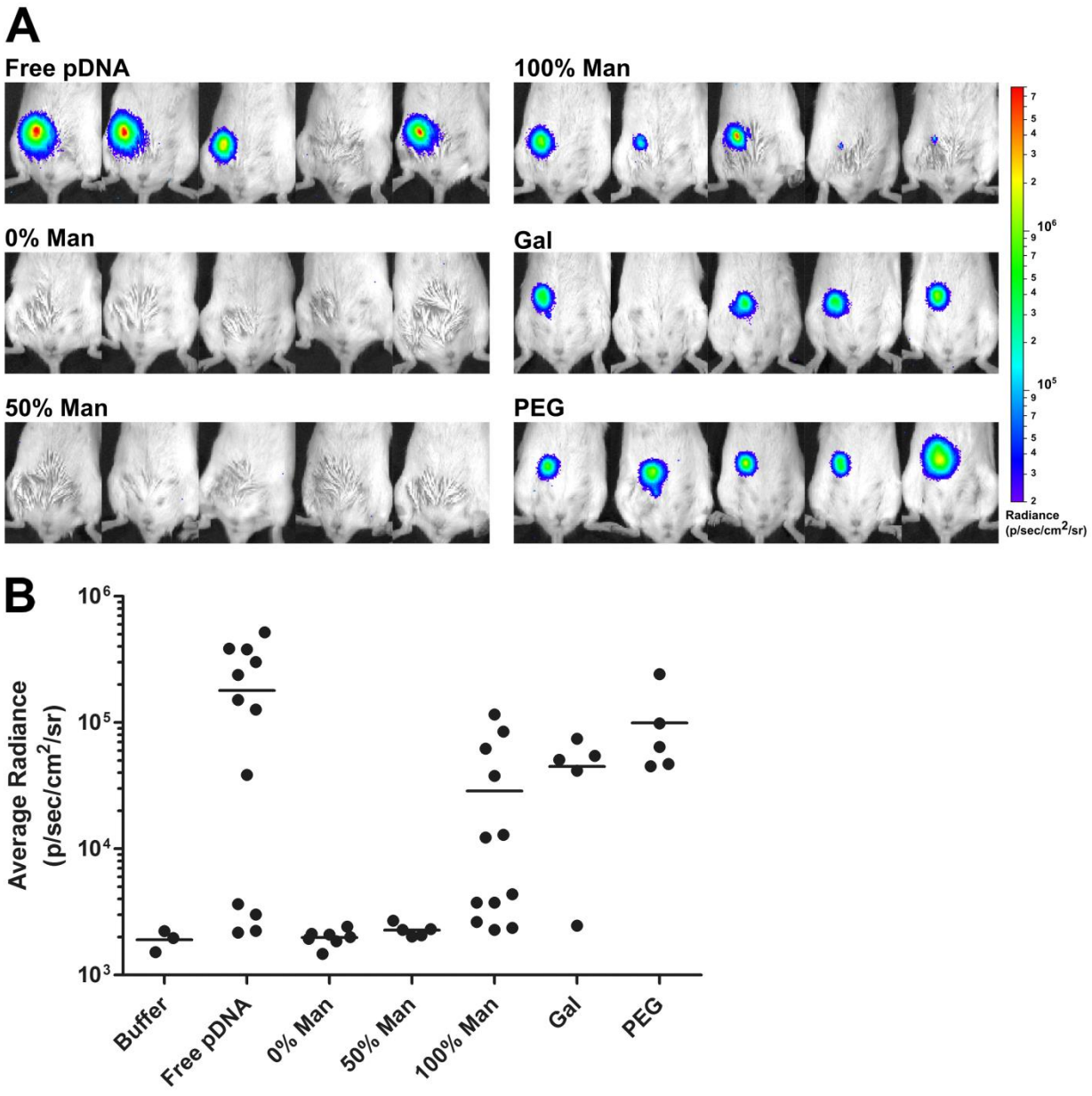

Figure 5.8. *In vivo* luciferase transfection mediated by pDNA polyplexes. Mice were injected subcutaneously with 5 μg free pDNA or pDNA polyplexes (n = 3-12 mice per group). (A) Representative luminescence images of mice at 24 h post-injection. (B) Average luminescence signal at the injection site at 24 h. pDNA is significantly different from 0% Man, 50% Man, and 100% Man ($p < 0.05$).

3.7. Polyplex trafficking to DCs in draining lymph nodes

Since antigen presentation by DCs to T cells in the lymph nodes is a prerequisite to the initiation of adaptive immunity, a trafficking study with Cy5-labeled pDNA was performed to determine whether polyplexes could mediate delivery to DCs in the lymph nodes. Based on the size range of the polyplexes (87-200 nm), it was anticipated that lymph node localization would occur primarily via active trafficking by DCs from the injection site [141–143], and thus the inguinal lymph nodes were analyzed 24 h post-injection to capture this population [141]. Polyplexes formulated with 100% Man generated the highest frequencies of Cy5+ CD11c+ MHCII+ DCs (13.7%), a significant increase compared to PEG (6.6%), free pDNA (5.2%) 0% Man (< 1%) and 50% Man (< 1%) (**Figure 5.9**).

High levels of lymph node DC uptake were also observed with Gal polyplexes (10.2%). Although Gal was not significantly different than 100% Man due to variability within each group, the maximum response for 100% Man was nearly 2-fold higher than the maximum for Gal (23.8% vs. 13.5%). Overall, these findings indicate that glycopolymer micelles enhance pDNA delivery to lymph node DCs, and that incorporation of mannose as a DC-targeting ligand may further improve trafficking efficacy. Additionally, in accordance with *in vivo* transfection results, shielding of cationic polyplex charge is critical for lymph node delivery, as micelles containing DMAEMA groups performed poorly compared to all other polyplex formulations and free pDNA.

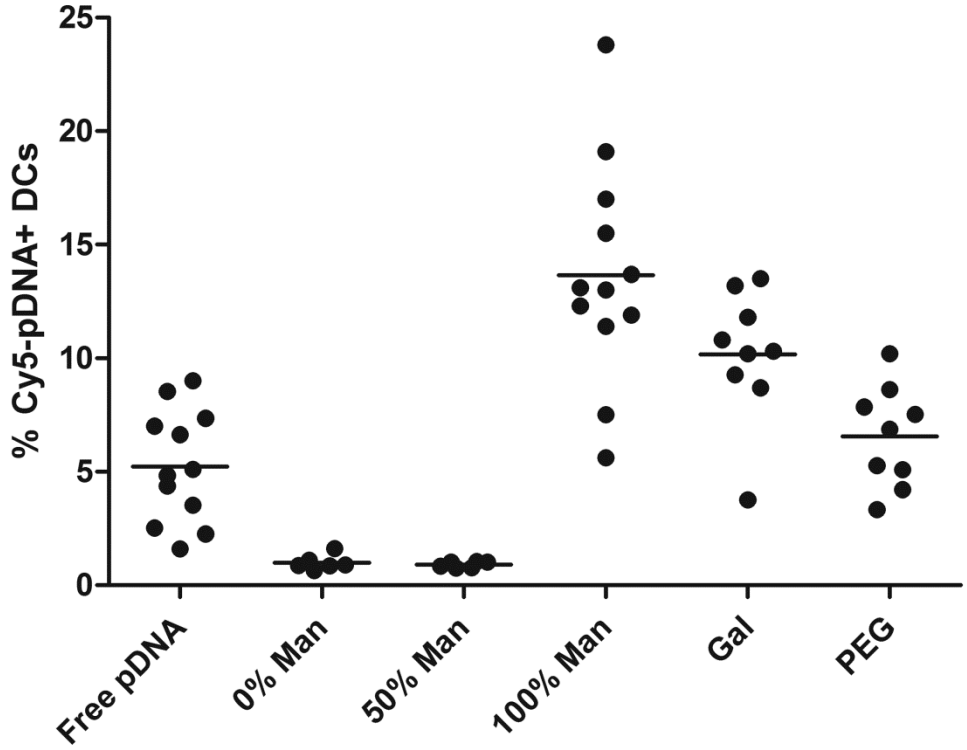

Figure 5.9. pDNA polyplex trafficking to DCs in the draining lymph nodes. Polyplexes were formulated with 5 μg Cy5 pDNA and administered via subcutaneous injection (n = 6-12 mice per group). At 24 h post-injection, inguinal lymph nodes were isolated and the frequency of Cy5+ CD11c+ MHCII+ DCs was determined by flow cytometry. Percent uptake was found to be significantly different for the 100% Man polyplexes as compared to free pDNA, 0% Man, 50% Man, and PEG, while uptake mediated by Gal polyplexes was significantly different from free pDNA, 0% Man, and 50% Man ($p < 0.05$). Uptake mediated by PEG polyplexes was not significant compared to free pDNA.

3.8. Evaluation of immune responses following pDNA vaccination

Based on the lymph node trafficking results, 100% Man, Gal, and PEG polyplexes were further evaluated for efficacy in a pDNA immunization study. Mice received three doses of ovalbumin pDNA at weekly intervals via subcutaneous injection, and were assessed for antibody and T cell responses on day 20 and 21, respectively. No response was observed in any of the experimental groups following *in vitro* splenocyte restimulation and intracellular cytokine staining (data not

shown), suggesting that sensitivity of the assay may be insufficient for this study. Analysis of ovalbumin-specific serum IgG levels revealed that 100% Man generated the highest antibody responses (50.0 ng/mL) compared to free pDNA (12.9 ng/mL), Gal (11.1 ng/mL), and PEG (15.3 ng/mL) (**Figure 5.10**). While the high variability within the 100% Man group underscores the need for additional studies to validate this data, these preliminary results suggest that the use of mannosylated polyplexes for pDNA vaccine delivery can increase the humoral immune response.

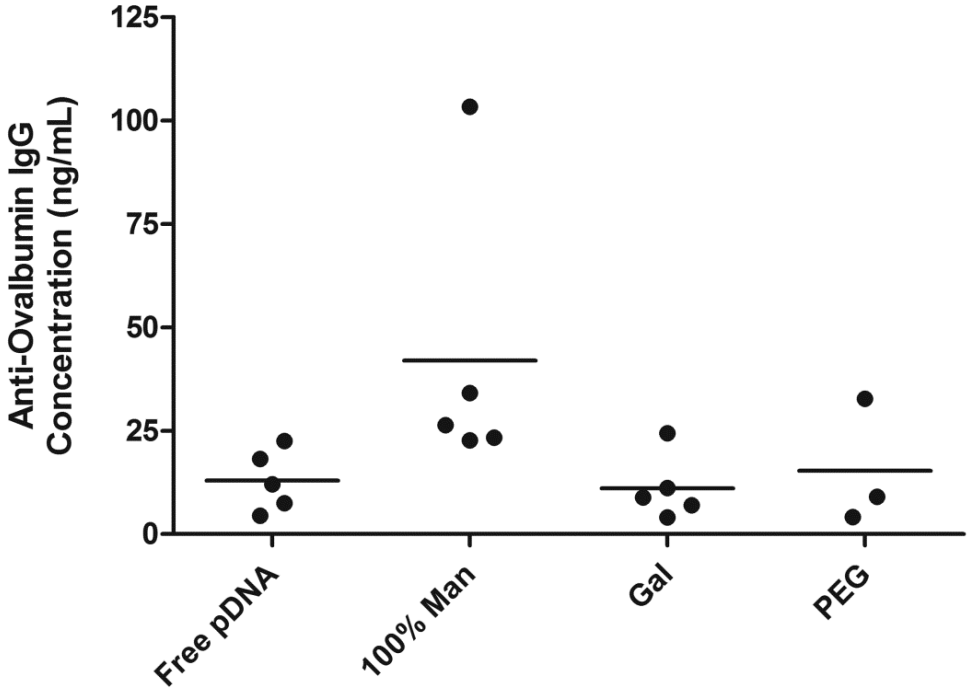

Figure 5.10. Ovalbumin-specific humoral responses in immunized mice. Polyplexes were formulated with 20 μg ovalbumin pDNA and injected subcutaneously on day 0, 7, and 14 (n = 3-5 mice per group). Serum samples were collected on day 20 and analyzed for anti-ovalbumin IgG by ELISA.

4. Discussion

RAFT-based glycopolymers are a highly promising approach for achieving targeted delivery of pDNA vaccines, but studies evaluating the *in vivo* performance of these systems are rare. Here, the development of a series of diblock copolymer micelles incorporating (1) varying ratios of ManEMA and DMAEMA, (2) GalEMA, or (3) PEGMA in the micelle corona is reported. This series was designed to investigate the effect of mannose glycotargeting on pDNA delivery *in vivo*. The core segment of these micelles utilized a pH-responsive copolymer of DEAEMA and BMA that had been previously described for *in vitro* pDNA delivery [72].

Polymeric gene delivery vehicles typically incorporate polycations for the electrostatic condensation of nucleic acids in order to confer protection against nuclease degradation and improve cellular uptake efficiency [26]. DMAEMA-based polymers have been successfully used for the *in vitro* delivery of a variety of nucleic acid therapeutics, including pDNA [72], siRNA [71], and mRNA [171]. However, while polycations have been shown to be extremely effective for *in vitro* models of transfection, recent reports suggest that cationic systems may actually be disadvantageous for *in vivo* delivery. Van den Berg *et al*. compared the expression of cationic lipoplexes and polyplexes *in vitro* and *in vivo*, and observed that while these vehicles generated high levels of expression in cell culture models, expression levels following intradermal administration proved to be significantly lower than that of naked pDNA [133]. PEGylation was sufficient to recover antigen expression and induction of antigen-specific T cell responses. The work of Palumbo *et al*. suggests that this discrepancy may be attributable to the tendency of highly cationic polyplexes to form impenetrable aggregates when injected in the skin, reducing the accessibility of the pDNA cargo for cellular uptake and transfection [135].

The findings here corroborate these studies. In an *in vitro* transfection assay using RAW 264.7 macrophages as a model APC cell line, observed transfection levels correlated negatively with increasing mannosylation and decreasing cationic charge. Although these mannose glycopolymers have been previously demonstrated to enhance *in vitro* and *in vivo* uptake by APCs [170], it appears that polycation-mediated cellular internalization is a stronger determinant of successful *in vitro* transfection. However, the exact opposite trend was observed when these polymers were evaluated for subcutaneous delivery in mice: all polyplexes incorporating DMAEMA failed to generate any detectable transfection, while mannosylated, galactosylated, and PEGylated polyplexes, which exhibited neutral or negative zeta potentials, successfully mediated expression. Unexpectedly, free pDNA produced the highest levels of *in vivo* transfection, despite being consistently ineffective *in vitro* (unpublished observations). Phua *et al*. observed a similar phenomenon when comparing naked mRNA to nanoparticulate mRNA, but noted that this trend only held for subcutaneous delivery, suggesting that this delivery route may be less favorable for materials-mediated transfection [136].

For vaccination applications, however, the link between local tissue transfection and immunogenicity is unclear. While it is possible that transfected "bystander" cells such as fibroblasts and keratinocytes may produce antigen for subsequent capture by DCs [5], achieving direct vaccine targeting to DCs remains the most certain method for inducing an immune response. Therefore, the vaccine potential of the glycopolymers was evaluated by investigating the efficacy of pDNA delivery to DCs in the draining lymph nodes. Polyplexes formulated with the 100% Man polymer demonstrated the highest uptake by lymph node DCs, outperforming free pDNA and PEGylated polyplexes by 2.6- and 2.1-fold, respectively. This is the first report of a

RAFT glycopolymer being used to enhance pDNA delivery to DCs in the lymph node. No uptake was observed for cationic polyplexes, further validating previous observations on the poor *in vivo* delivery characteristics of polycations.

Intriguingly, galactosylated polyplexes exhibited DC uptake rates comparable to mannosylated polyplexes, although the maximum uptake frequency for mannose was considerably higher than the maximum for galactose, suggesting that mannose glycotargeting may provide some additional benefit. While mannose has been the primary carbohydrate ligand explored for DC targeting, galactose may also play a role: the macrophage galactose-type lectin (MGL) is expressed on immature DCs and recognizes galactose-related structures [173,174].

These findings indicate that RAFT-based glycopolymers are a highly promising platform for enhancing *in vivo* pDNA delivery for vaccination applications. Most recently, preliminary immunization studies demonstrated the potential of mannosylated micelles for inducing antigen-specific antibody responses. Recommendations for future studies are to (1) further characterize the *in vivo* activity of glycopolymer polyplexes, quantifying uptake by specific DC subsets and *in situ* DC transfection, (2) optimize immunization protocols to increase the immunogenicity of glycopolymer polyplex vaccines, and (3) investigate the application of this delivery platform for use with other vaccine therapeutics, such as mRNA.

5. Conclusions

Achieving targeted delivery to DCs is a highly promising approach for improving the efficacy of pDNA vaccines. RAFT synthesis was used to develop a series of glycopolymer micelles

incorporating pendent mannose groups for enhancing uptake by DCs. Micelles incorporated a pH-responsive DEAEMA-*co*-BMA core segment to enable cytosolic delivery of the pDNA cargo. Following subcutaneous administration, glycotargeted polyplexes exhibited superior local tissue transfection and trafficking to lymph node DCs compared to conventional cationic polyplexes, demonstrating the potential of this platform for the delivery of pDNA vaccine therapeutics.

Chapter 6

Overall conclusions

1. Summary of findings

Nucleic acid vaccine technology holds significant potential as a versatile strategy for the treatment of a wide variety of diseases. Numerous research efforts have focused on improving the clinical performance of these therapeutics through the use of carrier systems to facilitate vaccine delivery to DCs. The goal of this work was to utilize RAFT synthetic methodologies to develop block copolymers for the delivery of two classes of nucleic acid therapeutics, mRNA and pDNA, and evaluate their *in vitro* and *in vivo* performance as vaccine vehicles.

1.1. Development of multifunctional block copolymers for mRNA delivery

mRNA is generating enormous research interest as an alternative to pDNA for nucleic acid-based vaccination strategies, but the existing literature on mRNA-specific delivery strategies is limited. A series of multifunctional block copolymers were developed in order to explore the effect of varying polymer architectures on mRNA delivery efficacy. These polymers were composed of three discrete segments: (1) DMAEMA for the electrostatic condensation of mRNA, (2) PEGMA for improving polyplex stability and biocompatibility, and (3) DEAEMA-co-BMA for enhancement of endolysosomal escape. In *in vitro* studies, the D-P-E blocking order was observed to be particularly favorable for intracellular delivery to hard-to-transfect APCs, a phenomenon that appeared to be correlated with the increased polyplex stability conferred by this polymer architecture. Furthermore, these polymers demonstrated the ability to

deliver a model mRNA vaccine vector to DCs for presentation and activation of T cells, a promising result that motivated the decision to investigate these polymers for *in vivo* delivery. However, the performance of these mRNA polyplexes in mouse models was unsatisfactory. Initial studies indicated that, following subcutaneous administration, mRNA polyplexes failed to mediate any observable local tissue transfection or mediate mRNA trafficking to lymph node DCs. Hypothetically, the incorporation of PEGMA to reduce cationic charge might be sufficient to improve *in vivo* delivery efficacy [133], but the findings here indicate that more significant refinements in polymer design are needed.

1.2. Evaluation of glycopolymer micelles for in vivo pDNA vaccine delivery

Glycotargeted polymer vehicles are a promising approach for enhancing vaccine delivery to DCs, the primary cell type of interest for vaccination-based therapies. A series of glycopolymer micelles were developed with DEAEMA-*co*-BMA in the micelle core and varying corona compositions: (1) ManEMA copolymerized with DMAEMA at varying molar ratios, (2) GalEMA as an untargeted glycopolymer control, and (3) PEGMA, as an untargeted nonglycosylated control. Initially, *in vitro* transfection results suggested that mannosylated polyplexes performed poorly relative to traditional cationic polyplexes. However, when applied to mice via subcutaneous injection, noncationic polyplexes successfully mediated pDNA transfection, while cationic polyplexes did not. Furthermore, mannosylated and galactosylated polyplexes exhibited superior trafficking to lymph node DCs compared to uncomplexed pDNA, indicating that glycotargeted micelles were capable of enhancing vaccine delivery to immunologically relevant cell types. Most recently, a preliminary immunization study demonstrated that mannosylated polyplexes induced higher antigen-specific humoral responses

compared to free pDNA and other polyplex formulations. These findings indicate that mannosylated polymer micelles are a promising platform for the *in vivo* delivery of pDNA and other nucleic acid vaccine therapeutics.

2. Conclusions

2.1. Utility of RAFT-based block copolymers as multifunctional delivery vehicles

These studies demonstrate the versatility of the RAFT synthetic methodology for the development of well-defined gene delivery vectors with complex architectures. A wide variety of polymer designs were investigated, and the findings confirmed that the resultant block copolymers exhibited the expected functional activities, *e.g.* pH-triggered membrane disruption, enhancement of polyplex stability, recognition of carbohydrate-specific lectins. Future work with RAFT-based vehicles could potentially explore other functionalities that would further improve vaccine efficacy, such as co-delivery of adjuvants for increased immunogenicity or incorporation of biodegradable segments for controlled release of the nucleic acid cargo.

2.2. Design considerations for polymeric gene delivery systems

In this work, the most successful delivery vectors incorporated neutral hydrophilic monomers that reduced the overall cationic charge. The PEGMA triblock copolymers, although ultimately unsuccessful for *in vivo* delivery, demonstrated superior polyplex stability and mRNA transfection *in vitro* compared to their unPEGylated counterpart. More significantly, mannosylated and galactosylated micelles outperformed cationic micelles for *in vivo* pDNA transfection and delivery to lymph node DCs. These findings have important implications for

gene delivery vector design given that the majority of polymeric carrier systems currently described in the literature are highly cationic. While such vehicles may be effective in cell culture models, the studies here indicate that cationic surface charge is detrimental for gene delivery *in vivo*, an observation that has been corroborated by other groups [133,135]. These results suggest a more promising polymer design: the glycopolymer micelles contain cationic units in the micelle core, but not the corona, thus enabling nucleic acid condensation while maintaining a neutral zeta potential.

An important caveat to be noted is that neutralization of cationic charge can adversely affect vaccine efficacy. Carstens *et al*. observed that while PEGylated liposomes demonstrated enhanced lymphatic trafficking, they did not generate higher immune responses, potentially due to reduced residence times in the lymph nodes [175]. The incorporation of DC targeting functionalities or vaccine adjuvants may be necessary in order to achieve an optimal balance between favorable *in vivo* biodistribution and sufficient vaccine immunogenicity. The mannosylated glycopolymers developed here appear to fulfill both criteria, by mediating improved pDNA delivery to lymph node DCs as well as eliciting higher humoral responses. Based on these promising findings, the mannosylated glycopolymer design merits further investigation in order to optimize its immunization efficacy and explore its potential for the delivery of other nucleic acid therapeutics.

References

1. Tang D, DeVit M, Johnston SA. Genetic immunization is a simple method for eliciting an immune response. Nature 1992;356:152–4.

2. Ulmer JB, Donnelly JJ, Parker SE, Rhodes GH, Felgner PL, Dwarki VJ, et al. Heterologous protection against influenza by injection of DNA encoding a viral protein. Science 1993;259:1745–9.

3. Kutzler MA, Weiner DB. DNA vaccines: ready for prime time? Nat Rev Genet 2008;9:776–88.

4. Liu MA. DNA vaccines: a review. J Intern Med 2003;253:402–10.

5. Gurunathan S, Klinman DM, Seder RA. DNA vaccines: immunology, application, and optimization. Ann Rev Immunol 2000;18:927–74.

6. Weide B, Garbe C, Rammensee H-G, Pascolo S. Plasmid DNA- and messenger RNA-based anti-cancer vaccination. Immunol Lett 2008;115:33–42.

7. Steinman RM, Banchereau J. Taking dendritic cells into medicine. Nature 2007;449:419–26.

8. Mellman I, Steinman RM. Dendritic cells: specialized and regulated antigen processing machines. Cell 2001;106:255–8.

9. Banchereau J, Briere F, Caux C, Davoust J, Lebecque S, Liu YJ, et al. Immunobiology of dendritic cells. Ann Rev Immunol 2000;18:767–811.

10. Shedlock DJ, Weiner DB. DNA vaccination: antigen presentation and the induction of immunity. J Leukoc Biol 2000;68:793–806.

11. Donnelly JJ, Wahren B, Liu MA. DNA vaccines: progress and challenges. J Immunol 2005;175:633–9.

12. Laddy DJ, Weiner DB. From plasmids to protection: a review of DNA vaccines against infectious diseases. Int Rev Immunol 2006;25:99–123.

13. Wolff JA, Malone RW, Williams P, Chong W, Acsadi G, Jani A, et al. Direct gene transfer into mouse muscle in vivo. Science 1990;247:1465–8.

14. Davidson A, Traub-Dargatz J, Rodeheaver R, Ostlund E, Pederson D, Moorhead R, et al. Immunologic responses to West Nile virus in vaccinated and clinically affected horses. J Am Vet Med Assoc 2005;226:240–5.

15. Garver K, LaPatra S, Kurath G. Efficacy of an infectious hematopoietic necrosis (IHN) virus DNA vaccine in Chinook *Oncorhynchus tshawytscha* and sockeye *O. nerka* salmon. Dis Aquat Organ 2005;64:13–22.

16. Bergman P, Camps-Palau M, McKnight J, Leibman N, Craft D, Leung C, et al. Development of a xenogeneic DNA vaccine program for canine malignant melanoma at the Animal Medical Center. Vaccine 2006;24:4582–5.

17. Saade F, Petrovsky N. Technologies for enhanced efficacy of DNA vaccines. Expert Rev Vaccines 2012;11:189–209.

18. Ramshaw IA, Ramsay AJ. The prime-boost strategy: exciting prospects for improved vaccination. Immunol Today 2000;21:163–5.

19. Wells DJ. Gene therapy progress and prospects: electroporation and other physical methods. Gene Ther 2004;11:1363–9.

20. Greenland JR, Letvin NL. Chemical adjuvants for plasmid DNA vaccines. Vaccine 2007;25:3731–41.

21. Hubbell JA, Thomas SN, Swartz MA. Materials engineering for immunomodulation. Nature 2009;462:449–60.

22. Yamamoto A, Kormann M, Rosenecker J, Rudolph C. Current prospects for mRNA gene delivery. Eur J Pharm Biopharm 2009;71:484–9.

23. Tavernier G, Andries O, Demeester J, Sanders NN, De Smedt SC, Rejman J. mRNA as gene therapeutic: How to control protein expression. J Control Release 2011;150:238–47.

24. Pollard H, Remy JS, Loussouarn G, Demolombe S, Behr JP, Escande D. Polyethylenimine but not cationic lipids promotes transgene delivery to the nucleus in mammalian cells. J Biol Chem 1998;273:7507–11.

25. Zabner J, Fasbender AJ, Moninger T, Poellinger KA, Welsh MJ. Cellular and molecular barriers to gene transfer by a cationic lipid. J Biol Chem 1995;270:18997–9007.

26. Pack DW, Hoffman AS, Pun S, Stayton PS. Design and development of polymers for gene delivery. Nat Rev Drug Discov 2005;4:581–93.

27. Zou S, Scarfo K, Nantz MH, Hecker JG. Lipid-mediated delivery of RNA is more efficient than delivery of DNA in non-dividing cells. Int J Pharm 2010;389:232–43.

28. Van Tendeloo VFI, Ponsaerts P, Lardon F, Nijs G, Lenjou M, Van Broeckhoven C, et al. Highly efficient gene delivery by mRNA electroporation in human hematopoietic cells: superiority to lipofection and passive pulsing of mRNA and to electroporation of plasmid cDNA for tumor antigen loading of dendritic cells. Blood 2001;98:49–56.

29. Elouahabi A, Ruysschaert J-M. Formation and intracellular trafficking of lipoplexes and polyplexes. Mol Ther 2005;11:336–47.

30. Pascolo S. Messenger RNA-based vaccines. Expert Opin Biol Ther 2004;4:1285–94.

31. Martinon F, Krishnan S, Lenzen G, Magné R, Gomard E, Guillet J-G, et al. Induction of virus-specific cytotoxic T lymphocytes in vivo by liposome-entrapped mRNA. Eur J Immunol 1993;23:1719–22.

32. Boczkowski D, Nair SK, Snyder D, Gilboa E. Dendritic cells pulsed with RNA are potent antigen-presenting cells in vitro and in vivo. J Exp Med 1996;184:465–72.

33. Saenz-Badillos J, Amin SP, Granstein RD. RNA as a tumor vaccine: a review of the literature. Exp Dermatol 2001;10:143–54.

34. Ponsaerts P, Van Tendeloo VFI, Berneman ZN. Cancer immunotherapy using RNA-loaded dendritic cells. Clin Exp Immunol 2003;134:378–84.

35. Gilboa E, Vieweg J. Cancer immunotherapy with mRNA-transfected dendritic cells. Immunol Rev 2004;199:251–63.

36. Grünebach F, Müller MR, Brossart P. New developments in dendritic cell-based vaccinations: RNA translated into clinics. Cancer Immunol Immunother 2005;54:517–25.

37. Kyte JA, Gaudernack G. Immuno-gene therapy of cancer with tumour-mRNA transfected dendritic cells. Cancer Immunol Immunother 2006;55:1432–42.

38. Kreiter S, Diken M, Selmi A, Türeci Ö, Sahin U. Tumor vaccination using messenger RNA: prospects of a future therapy. Curr Opin Immunol 2011;23:399–406.

39. Heiser A, Coleman D, Dannull J, Yancey D, Maurice MA, Lallas CD, et al. Autologous dendritic cells transfected with prostate-specific antigen RNA stimulate CTL responses against metastatic prostate tumors. J Clin Invest 2002;109:311–2.

40. Su Z, Dannull J, Heiser A, Dendritic TR, Yancey D, Pruitt S, et al. Immunological and clinical responses in metastatic renal cancer patients vaccinated with tumor RNA-transfected dendritic cells. Cancer Res 2003;63:2127–33.

41. Nair SK, Morse M, Boczkowski D, Cumming RI, Vasovic L, Gilboa E, et al. Induction of tumor-specific cytotoxic T lymphocytes in cancer patients by autologous tumor RNA-transfected dendritic cells. Ann Surg 2002;235:540–9.

42. Rains N, Cannan RJ, Chen W, S SR. Development of a dendritic cell (DC)-based vaccine for patients with advanced colorectal cancer. Hepatogastroenterology 2001;48:347–51.

43. Morse MA, Nair SK, Boczkowski D, Tyler D, Hurwitz HI, Proia A, et al. The feasibility and safety of immunotherapy with dendritic cells loaded with CEA mRNA following neoadjuvant chemoradiotherapy and resection of pancreatic cancer. Int J Gastrointest Cancer 2002;32:1–6.

44. Morse MA, Nair SK, Mosca PJ, Hobeika AC, Clay TM, Deng Y, et al. Immunotherapy with autologus, human dendritic cells transfected with carcinoembryonic antigen mRNA. Cancer Invest 2003;21:341–9.

45. Caruso DA, Orme LM, Neale AM, Radcliff FJ, Amor GM, Maixner W, et al. Results of a phase 1 study utilizing monocyte-derived dendritic cells pulsed with tumor RNA in children and young adults with brain cancer. Neuro Oncol 2004;6:236–46.

46. Caruso DA, Orme LM, Amor GM, Neale AM, Radcliff FJ, Downie P, et al. Results of a Phase I study utilizing monocyte-derived dendritic cells pulsed with tumor RNA in children with Stage 4 neuroblastoma. Cancer 2005;103:1280–91.

47. Weide B, Carralot J-P, Reese A, Scheel B, Eigentler TK, Hoerr I, et al. Results of the first phase I/II clinical vaccination trial with direct injection of mRNA. J Immunother 2008;31:180–8.

48. Rittig SM, Haentschel M, Weimer KJ, Heine A, Muller MR, Brugger W, et al. Intradermal vaccinations with RNA coding for TAA generate CD8+ and CD4+ immune responses and induce clinical benefit in vaccinated patients. Mol Ther 2011;19:990–9.

49. Su Z, Dannull J, Yang BK, Dahm P, Coleman D, Yancey D, et al. Telomerase mRNA-transfected dendritic cells stimulate antigen-specific CD8+ and CD4+ T cell responses in patients with metastatic prostate cancer. J Immunol 2005;174:3798–807.

50. Mu LJ, Kyte JA, Kvalheim G, Aamdal S, Dueland S, Hauser M, et al. Immunotherapy with allotumour mRNA-transfected dendritic cells in androgen-resistant prostate cancer patients. Br J Cancer 2005;93:749–56.

51. Kyte JA, Mu L, Aamdal S, Kvalheim G, Dueland S, Hauser M, et al. Phase I/II trial of melanoma therapy with dendritic cells transfected with autologous tumor-mRNA. Cancer Gene Ther 2006;13:905–18.

52. Dannull J, Su Z, Rizzieri D, Yang BK, Coleman D, Yancey D, et al. Enhancement of vaccine-mediated antitumor immunity in cancer patients after depletion of regulatory T cells. J Clin Invest 2005;115:3623–33.

53. Schuurhuis DH, Verdijk P, Schreibelt G, Aarntzen EHJG, Scharenborg N, De Boer A, et al. In situ expression of tumor antigens by messenger RNA-electroporated dendritic cells in lymph nodes of melanoma patients. Cancer Res 2009;69:2927–34.

54. Kobayashi T, Yamanaka R, Homma J, Tsuchiya N, Yajima N, Yoshida S, et al. Tumor mRNA-loaded dendritic cells elicit tumor-specific CD8+ cytotoxic T cells in patients with malignant glioma. Cancer Immunol Immunother 2003;52:632–7.

55. Petsch B, Schnee M, Vogel AB, Lange E, Hoffmann B, Voss D, et al. Protective efficacy of in vitro synthesized, specific mRNA vaccines against influenza A virus infection. Nat Biotechnol 2012;30:1210–6.

56. Zarei S, Arrighi J-F, Ongaro G, Calzascia T, Haller O, Frossard C, et al. Efficient induction of CD8 T-associated immune protection by vaccination with mRNA transfected dendritic cells. J Invest Dermatol 2003;121:745–50.

57. Yu H, Babiuk LA, Van Drunen Littel-van den Hurk S. Immunity and protection by adoptive transfer of dendritic cells transfected with hepatitis C NS3/4A mRNA. Vaccine 2007;25:1701–11.

58. Dell K, Klein C, Gissmann L. Comparison of DNA- and mRNA-transfected mouse dendritic cells as potential vaccines against the human papillomavirus type 16 associated oncoprotein E7. Antivir Ther 2008;13:495–509.

59. Pollard C, Rejman J, De Haes W, Verrier B, Van Gulck E, Naessens T, et al. Type I IFN counteracts the induction of antigen-specific immune responses by lipid-based delivery of mRNA vaccines. Mol Ther 2012;21:251–9.

60. Roesler E, Weiss R, Weinberger EE, Fruehwirth A, Stoecklinger A, Mostböck S, et al. Immunize and disappear-safety-optimized mRNA vaccination with a panel of 29 allergens. J Allergy Clin Immunol 2009;124:1070–7.

61. Nguyen DN, Green JJ, Chan JM, Langer R, Anderson DG. Polymeric materials for gene delivery and DNA vaccination. Adv Mater 2009;21:847–67.

62. De Smedt SC, Demeester J, Hennink WE. Cationic polymer based gene delivery systems. Pharm Res 2000;17:113–26.

63. Morille M, Passirani C, Vonarbourg A, Clavreul A, Benoit J-P. Progress in developing cationic vectors for non-viral systemic gene therapy against cancer. Biomaterials 2008;29:3477–96.

64. Merdan T, Kopecek J, Kissel T. Prospects for cationic polymers in gene and oligonucleotide therapy against cancer. Adv Drug Deliver Rev 2002;54:715–58.

65. Foged C, Sundblad A, Hovgaard L. Targeting vaccines to dendritic cells. Pharm Res 2002;19:229–38.

66. Tacken PJ, De Vries IJM, Torensma R, Figdor CG. Dendritic-cell immunotherapy: from ex vivo loading to in vivo targeting. Nat Rev Immunol 2007;7:790–802.

67. Mukherjee S, Ghosh RN, Maxfield FR. Endocytosis. Physiol Rev 1997;77:759–803.

68. Gruenberg J, Van der Goot FG. Mechanisms of pathogen entry through the endosomal compartments. Nat Rev Mol Cell Bio 2006;7:495–504.

69. Varkouhi AK, Scholte M, Storm G, Haisma HJ. Endosomal escape pathways for delivery of biologicals. J Control Release 2011;151:220–8.

70. Sonawane ND, Szoka FC, Verkman AS. Chloride accumulation and swelling in endosomes enhances DNA transfer by polyamine-DNA polyplexes. J Biol Chem 2003;278:44826–31.

71. Convertine AJ, Benoit DSW, Duvall CL, Hoffman AS, Stayton PS. Development of a novel endosomolytic diblock copolymer for siRNA delivery. J Control Release 2009;133:221–9.

72. Manganiello MJ, Cheng C, Convertine AJ, Bryers JD, Stayton PS. Diblock copolymers with tunable pH transitions for gene delivery. Biomaterials 2012;33:2301–9.

73. Okuda T, Niidome T, Aoyagi H. Cytosolic soluble proteins induce DNA release from DNA-gene carrier complexes. J Control Release 2004;98:325–32.

74. Huth S, Hoffmann F, Gersdorff K Von, Laner A, Reinhardt D, Rosenecker J, et al. Interaction of polyamine gene vectors with RNA leads to the dissociation of plasmid DNA-carrier complexes. J Gene Med 2006;8:1416–24.

75. Iida T, Mori T, Katayama Y, Niidome T. Overall interaction of cytosolic proteins with the PEI/DNA complex. J Control Release 2007;118:364–9.

76. Schaffer D V, Fidelman NA, Dan N, Lauffenburger DA. Vector unpacking as a potential barrier for receptor-mediated polyplex gene delivery. Biotechnol Bioeng 2000;67:598–606.

77. Wong S, Pelet J, Putnam D. Polymer systems for gene delivery - past, present, and future. Prog Polym Sci 2007;32:799–837.

78. Cartier R, Reszka R. Utilization of synthetic peptides containing nuclear localization signals for nonviral gene transfer systems. Gene Ther 2002;9:157–67.

79. Dean DA, Strong DD, Zimmer WE. Nuclear entry of nonviral vectors. Gene Ther 2005;12:881–90.

80. Xu FJ, Yang WT. Polymer vectors via controlled/living radical polymerization for gene delivery. Prog Polym Sci 2011;36:1099–131.

81. Mishra S, Webster P, Davis ME. PEGylation significantly affects cellular uptake and intracellular trafficking of non-viral gene delivery particles. Eur J Cell Bio 2004;83:97–111.

82. Kakizawa Y, Kataoka K. Block copolymer micelles for delivery of gene and related compounds. Adv Drug Deliver Rev 2002;54:203–22.

83. York AW, Kirkland SE, McCormick CL. Advances in the synthesis of amphiphilic block copolymers via RAFT polymerization: stimuli-responsive drug and gene delivery. Adv Drug Deliver Rev 2008;60:1018–36.

84. Gary DJ, Lee H, Sharma R, Lee J-S, Kim Y, Cui ZY, et al. Influence of nano-carrier architecture on in vitro siRNA delivery performance and in vivo biodistribution: polyplexes vs micelleplexes. ACS Nano 2011;5:3493–505.

85. Chu DSH, Schellinger JG, Shi J, Convertine AJ, Stayton PS, Pun SH. Application of living free radical polymerization for nucleic acid delivery. Acc Chem Res 2012;45:1089–99.

86. Chiefari J, Chong YK, Ercole F, Krstina J, Jeffery J, Le TPT, et al. Living free-radical polymerization by reversible addition-fragmentation chain transfer: the RAFT process. Macromolecules 1998;31:5559–62.

87. Bettinger T, Carlisle RC, Read ML, Ogris M, Seymour LW. Peptide-mediated RNA delivery: a novel approach for enhanced transfection of primary and post-mitotic cells. Nucleic Acids Res 2001;29:3882–91.

88. Rejman J, Tavernier G, Bavarsad N, Demeester J, De Smedt SC. mRNA transfection of cervical carcinoma and mesenchymal stem cells mediated by cationic carriers. J Control Release 2010;147:385–91.

89. Parker AL, Seymour LW. Targeting of polyelectrolyte RNA complexes to cell surface integrins as an efficient cytoplasmic transfection mechanism. J Bioact Compat Pol 2002;17:229–38.

90. Read ML, Singh S, Ahmed Z, Stevenson M, Briggs SS, Oupicky D, et al. A versatile reducible polycation-based system for efficient delivery of a broad range of nucleic acids. Nucleic Acids Res 2005;33:e86.

91. Üzgün S, Nica G, Pfeifer C, Bosinco M, Michaelis K, Lutz J-F, et al. PEGylation improves nanoparticle formation and transfection efficiency of messenger RNA. Pharm Res 2011;28:2223–32.

92. Debus H, Baumhof P, Probst J, Kissel T. Delivery of messenger RNA using poly(ethylene imine)-poly(ethylene glycol)-copolymer blends for polyplex formation: biophysical characterization and in vitro transfection properties. J Control Release 2010;148:334–43.

93. Uchida S, Itaka K, Uchida H, Hayakawa K, Ogata T, Ishii T, et al. In vivo messenger RNA introduction into the central nervous system using polyplex nanomicelle. PLOS ONE 2013;8:1–8.

94. Manickam DS, Li J, Putt DA, Zhou Q-H, Wu C, Lash LH, et al. Effect of innate glutathione levels on activity of redox-responsive gene delivery vectors. J Control Release 2010;141:77–84.

95. Su X, Fricke J, Kavanagh DG, Irvine DJ. In vitro and in vivo mRNA delivery using lipid-enveloped pH-responsive polymer nanoparticles. Mol Pharm 2011;8:774–87.

96. Mockey M, Bourseau E, Chandrashekhar V, Chaudhuri A, Lafosse S, Le Cam E, et al. mRNA-based cancer vaccine: prevention of B16 melanoma progression and metastasis by systemic injection of MART1 mRNA histidylated lipopolyplexes. Cancer Gene Ther 2007;14:802–14.

97. Xiong X-B, Falamarzian A, Garg SM, Lavasanifar A. Engineering of amphiphilic block copolymers for polymeric micellar drug and gene delivery. J Control Release 2011;155:248–61.

98. Oishi M, Kataoka K, Nagasaki Y. pH-responsive three-layered PEGylated polyplex micelle based on a lactosylated ABC triblock copolymer as a targetable and endosome-disruptive nonviral gene vector. Bioconjugate Chem 2006;17:677–88.

99. Fukushima S, Miyata K, Nishiyama N, Kanayama N, Yamasaki Y, Kataoka K. PEGylated polyplex micelles from triblock catiomers with spatially ordered layering of condensed pDNA and buffering units for enhanced intracellular gene delivery. J Am Chem Soc 2005;127:2810–1.

100. Miyata K, Oba M, Kano MR, Fukushima S, Vachutinsky Y, Han M, et al. Polyplex micelles from triblock copolymers composed of tandemly aligned segments with biocompatible, endosomal escaping, and DNA-condensing functions for systemic gene delivery to pancreatic tumor tissue. Pharm Res 2008;25:2924–36.

101. Sharma R, Lee J-S, Bettencourt RC, Xiao C, Konieczny SF, Won Y-Y. Effects of the incorporation of a hydrophobic middle block into a PEG-polycation diblock copolymer on the physicochemical and cell interaction properties of the polymer-DNA complexes. Biomacromolecules 2008;9:3294–307.

102. Dai J, Zou S, Pei Y, Cheng D, Ai H, Shuai X. Polyethylenimine-grafted copolymer of poly(l-lysine) and poly(ethylene glycol) for gene delivery. Biomaterials 2011;32:1694–705.

103. Yuan Z-F, Li F, Ma M, Cheng S-X, Zhuo R-X. Synthesis and characterization of poly(ethylene glycol)-b- poly(ε-caprolactone)-b-poly(2-(2-aminoethyl amino)ethyl

methacrylate) triblock copolymers as efficient gene delivery vectors. J Appl Polym Sci 2011;121:666–74.

104. Zhang W, He J, Liu Z, Ni P, Zhu X. Biocompatible and pH-responsive triblock copolymer mPEG-b-PCL-b-PDMAEMA: synthesis, self-assembly, and application. J Polym Sci A Polym Chem 2010;48:1079–91.

105. Sun T-M, Du J-Z, Yan L-F, Mao H-Q, Wang J. Self-assembled biodegradable micellar nanoparticles of amphiphilic and cationic block copolymer for siRNA delivery. Biomaterials 2008;29:4348–55.

106. Liu Y, Samsonova O, Sproat B, Merkel O, Kissel T. Biophysical characterization of hyper-branched polyethylenimine-graft-polycaprolactone-block-mono-methoxyl-poly(ethylene glycol) copolymers (hy-PEI-PCL-mPEG) for siRNA delivery. J Control Release 2011;153:262–8.

107. Segura T, Hubbell JA. Synthesis and in vitro characterization of an ABC triblock copolymer for siRNA delivery. Bioconjugate Chem 2007;18:736–45.

108. Van de Wetering P, Cherng J-Y, Talsma H, Crommelin DJ, Hennink WE. 2-(Dimethylamino)ethyl methacrylate based (co)polymers as gene transfer agents. J Control Release 1998;53:145–53.

109. Van De Wetering P, Moret EE, Schuurmans-Nieuwenbroek NM, Van Steenbergen MJ, Hennink WE. Structure-activity relationships of water-soluble cationic methacrylate/methacrylamide polymers for nonviral gene delivery. Bioconjugate Chem 1999;10:589–97.

110. You Y-Z, Manickam DS, Zhou Q-H, Oupický D. Reducible poly(2-dimethylaminoethyl methacrylate): synthesis, cytotoxicity, and gene delivery activity. J Control Release 2007;122:217–25.

111. Zhu C, Jung S, Luo S, Meng F, Zhu X, Park TG, et al. Co-delivery of siRNA and paclitaxel into cancer cells by biodegradable cationic micelles based on PDMAEMA-PCL-PDMAEMA triblock copolymers. Biomaterials 2010;31:2408–16.

112. Zhu C, Zheng M, Meng F, Mickler FM, Ruthardt N, Zhu X, et al. Reversibly shielded DNA polyplexes based on bioreducible PDMAEMA-SS-PEG-SS-PDMAEMA triblock copolymers mediate markedly enahnced nonviral gene transfection. Biomacromolecules 2012;13:769–78.

113. Zhang Y, Zheng M, Kissel T, Agarwal S. Design and biophysical characterization of bioresponsive degradable poly(dimethylaminoethyl methacrylate) based polymers for in vitro DNA transfection. Biomacromolecules 2012;13:313–22.

114. Van de Wetering P, Zuidam NJ, Van Steenbergen MJ, Van der Houwen OAGJ, Underberg WJM, Hennink WE. A mechanistic study of the hydrolytic stability of poly(2-(dimethylamino)ethyl methacrylate). Macromolecules 1998;31:8063–8.

115. Van de Wetering P, Cherng J-Y, Talsma H, Hennink WE. Relation between transfection efficiency and cytotoxicity of poly(2-dimethylamino)ethyl methacrylate)/plasmid complexes. J Control Release 1997;49:59–69.

116. Synatschke C V, Schallon A, Jérôme V, Freitag R, Müller AHE. Influence of polymer architecture and molecular weight of poly(2-(dimethylamino)ethyl methacrylate) polycations on transfection efficiency and cell viability in gene delivery. Biomacromolecules 2011;12:4247–55.

117. Murthy N, Robichaud JR, Tirrell DA, Stayton PS, Hoffman AS. The design and synthesis of polymers for eukaryotic membrane disruption. J Control Release 1999;61:137–43.

118. Deshpande MC, Davies MC, Garnett MC, Williams PM, Armitage D, Bailey L, et al. The effect of poly(ethylene glycol) molecular architecture on cellular interaction and uptake of DNA complexes. J Control Release 2004;97:143–56.

119. Venkataraman S, Ong WL, Ong ZY, Joachim Loo SC, Ee PLR, Yang YY. The role of PEG architecture and molecular weight in the gene transfection performance of PEGylated poly(dimethylaminoethyl methacrylate) based cationic polymers. Biomaterials 2011;32:2369–78.

120. Van Tendeloo VF, Snoeck HW, Lardon F, Vanham GL, Nijs G, Lenjou M, et al. Nonviral transfection of distinct types of human dendritic cells: high-efficiency gene transfer by electroporation into hematopoietic progenitor- but not monocyte-derived dendritic cells. Gene Ther 1998;5:700–7.

121. Irvine AS, Trinder PK, Laughton DL, Ketteringham H, McDermott RH, Reid SC, et al. Efficient nonviral transfection of dendritic cells and their use for in vivo immunization. Nat Biotechnol 2000;18:1273–8.

122. Strobel I, Berchtold S, Götze A, Schulze U, Schuler G, Steinkasserer A. Human dendritic cells transfected with either RNA or DNA encoding influenza matrix protein M1 differ in their ability to stimulate cytotoxic T lymphocytes. Gene Ther 2000;7:2028–35.

123. Melhem NM, Gleason SM, Liu XD, Barratt-Boyes SM. High-level antigen expression and sustained antigen presentation in dendritic cells nucleofected with wild-type viral mRNA but not DNA. Clin Vaccine Immunol 2008;15:1337–44.

124. Van De Parre TJL, Martinet W, Schrijvers DM, Herman AG, De Meyer GRY. mRNA but not plasmid DNA is efficiently transfected in murine J774A.1 macrophages. Biochem Biophys Res Commun 2005;327:356–60.

125. Boczkowski D, Nair SK, Nam J-H, Lyerly HK, Gilboa E. Induction of tumor immunity and cytotoxic T lymphocyte responses using dendritic cells transfected with messenger RNA amplified from tumor cells. Cancer Res 2000;60:1028–34.

126. Moore MW, Carbone FR, Bevan MJ. Introduction of soluble protein into the class I pathway of antigen processing and presentation. Cell 1988;54:777–85.

127. Diken M, Kreiter S, Selmi A, Britten CM, Huber C, Türeci O, et al. Selective uptake of naked vaccine RNA by dendritic cells is driven by macropinocytosis and abrogated upon DC maturation. Gene Ther 2011;18:702–8.

128. Kattunen J, Sanderson S, Shastri N. Detection of rare antigen-presenting cells by the lacZ T-cell activation assay suggests an expression cloning strategy for T-cell antigens. Proc Natl Acad Sci USA 1992;89:6020–4.

129. Burke RS, Pun SH. Extracellular barriers to in vivo PEI and PEGylated PEI polyplex-mediated gene delivery to the liver. Bioconjugate Chem 2008;19:693–704.

130. Ruponen M, Honkakoski P, Tammi M, Urtti A. Cell-surface glycosaminoglycans inhibit cation-mediated gene transfer. J Gene Med 2004;6:405–14.

131. Oupicky D, Ogris M, Howard KA, Dash PR, Ulbrich K, Seymour LW. Importance of lateral and steric stabilization of polyelectrolyte gene delivery vectors for extended systemic circulation. Mol Ther 2002;5:463–72.

132. Toncheva V, Wolfert MA, Dash PR, Oupicky D, Ulbrich K, Seymour LW, et al. Novel vectors for gene delivery formed by self-assembly of DNA with poly(L-lysine) grafted with hydrophilic polymers. BBA-Gen Subjects 1998;1380:354–68.

133. Van den Berg JH, Oosterhuis K, Hennink WE, Storm G, Van der Aa LJ, Engbersen JFJ, et al. Shielding the cationic charge of nanoparticle-formulated dermal DNA vaccines is essential for antigen expression and immunogenicity. J Control Release 2010;141:234–40.

134. Uzgün S, Akdemir O, Hasenpusch G, Maucksch C, Golas MM, Sander B, et al. Characterization of tailor-made copolymers of oligo(ethylene glycol) methyl ether methacrylate and N,N-dimethylaminoethyl methacrylate as nonviral gene transfer agents: influence of macromolecular structure on gene vector particle properties and transfection efficiency. Biomacromolecules 2010;11:39–50.

135. Palumbo RN, Zhong X, Panus D, Han W, Ji W, Wang C. Transgene expression and local tissue distribution of naked and polymer-condensed plasmid DNA after intradermal administration in mice. J Control Release 2012;159:232–9.

136. Phua KKL, Leong KW, Nair SK. Transfection efficiency and transgene expression kinetics of mRNA delivered in naked and nanoparticle format. J Control Release 2013;166:227–33.

137. Probst J, Weide B, Scheel B, Pichler BJ, Hoerr I, Rammensee H-G, et al. Spontaneous cellular uptake of exogenous messenger RNA in vivo is nucleic acid-specific, saturable and ion dependent. Gene Ther 2007;14:1175–80.

138. Randolph GJ, Angeli V, Swartz MA. Dendritic-cell trafficking to lymph nodes through lymphatic vessels. Nat Rev Immunol 2005;5:617–28.

139. Reddy ST, Swartz MA, Hubbell JA. Targeting dendritic cells with biomaterials: developing the next generation of vaccines. Trends Immunol 2006;27:573–9.

140. Kim J, Mooney DJ. In vivo modulation of dendritic cells by engineered materials: towards new cancer vaccines. Nano Today 2011;6:466–77.

141. Manolova V, Flace A, Bauer M, Schwarz K, Saudan P, Bachmann MF. Nanoparticles target distinct dendritic cell populations according to their size. Eur J Immunol 2008;38:1404–13.

142. Reddy ST, Rehor A, Schmoekel HG, Hubbell JA, Swartz MA. In vivo targeting of dendritic cells in lymph nodes with poly(propylene sulfide) nanoparticles. J Control Release 2006;112:26–34.

143. Reddy ST, Van der Vlies AJ, Simeoni E, Angeli V, Randolph GJ, O'Neil CP, et al. Exploiting lymphatic transport and complement activation in nanoparticle vaccines. Nat Biotechnol 2007;25:1159–64.

144. Liu MA. DNA vaccines: an historical perspective and view to the future. Immunol Rev 2011;239:62–84.

145. Banchereau J, Steinman RM. Dendritic cells and the control of immunity. Nature 1998;392:245–52.

146. Keler T, Ramakrishna V, Fanger MW. Mannose receptor-targeted vaccines. Expert Opin Biol Ther 2004;4:1953–62.

147. Figdor CG, Kooyk Y Van, Adema GJ. C-type lectin receptors on dendritic cells and langerhans cells. Nat Rev Immunol 2002;2:77–84.

148. Stahl PD, Ezekowitz RA. The mannose receptor is a pattern recognition receptor involved in host defense. Curr Opin Immunol 1998;10:50–5.

149. Sallusto F, Cella M, Danieli C, Lanzavecchia A. Dendritic cells use macropinocytosis and the mannose receptor to concentrate macromolecules in the major histocompatibility complex class II compartment: downregulation by cytokines and bacterial products. J Exp Med 1995;182:389–400.

150. Engering AJ, Cella M, Fluitsma D, Brockbaus M, Hoefsmie ECM, Lanzavecchia A, et al. The mannose receptor functions as a high capacity and broad specificity antigen receptor in human dendritic cells. Eur J Immunol 1997;27:2417–25.

151. Tan MC, Mommaas AM, Drijfhout JW, Jordens R, Onderwater JJ, Verwoerd D, et al. Mannose receptor-mediated uptake of antigens strongly enhances HLA class II-restricted antigen presentation by cultured dendritic cells. Eur J Immunol 1997;27:2426–35.

152. Toda S, Ishii N, Okada E, Kusakabe KI, Arai H, Hamajima K, et al. HIV-1-specific cell-mediated immune responses induced by DNA vaccination were enhanced by mannan-coated liposomes and inhibited by anti-interferon-gamma antibody. Immunology 1997;92:111–7.

153. Sasaki S, Fukushima J, Arai H, Kusakabe KI, Hamajima K, Ishii N, et al. Human immunodeficiency virus type-1-specific immune responses induced by DNA vaccination are greatly enhanced by mannan-coated diC14-amidine. Eur J Immunol 1997;27:3121–9.

154. Hattori Y, Kawakami S, Suzuki S, Yamashita F, Hashida M. Enhancement of immune responses by DNA vaccination through targeted gene delivery using mannosylated cationic liposome formulations following intravenous administration in mice. Biochem Biophys Res Commun 2004;317:992–9.

155. Diebold SS, Kursa M, Wagner E, Cotten M, Zenke M. Mannose polyethylenimine conjugates for targeted DNA delivery into dendritic cells. J Biol Chem 1999;274:19087–94.

156. Tang CK, Lodding J, Minigo G, Pouniotis DS, Plebanski M, Scholzen A, et al. Mannan-mediated gene delivery for cancer immunotherapy. Immunology 2007;120:325–35.

157. Lu Y, Kawakami S, Yamashita F, Hashida M. Development of an antigen-presenting cell-targeted DNA vaccine against melanoma by mannosylated liposomes. Biomaterials 2007;28:3255–62.

158. Lisziewicz J, Trocio J, Whitman L, Varga G, Xu J, Bakare N, et al. DermaVir: a novel topical vaccine for HIV/AIDS. J Invest Dermatol 2005;124:160–9.

159. Cui Z, Mumper RJ. Topical immunization using nanoengineered genetic vaccines. J Control Release 2002;81:173–84.

160. Zhou X, Liu B, Yu X, Zha X, Zhang X, Chen Y, et al. Controlled release of PEI/DNA complexes from mannose-bearing chitosan microspheres as a potent delivery system to enhance immune response to HBV DNA vaccine. J Control Release 2007;121:200–7.

161. Lee RT, Ichikawa Y, Kawasaki T, Drickamer K, Lee YC. Multivalent ligand binding by serum mannose-binding protein. Arch Biochem Biophys 1992;299:129–36.

162. Mammen M, Choi S-K, Whitesides GM. Polyvalent interactions in biological systems: implications for design and use of multivalent ligands and inhibitors. Angew Chem Int Ed 1998;37:2754–94.

163. Lowe AB, Sumerlin BS, McCormick CL. The direct polymerization of 2-methacryloxyethyl glucoside via aqueous reversible addition-fragmentation chain transfer (RAFT) polymerization. Polymer 2003;44:6761–5.

164. Xiao N-Y, Li A-L, Liang H, Lu J. A well-defined novel aldehyde-functionalized glycopolymer: synthesis, micelle formation, and its protein immobilization. Macromolecules 2008;41:2374–80.

165. Wang Y, Li X, Hong C, Pan C. Synthesis and micellization of thermoresponsive galactose-based diblock copolymers. J Polym Sci A Polym Chem 2011;49:3280–90.

166. Bernard J, Hao X, Davis TP, Barner-Kowollik C, Stenzel MH. Synthesis of various glycopolymer architectures via RAFT polymerization: from block copolymers to stars. Biomacromolecules 2006;7:232–8.

167. Lowe AB, Wang R. Synthesis of controlled-structure AB diblock copolymers of 3-O-methacryloyl-1,2:3,4-di-O-isopropylidene-d-galactopyranose and 2-(dimethylamino)ethyl methacrylate. Polymer 2007;48:2221–30.

168. Albertin L, Stenzel M, Barner-Kowollik C, Foster LJR, Davis TP. Well-defined glycopolymers from RAFT polymerization: poly(methyl 6-O-methylacryloyl-α-D-glucoside) and its block copolymer with 2-hydroxyethyl methacrylte. Macromolecules 2004;37:7530–7.

169. Obata M, Kobori T, Hirohara S, Tanihara M. Synthesis of poly[2-(α-d-mannopyranosyloxy)ethyl-co-2-dimethylaminoethyl methacrylates] and its lectin-binding and DNA-condensing properties. Polymer 2012;53:4672–7.

170. Song E-H, Manganiello MJ, Chow Y-H, Ghosn B, Convertine AJ, Stayton PS, et al. In vivo targeting of alveolar macrophages via RAFT-based glycopolymers. Biomaterials 2012;33:6889–97.

171. Cheng C, Convertine AJ, Stayton PS, Bryers JD. Multifunctional triblock copolymers for intracellular messenger RNA delivery. Biomaterials 2012;33:6868–76.

172. Edelman GM, Cunningham BA, Reeke GN, Becker JW, Waxdal MJ, Wang JL. The covalent and three-dimensional structure of concanavalin A. Proc Natl Acad Sci USA 1972;69:2580–4.

173. Higashi N, Fujioka K, Denda-Nagai K, Hashimoto S-I, Nagai S, Sato T, et al. The macrophage C-type lectin specific for galactose/N-acetylgalactosamine is an endocytic

receptor expressed on monocyte-derived immature dendritic cells. J Biol Chem 2002;277:20686–93.

174. Van Vliet SJ, Saeland E, Van Kooyk Y. Sweet preferences of MGL: carbohydrate specificity and function. Trends Immunol 2008;29:83–90.

175. Carstens MG, Camps MGM, Henriksen-Lacey M, Franken K, Ottenhoff THM, Perrie Y, et al. Effect of vesicle size on tissue localization and immunogenicity of liposomal DNA vaccines. Vaccine 2011;29:4761–70.

Vita

Connie Cheng was born in St. Paul, Minnesota in 1986. She graduated from Harvard University in 2008 with a S.B. degree in Engineering Sciences. During her undergraduate career, she conducted research in the laboratory groups of Dr. Linda Griffith, Department of Biological Engineering, and Dr. Michael Rubner, Department of Materials Science and Engineering, at the Massachusetts Institute of Technology. She pursued her Ph.D. degree in the Department of Bioengineering at the University of Washington under the guidance of Dr. James Bryers, and completed her doctoral dissertation in 2013.